ISSN 1881-7831 Online ISSN 1881-784X

DD&T

Drug Discoveries & Therapeutics

Volume 8, Number 4
August, 2014

IRCA
BSSA
IACMHR

www.ddtjournal.com

DD&T
Drug Discoveries & Therapeutics

ISSN: 1881-7831
Online ISSN: 1881-784X
CODEN: DDTRBX
Issues/Year: 6
Language: English
Publisher: IACMHR Co., Ltd.

Drug Discoveries & Therapeutics is one of a series of peer-reviewed journals of the International Research and Cooperation Association for Bio & Socio-Sciences Advancement (IRCA-BSSA) Group and is published bimonthly by the International Advancement Center for Medicine & Health Research Co., Ltd. (IACMHR Co., Ltd.) and supported by the IRCA-BSSA and Shandong University China-Japan Cooperation Center for Drug Discovery & Screening (SDU-DDSC).

Drug Discoveries & Therapeutics publishes contributions in all fields of pharmaceutical and therapeutic research such as medicinal chemistry, pharmacology, pharmaceutical analysis, pharmaceutics, pharmaceutical administration, and experimental and clinical studies of effects, mechanisms, or uses of various treatments. Studies in drug-related fields such as biology, biochemistry, physiology, microbiology, and immunology are also within the scope of this journal.

Drug Discoveries & Therapeutics publishes Original Articles, Brief Reports, Reviews, Policy Forum articles, Case Reports, News, and Letters on all aspects of the field of pharmaceutical research. All contributions should seek to promote international collaboration in pharmaceutical science.

Editorial Board

Editorial and Head Office:

Pearl City Koishikawa 603,
2-4-5 Kasuga, Bunkyo-ku,
Tokyo 112-0003, Japan
Tel.: +81-3-5840-9697
Fax: +81-3-5840-9698
E-mail: office@ddtjournal.com

Drug Discoveries & Therapeutics

Editorial and Head Office

Pearl City Koishikawa 603, 2-4-5 Kasuga, Bunkyo-ku,
Tokyo 112-0003, Japan

Tel: +81-3-5840-9697, Fax: +81-3-5840-9698
E-mail: office@ddtjournal.com
URL: www.ddtjournal.com

Editorial Board Members

Reviews

Original Articles

CONTENTS (*Continued*)

Review

DOI: 10.5582/ddt.2014.01032

A map describing the association between effective components of traditional Chinese medicine and signaling pathways in cancer cells *in vitro* and *in vivo*

Jufeng Xia[1], Jialu Chen[2], Zhongmin Zhang[2], Peipei Song[1], Wei Tang[1,*], Norihiro Kokudo[1]

[1] *Hepato-Biliary-Pancreatic Surgery Division, Department of Surgery, Graduate School of Medicine, The University of Tokyo, Tokyo, Japan;*
[2] *Department of Chemistry, Fudan University, Shanghai, China.*

Summary **Cancer is the second leading cause of death by disease in the world. Chemotherapy is one of three major therapeutic methods for cancer treatment, but cancer cells gradually evolve resistance to chemotherapeutic reagents. For centuries, traditional Chinese medicine (TCM) was used to fight against cancer. In recent years, a number of effective component mechanisms of TCM have been increasingly illuminated. As we know, chemical structures of reagents decide or affect their activities on target pathways. Thus, we classified some antitumor-related TCM components reported in the last five years into thirteen groups by their chemical structures, such as, alkaloids, diterpenoids, triterpenes, sesquiterpenes, anthraquinones, benzoquinones, flavonoids, berbamines, xanthones, saponins, steroids, polysaccharides, and glycosides. In various cancer cell lines, these constituents target dozens of signaling pathways *in vitro* and *in vivo*. Among these components, there are three sets: *i*) mainly apoptosis-related groups, such as, alkaloids, diterpenoids, anthraquinones, berbamines, and xanthones, target pathways like the mitochondrial pathway, NF-κB pathway, p53 pathway and so on; *ii*) mainly proliferation, invasion and metastasis-related groups, such as, triterpenes, sesquiterpenes, polysaccharides, and glycosides, target pathways like the mTOR pathway, β-catenin pathway, ERK pathway and so on; *iii*) both apoptosis and proliferation, invasion and metastasis-related groups, such as benzoquinones, flavonoids, saponins, and steroids, target the pathways in *i*) and *ii*) synchronously. These will provide association information between TCM components and signaling pathways to promote studies on mechanisms of effective constituents, target drug development, and combinational chemotherapy. TCM could be alternative medicine for cancer treatment in the future.**

Keywords: Traditional Chinese medicine, signaling pathway, chemical structure, alternative medicine, combination therapy

1. Introduction

In 2008, approximately 12.7 million cancers were diagnosed (excluding non-melanoma skin cancers and other non-invasive cancers) (*1*), and in 2010 nearly 7.98 million people died. Cancers as a group account for approximately 13% of all deaths each year with the most common being: lung cancer (1.4 million deaths), stomach cancer (740,000 deaths), liver cancer (700,000 deaths), colorectal cancer (610,000 deaths), and breast cancer (460,000 deaths) (*2*). This makes invasive cancer the leading cause of death in the developed world and the second leading cause of death in the developing world. Over half of the cases occur in the developing world.

Chemoprevention is one of the major approaches for decreasing cancer morbidity and mortality (*3*). However, resistance to chemotherapy and molecular target therapies is becoming a big barrier for current cancer research. Because of the high cost of developing novel

**Address correspondence to:*
Dr. Wei Tang, Hepato-Biliary-Pancreatic Surgery Division, Department of Surgery, Graduate School of Medicine, The University of Tokyo, 7-3-1 Hongo, Bunkyo-ku, Tokyo 113-8655, Japan.
E-mail: tang-sur@h.u-tokyo.ac.jp

chemotherapeutic or targeted drugs, there is an emergent requirement for alternative medication.

It was reported that traditional Chinese medicine (TCM) had been widely applied for cancer care in China and there has been a great number of controlled clinical studies reported in Chinese papers (*4*). TCM uses a combinational medication of different natural components. To better understand the therapeutic effects of TCM, many efforts have been made to identify the constituents of TCM and to lift the veil of molecular mechanisms from it.

In recent years, a few reports suggested that certain kinds of chemical structures may relate to some corresponding cellular signaling pathways (*5*). Thus, we summarized the last five years' studies on TCM components functions on cancer cell signaling pathways and aimed at looking for association between chemical structure of TCM constituents and cancer cell signaling pathways.

2. Association between chemical structure of TCM constituents and cancer cell signaling pathways

Based on the last five years' papers on TCM components related cellular signal pathway research, the chemical structure of dozens of TCM constituents have been analyzed and relationships to signal pathways has been summarized (Table 1).

2.1. *Alkaloid*

Alkaloids are a group of naturally occurring chemical

Table 1. Components of TCM commonly used in cancer treatment

Components	Cell lines	Animals	Pathways	*Ref.*
Alkaloid	9KB, L1210, HeLa, MCF-7,HCT116, A549,MNNG/HOS,M21,A375, 95D	Mice	mTOR, NF-κB, p53, HIF-1α,FOXO3α, mitochondria,	*6-19*
Diterpenoid	β-TC-6,SGC996, NOZ,MDA-MB-231, SW620	Mice	PI3K/Akt,FAK,p38 MAPK, NF-κB,HIF-1α, mitochondria	*20-29*
Triterpene	HeLa,T24, HepG2, MDA-MB-231, HEK293, HCT15, CO115	Mice Zebrafish	NF-κB, angpt2/tie2, STAT3, β-catenin, EGFR, FAK-SRC-Paxillin	*30-39*
Sesquiterpene	HUVECs, MCF-7, MKN-45, A2780/CP70,MCAS	Mice	Akt/GSK3β, mTOR, Smad3,JNK,Notch-1,Snail/E-cadherin,	*40-44*
Anthraquinone	MCF-7,HeLa,MDA-MB-231,HepG2,U87,NPC-TW-039, NPC-TW-076	Mice	NF-κB, p53, MAPK, mitochondria,	*45-50*
Benzoquinone	HeLa,AGS,BXPC-3, PANC-1, ASPC-1, A549,NTHY-0RI 3-1 CL1-0, CL1-5, DU145,	Mice	NF-κB, PI3K/Akt, ERK1/2, mitochondria	*51-58*
Flavonoid	MDA-MB-231, MCF-7, T24, U87MG, U251MG, MHCC97H, AGS, A549, PC-3, A431, SKBr3, BGC-823, HT-29, 5637, A2780/CP70, OVCAR-3,	Mice	NF-κB, mTOR, p38 MAPK,mitochondria, ROS, TGF-β, ERK, p53, Rac1	*59-74*
Berbamine	HepG2, PLC/PRF/5, SK-Hep-1, SNU398, Bxpc-3, Panc-1, A2058, A375, G361, SK-MEL-28, U87, SK-MEL-5, Raji, L428, Namalwa, Jurkat, HCT116, HCT8, MCF-7, HUVECs	Mice	NF-κB,TGF-β/Smad, STAT3, JNK, mTOR, HIF-1α	*75-80*
Xanthone	HepG2,Hep3B, Huh-7,Bel7404, BGC-823, SGC-7901, SK-Hep-1, MIAPaCa-2, BxPC-3, PC-3	Mice	STAT3, ERK, JNK, mitochondria	*81-86*
Saponin	HL-60,T47D,HeLa, MDA-MA-231, MDA-MB-453, NCI-H157, SKOV3, NCI-H460, A549, MCF-7, SPCA-1, H1975, NCI-H446, NCI-H292, NCI-H69, HO-8910PM	Mice	JNK, p38 MAPK, mitochondria, mTOR, AIF, ROS, p53/p21, β-catenin	*87-95*
Steroid	HCCLM3, HepG2, A549,MDAMB-231,LNCaP,DU145,PC3,HL-60,MGc-803, SW620, HeLa, 4T1	Mice	Met/PI3K/Akt, STAT3, NF-κB, AKT/GSK3β/β-catenin, FAK/Rac1, MAPK	*96-104*
Polysaccharide	HT-29, LOVO, CL1-5,A549, Hca-F, 4T1, HL-60, U-2	Mice	ErbB, IGF-1R, TGFR/Smad7, NF-κB, ERK, death receptor,β-catenin, mitochondria	*105-113*
Glycoside	TEU-2, A549, H22, MCF-7, YD-10B	Mice	mTOR, MAPK, ERK, NF-κB, Rac1, β-catenin, mitochondria	*114-119*

compounds (natural products) that contain mostly basic nitrogen atoms. Alkaloids are produced by a large variety of organisms including bacteria, fungi, plants, and animals. They often have pharmacological effects and are used as medications, as recreational drugs, or in entheogenic rituals (*6*). The following are some TCM components which were reported in recent years.

Camptothecin, which is extracted from *Camptoteca acuminata Decne*, and its derivatives can inhibit cancer cell proliferation by suppressing DNA topoisomerase I by stabilizing certain intermediate complexes during DNA synthesis (*7*). It has been applied to 9KB (human oral epidermoid carcinoma cell line) and L1210 (human leukemia cell line). It also can induce p53-dependent DNA damage in renal cell carcinoma (*8*). In another report, camptothecin induces apoptosis through the hypoxia-inducible factor-1α (HIF-1α) pathway in HeLa (human cervix adenocarcinoma cell line) (*9*). In the HCT116 coloretctal cancer cell, camptothecin can induce apoptosis through the AMPK-TSC2-mTOR pathway (*10*).

Vinblastine, which is derived from *Vinca rosea* L., can arrest the cell cycle through inhibiting assembly of microtubules and binding to subunits of tubulin in S phase. Anticancer activity was assayed against MCF-7 (human breast cancer cell line) (*11*). An *in vitro* and *in vivo* study suggests a synergistic anticancer activity of a nanoliposomal C6-ceramide and vinblastine combination, potentially lead by an autophagy mechanism (*12*).

Berberine is a natural product extracted from roots of *Coptis chinensis* Franch which has been shown to have anticancer activities. In HCT116 (human colon cancer cell line), it suppresses proliferation *via* AMPK dependent inhibition of mTOR activity and induces apoptosis by AMPK dependent inhibition of NF-κB. *In vivo*, it also inhibits mTOR and activates caspase-3 cleavage (*13*). In A549 (human lung adenocarcinoma cell line), berberine inhibits proliferation and induces apoptosis of adenocarcinoma cells by activating the p38α MAPK signaling pathway followed by inducing p53 and FOXO3α (*14*).

Oxymatrine, the main constituent in the traditional Chinese herbal medicine *Sophora japonica*, has been reported to have antitumor properties. In human osteosarcoma MNNG/HOS cell line, oxymatrine induces mitochondria dependent apoptosis by inhibiting the PI3K/Akt pathway (*15*). In an *in intro* and *in vivo* experiment, oxymatrine shows an antiangiogenic effect on pancreatic cancer through inhibition of the NF-κB-mediated VEGF signaling pathway (*16*).

Matrine is a major active component in traditional Chinese medicine *Sophora flavescens*. It has been reported that matrine induces growth inhibition and apoptosis of M21 and A375 (human melanoma cell lines) by activating the PTEN pathway (*17*). Matrine also induces apoptosis of A549 and 95D (human lung cancer cell lines) *via* the PI3K/Akt/mTOR signaling pathway and down-regulation of inhibitor of apoptosis proteins (*18*). Another study reports that matrine inhibits the invasive activities of human osteosarcoma cells through down-regulation of the ERK/NF-κB pathway *in intro* and *in vivo* (*19*).

These alkaloid components can suppress proliferation, invasion, or apoptosis of cancer cells by the following pathways: *i*) AMPK/mTOR pathway; *ii*) MAPK/Akt/mTOR pathway; *iii*) NF-κB pathway; *iv*) p53 apoptosis pathway; *v*) HIF-1α pathway; *vi*) mitochondria-dependent pathway; and *vii*) FOXO3α pathway. The first three pathways are major signaling pathways activated by alkaloids from TCM.

2.2. *Diterpenoid*

The terpenoids are a large and diverse class of naturally occurring organic chemicals similar to terpenes, derived from five-carbon isoprene units assembled and modified in thousands of ways. Most are multicyclic structures that differ from one another not only in functional groups but also in their basic carbon skeletons. These lipids can be found in all classes of living things, and are the largest group of natural products (*20*). Diterpenoids, a member of the terpenoid family, with their twenty-carbon backbone constitute roughly a fourth of all known plant terpenoids, which currently are more than 12,000 (and counting) structures known. The followings are some TCM-derived diterpenoid components.

Andrographolide is a diterpenoid lactone derived from *Andrographis paniculata*. The combination of andrographolide and taxifolin inhibit proliferation and trigger apoptosis of breast cancer cells by disrupting microtubule dynamics and acitivating the spindle assembly checkpoint (SAC) (*21*). In other studies, andrographolide alone can inhibit proliferation of breast cancer cells and non-small cell lung cancer (NSCLC) cells by downregulating the PI3K/Akt pathway (*22,23*). NSCLC cells also can be suppressed by andrographolide through the HIF-1α pathway (*24*). In the β-TC-6 (human insulinoma cell line), andrographolide suppress growth of cancer cells through inhibition of the TLR4/NF-κB signaling pathway *in intro* and *in vivo* (*25*).

Oridonin is isolated from the plant *Rabdosia rubescens*. It can inhibit growth of prostate cancer cells by suppressing the NF-κB signaling pathway *in intro* and *in vivo* (*26*). In human gallbladder cancer cell lines SGC996 and NOZ, oridonin induces apoptosis and cell cycle arrest *via* the mitochondrial pathway (*27*). It is also reported to suppress invasion and metastasis of human breast cancer cell line MDA-MB-231 *in vitro* by decreasing the expression of MMPs and regulating the Integrinβ/FAK pathway *in vitro* (*28*).

Diterpenoid C is isolated from *Radix Curcumae* which is the dry root of Curcuma wenyujin. In a study on human colon adenocarcinoma cell line SW620,

diterpenoid C functions as an inhibitor of proliferation and inducer of apoptosis through the MAPK signaling pathway (*29*).

The diterpenoids can induce apoptosis and inhibit invasion of cancer cells *via* the following pathways: *i*) PI3K/Akt pathway; *ii*) p38 MAPK pathway; *iii*) NF-κB pathway; *iv*) HIF-1α pathway; *v*) mitochondria-dependant pathway; *vi*) FAK pathway; and *vii*) disrupting microtubule dynamics and acitivating SAC. The first three pathways are affected by most diterpenoids above and they have crosstalk between each other.

2.3. *Triterpene*

Triterpenes are terpenes consisting of six isoprene units and have the molecular formula $C_{30}H_{48}$. The pentacyclic triterpenes can be classified into lupane, oleanane or ursane groups. A notable pentacyclic triterpene is Boswellic acid.

Ganoderic acid is a triterpene derived from *Ganoderma lucidum*. It induces mitochondria-dependent apoptosis in human cervical carcinoma HeLa cells *in vitro* (*30*). Ganoderic acid can also inhibit growth and angiogenesis of human breast cancer cell line MDA-MB-231 by modulating the NF-κB signaling pathway (*31*). On the other hand, ganoderic acid can enhance chemosensitivity of human hepatocellular carcinoma (HCC) cell line HepG2 to cisplatin by inhibiting the JAK-STAT3 signaling pathway (*32*). This suggests that ganoderic acid can be used in combination with chemotherapeutic agents for cancer treatment.

Ursolic acid is a triterpene compound isolated from certain traditional medicinal plants, such as *Mirabilis jalapa*. Ursolic acid was proved to suppress the proliferation of colon cancer cell line HEK293 by promoting degradation of β-catenin (*33*). In Enrlich ascites carcinoma cell line, ursolic acid acts as an inducer of apoptosis through the mitochondrial signaling pathway *in intro* and *in vivo* (*34*), and in T24 human bladder cancer cells, it induces apoptosis *via* the Akt/NF-κB pathway (*35*). Ursolic acid also can induce cell death and modulate autophagy by the JNK pathway in the apoptosis-resistant human colon carcinoma cell line HCT15 and CO115 (*36*).

Ganoderiol A is a natural product isolated from traditional Chinese medicine *Ganoderma lucidum*. It inhibits migration and adhesion of highly metastatic breast cancer cell line MDA-MB-231 by suppressing the FAK-SRC-Paxillin cascade pathway (*37*).

The fruit of *Poncirus trifoliate* has been used as traditional medicine for many years, and 25-Methoxyhispidol A is derived from it. In MDA-MB-231 breast cancer cells, 25-Methoxyhispidol A suppresses cell growth through modulation of the EGFR/c-Src signaling pathway *in vitro* (*38*).

Friedelan-3-one and 29-hydroxyfriedelan-3-one are exacted from *Tripterygium wilfordii* which has been traditionally used as folk medicine for treatment of inflammatory diseases. They show antiangiogenic activity against vessel formation in the zebrafish model by inhibiting the angpt2/tie2 signaling pathway. (*39*)

The triterpenes above mainly fight against cancer cells *via* the following pathways: *i*) mitochondria pathway; *ii*) NF-κB pathway; *iii*) angpt2/tie2 signaling pathway; *iv*) JAK-STAT3 pathway; *v*) β-catenin pathway; *vi*) FAK-SRC-Paxillin cascade pathway; and *vii*) EGFR/c-Src pathway. The first three pathways are affected by more than two components.

2.4. *Sesquiterpene*

Sesquiterpenes are a class of terpenes that consist of three isoprene units and have the molecular formula $C_{15}H_{24}$. Like monoterpenes, sesquiterpenes may be acyclic or contain rings, including many unique combinations.

Dehydrocostus lactone is a TCM component derived from *Saussurea costus* (Falc.) Lipschitz. In human umbilical vein endothelial cells (HUVECs), it suppresses angiogenesis by inhibiting Akt/GSK3β and mTOR signaling pathways *in intro* and *in vivo* (*40*).

β-Elemene, a naturally occurring component isolated from *Curcumae Radix*, has been used as an antitumor drug for various cancers in China. It has been reported to be able to block epithelial-mesenchymal transition (EMT) in MCF-7, a human breast cancer cell line, by Smad3-mediated down-regulation of nuclear transcription factors (SNAI1, SNAI2, TWIST and SIP1) (*41*). In the same cell line, other research proves that β-elemene decreases cell invasion through up-regulation of E-cadherin expression (*42*). In research on gastric cancer stem-like cells, β-elemene is effective in attenuating angiogenesis by targeting Notch-1 *in intro* and *in vivo* (*43*). A study on a combination of β-elemene and cisplatin suggests that in resistant ovarian carcinoma cells β-elemene increases susceptibility to cisplatin by inactivating the JNK pathway (*44*).

These sesquiterpenes block proliferation and invasion of cancer cells by some different pathways as follows: *i*) Akt/GSK3β pathway; *ii*) mTOR pathway; *iii*) Smad3 pathway; *iv*) Snail/E-cadherin pathway; *v*) Notch-1 pathway; and *vi*) JNK pahway.

2.5. *Anthraquinone*

Anthraquinone, also called anthracenedione or dioxoanthracene, is an aromatic organic compound with formula $C_{14}H_8O_2$. Several isomers are possible, each of which can be viewed as a quinone derivative. The term anthraquinone, however, almost invariably refers to one specific isomer, 9,10-anthraquinone wherein the keto groups are located on the central ring.

Emodin, a naturally occurring anthraquinone component derived from *Polygoni cuspidati radix*, has

been reported to have anti-cancer and anti-inflammatory activities. In MCF-7 and MDA-MB-231 human breast cell lines, emodin leads to inhibition of proliferation through the ERα-MAPK/Akt-Cyclin D1/Bcl-2 signaling pathway (*45*). Emodin induces apoptosis of the HeLa human cervical cell line by activation of the mitochondria apoptotic pathway (*46*). Cancer cell apoptosis also can be induced by emodin in the HepG2 human HCC cell line through activation of the p53 pathway and inhibition of the NF-κB/p65 pathway (*47*).

Aloe emodin, one of the active compounds isolated from *Aloe vera* leaves, plays an important role in the regulation of cell growth and death. It induces cell cycle arrest and apoptosis *via* the mitochondria dependent signaling pathway in human U87 malignant glioma cells (*48*). Another study proved that aloe emodin induces invasive inhibition of NPC-TW 039 and NPC-TW 076 human nasopharyngeal carcinoma cell lines by decreasing expression levels of MMP-2 through the p38 MAPK/NF-κB signaling pathway (*49*).

2-methyl-1,3,6-trihydroxy-9,10-anthraquinone is one of the major constituents derived from the TCM *Rubia yunnanensis* which exhibits inhibitory activity of proliferation of several human cancer cell lines. In the HeLa human cervical cancer cell line, 2-methyl-1,3,6-trihydroxy-9,10-anthraquinone was demonstrated to induce cell cycle arrest and apoptosis of cancer cells through the p53/p21/Cdc2-cyclin B1 signaling pathway (*50*).

These anthraquinones above show antitumor activities through several pathways: *i*) mitochondria-dependent pathway; *ii*) NF-κB pathway; *iii*) MAPK/Cyclin D1/Bcl-2 pathway; *iv*) p53 pathway; and *v*) Cdc2/Cyclin B1 pathway. The first two pathways play a role as frequent targets.

2.6. *Benzoquinone*

Benzoquinone is a quinone with a single benzene ring, of which there are only two members: *i*) 1,4-Benzoquinone, most commonly; and *ii*) 1,2-Benzoquinone, less commonly.

Rhinacanthone, a main bioactive component derived from *Rhinacanthus nasutus* KURZ, has been reported to possess antitumor activities. Recent research demonstrates that rhinacanthone leads to apoptosis of HeLa human cervical carcinoma cells through the mitochondria-dependent signaling pathway.

Shikonin, a natural product derived from the Chinese medical herb *Lithospermum erythrorhizon*, has been widely used as a traditional Chinese medicine for thousands of years. In the BXPC-3 human pancreatic carcinoma cell line, it promotes autophagy through the PI3K/Akt signaling pathway (*51*). In another human pancreatic carcinoma study, PANC-1, BXPC-3, and ASPC-1 cell lines were employed. Shikonin is combined with gemcitabine, a nucleoside analog used as chemotherapy, and the combination group is demonstrated to suppress tumor growth *in vitro* and *in vivo* through the NF-κB pathway (*52*). In a human gastric cancer study, shikonin induced cell cycle arrest of the AGS cell line by the early growth response 1 (Egr1)/p21 signaling pathway (*53*). In A549 lung cancer cell line, Shikonin attenuates adhesion of cells to extracellular matrix and metastasis through inhibition of the ERK1/2 signaling pathway (*54*). In the NTHY-0RI 3-1 human papillary thyroid carcinoma cell line, shikonin plays a role in inducing apoptosis through the mitochondrial pathway (*55*).

Tanshinone I, a bioactive constituent of *Salvia miltiorrhiza* Bunge, has been used in China for thousands of years to treat various diseases, such as heart disease, hepatitis, and cancer. In A549, CL1-0, and CL1-5 cell lines, tanshinone I inhibits cancer progress by blocking the cell cycle pathway and VEGF protein *in vitro* and *in vivo* (*56*). In the DU145 human prostate cancer cell line, tanshinone I induces apoptosis of cancer cells by activating the mitochondrial pathway (*57*). In a paper published in 2008, Tanshinone I was reported to suppress proliferation of NSCLC cells through the NF-κB pathway (*58*).

These benzoquinones target several pathways: *i*) mitochondrial pathway; *ii*) NF-κB pathway; *iii*) PI3K/Akt pathway; *iv*) ERK1/2 pathway; and *v*) cell cycle pathway. The first two pathways are targets of all of these benzoquinones.

2.7. *Flavonoid*

Flavonoids are a class of plant secondary metabolites. Flavonoids were referred to as Vitamin P from the mid-1930s to early 50s, but the term has since fallen out of use. Chemically, they have the general structure of a 15-carbon skeleton, which consists of two phenyl rings (A and B) and a heterocyclic ring (C). This carbon structure can be abbreviated C6-C3-C6. Flavonoids have been reported to possess various therapeutic effects for inflammation, cancer, and cardiovascular diseases.

Baicalein (5,6,7-trihydroxyflavone) is a flavone, a type of flavonoid, originally isolated from the roots of *Scutellaria baicalensis*. It has been reported to inhibit migration and invasion of human gastric cancer cells by suppressing the TGF-β signaling pathway (*59*). In the human breast carcinoma cell line MDA-MB-231, baicalein shows its ability to induce autophagic cell death *via* activation of the AMPK/ULK1 pathway and inhibition of the mTOR pathway (*60*). Baicalein also can lead to apoptosis of MCF-7 human breast cancer cells and T24 human bladder cancer cells through a decrease of the reactive oxygen species (ROS)-dependent apoptosis pathway and mitochondrial-dependent caspase activation pathway respectively (*61,62*). A study on invasion of glioma cells shows

that baicalein attenuates the invasion of U87MG and U251MG cell lines by inhibition of the activity of the p38 MAPK signaling pathway (*63*). Through MAPK family pathways, baicalein also is reported to suppress the invasion and metastasis of the MHCC97H human HCC cell line *via* down-regulation of the ERK signaling pathway (*64*).

Quercetin, a flavonol, is a flavonoid, in other words, a plant pigment with a molecular structure like or derived from flavone. In AGS human gastric cancer cells, quercetin induces apoptosis through inhibition of the p38 MAPK signaling pathway (*65*). In combination with trichostatin A, a eukaryotic cell cycle inhibitor, quercetin enhances treatment effects by inhibiting proliferation of A549 human NSCLC cells through the p53 signaling pathway *in vitro* and *in vivo* (*66*). In a study on human prostate tumors, quercetin was shown to inhibit angiogenesis by targeting the VEGFR-2 mediated mTOR signaling pathway *in vitro* and *in vivo* (*67*). Quercetin has been reported to induce apoptosis of human prostate cancer PC-3 cells through endoplasmic reticulum (ER) stress and the mitochondrial apoptotic signaling pathway (*68*).

Icariin is a flavonol glycoside, a type of flavonoid. It is the 8-prenyl derivative of kaempferol 3,7-O-diglucoside. The compound is derived from several species of plants belonging to the genus *Epimedium Berberidaceae*. It induces apoptosis of A431 human epidermoid carcinoma cells by inhibiting the EGFR pathway (*69*). Similarly, other research also proves that icariin inhibits proliferation of SKBr3 breast cancer cells *via* the EGFR-MAPK signaling pathway (*70*). In the BGC-823 human gastric cancer cell line, icariin exterts negative effects on invasion and migration through the Rac1 pathway (*71*).

Kaempferol is a natural flavonol, a type of flavonoid, that has been isolated from tea, broccoli, *Delphinium*, Witch-hazel, grapefruit, grapes, and other plant sources. It promotes apoptosis of HT-29 human colon cancer cells through activating cell surface death receptors and the mitochondrial pathway (*72*). In a recent paper, it was revealed that kaemperol attenuates the growth of 5637 and T24 human bladder cancer cells by inhibition of the c-Met/p38 MAPK signaling pathway *in vitro* and *in vivo* (*73*). The antitumor activity of kaempferol also has been shown in OVCAR-3 and A2780/CP70 human ovarian cancer cell lines, it suppresses expression of VEGF and angiogenesis by inhibiting the ERK-NF-κB pathway (*74*).

The above flavonoids play an efficient role against cancer cells by targeting various pathways: *i*) mTOR pathway; *ii*) mitochondrial pathway; *iii*) p38 MAPK pathway; *iv*) NF-κB pathway; *v*) TGF-β pathway; *vi*) ROS-dependant pathway; *vii*) ERK pathway; *viii*) p53 pathway; and *ix*) Rac1 pathway. MAPK pathway, mTOR pathway, the mitochondrial pathway, and NF-κB pathway all are inhibited by at least half of the listed flavonoids. That may suggest there is a certain association between these signaling pathways and flavonoids.

2.8. *Berbamine and its structural analogues*

Berbamine is a natural bisbenzylisoquinoline product derived from traditional Chinese herbal medicine *Berberis amurensis* and has been used to treat inflammatory and other diseases for centuries. In HepG2, PLC/PRF/5, SK-Hep-1, and SNU398 cells, berbamine plays a role in blocking the Ca^{2+} channel through inhibition of Ca^{2+}/calmodulin-dependent protein kinase II (introduction). In Bxpc-3 and Panc-1 human pancreatic cancer cell lines, berbamine can enhance antitumor activity of gemcitabine through activating the TGF-β/Smad pathway (*75*). A derivative of berbamine is reported to induce apoptosis of A2058, A375, G361, SK-MEL-28, and SK-MEL-5 human melanoma cell lines *via* inhibition of the jak2/STAT3 signaling pathway (*76*). Another berbamine derivative was proved to inhibit cell viability and lead to apoptosis of the U87 human glioblastoma cell line through up-regulation of the miRNA-4284 and JNK/AP-1 signaling pathway (*77*). 4-Chlorobenzoyl berbamine, a derivative of berbamine, was demonstrated to inhibit proliferation and induce apoptosis of Raji, L428, Namalwa, and Jurkat lymphoma cell lines through the PI3K/Akt and NF-κB pathway (*78*).

Dauricine, a natural product isolated from the rhizome of *Menispermum dauricum* DC, has been found to have antiarrhythmic and anti-inflammatory effects. It was proved to suppress proliferation and invasion and induce apoptosis of HCT116 and HCT8 human colon cancer cells by blocking the NF-κB signaling pathway (*79*). In the MCF-7 human breast cancer line and HUVECs human umbilical vein endothelial cells, dauricine plays a role in inhibiting angiogenesis of cancer cells by blocking the PI3K/Akt/mTOR pathway and HIF-1α pathway (*80*).

In brief, berbamine, its derivatives, and its analogues stand up to cancer cells through the following pathways: *i*) TGF-β/Smad pathway; *ii*) jak2/STAT3 pathway; *iii*) JNK/AP-1 pathway; *iv*) PI3K/Akt/mTOR pathway; *v*) NF-κB pathway; and *vi*) HIF-1α pathway. The PI3K/Akt/mTOR pathway and NF-κB pathway are both targeted by these components.

2.9. *Xanthone*

Xanthone is an organic compound with the molecular formula C13H8O2. It can be prepared by the heating of phenyl salicylate. Up to now, over 200 xanthones have been identified.

1,3,5-Trihydroxy-13,13-dimethyl-2H-pyran [7,6-b] xanthone (TDP), is isolated from the traditional Chinese medicinal herb *Garcinia oblongifolia*. Research on

this component is focused on human hepatocellular carcinoma. In this research, TDP is reported to induce apoptosis of cells by targeting the heat shock protein 27 (Hsp27) related signaling pathway (*81*). In another study, TDP was proved to lead to apoptosis of cells through activation of the mitochondrial signaling pathway (*82*).

α-Mangostin, a main xanthone component isolated from the pericarp of mangosteen (*Garcinia mangostana* Linn), possesses unique biological activities, including antioxidant, antitumor and anti-inflammatory effects. It has been identified to be able to increase apoptosis of BGC-823 and SGC-7901 human gastric adenocarcinoma cell lines by blocking the STAT3 siganaling pathway (*83*). In human hepatoma SK-Hep-1 cells, α-mangostin leads to mitochondrial dependent apoptosis *via* inhibition of the p38 MAPK signaling pathway (84). In MIAPaCa-2 and BxPC-3 human pancreatic cancer cell lines, α-mangostin can suppress the invasion and metastasis of pancreatic cancer cells by decreasing MMP-2 and MMP-9 expression, increasing E-cadherin expression and inhibiting the ERK signaling pathway (*85*). In the PC-3 human prostate carcinoma cell line, α-mangostin can also inhibit metastasis of cancer cells through inhibition of MMP-2 and MMP-9 *via* the JNK signaling pathway (*86*).

These xanthones mainly target the following pathways: *i*) mitochondrial pathway; *ii*) STAT3 pathway; *iii*) ERK pathway; and *iv*) JNK pathway. The mitochondrial pathway is targeted more frequently.

2.10. *Saponin*

Saponins are a class of chemical compounds found in particular abundance in various plant species. More specifically, they are amphipathic glycosides grouped phenomenologically by the soap-like foaming they produce when shaken in aqueous solutions, and structurally by having one or more hydrophilic glycoside moieties combined with a lipophilic triterpene derivative.

Dioscin, a plant steroidal glycoside isolated from *Polygonatum zanlanscianense* pump, exhibits cytotoxicity against a number of human malignant cell lines. In human myeloblast leukemia HL-60 cells, dioscin induces apoptosis of cancer cells by activating p38 MAPK and JNK through the caspase dependent mitochondrial signaling pathway (*87*). In MDA-MA-231, MDA-MB-453, and T47D human breast cancer cell lines, dioscin induces cell death through the apoptosis inducing factor (AIF) signaling pathway (*88*).

Ophiopogonin B (OP-B) is a bioactive component of Radix Ophiopogon Japonicus, which is often used in Chinese traditional medicine to treat pulmonary disease. In a paper published in Chinese, OP-B was proved to increase the autophage of human HeLa cells through repression of the Akt/mTOR signaling pathway (*89*). In human NSCLC cell lines NCI-H157 and NCI-H460, OP-B was proved to induce autophage of cancer cells *via* inhibition of the PI3K/Akt signaling pathway (*90*).

Saikosaponin, a naturally occurring compound isolated from *Bupleurum radix*, has been shown to exert anti-cancer activity in several cancer cell lines. In HeLa and Siha cervical cancer cell lines, SKOV3 ovarian cancer cell line, and A549 NSCLC cell line, combination administration of saikosaponin and cisplatin can sensitize cancer cells to cisplatin through the ROS-mediated apoptotic pathway (*91*). In MDA-MB-231 and MCF-7 human breast cancer cells, saikosaponin increases apoptosis through the p53/021 dependant pathway (*92*).

Periplocin is a natural product derived from *Cortex periplocae*. It is demonstrated to suppress proliferation and induce apoptosis of SW480 human colon carcinoma cells through the β-catenin/Tcf signaling pathway *in vitro* and *in vivo* (*93*). In human lung cancer cell lines A549, SPCA-1, H1975, NCI-H446, NCI-H460, NCI-H292 and NCI-H69, periplocin can inhibit proliferation and induce apoptosis of cancer cells by the Akt and ERK signaling pathway *in vitro* and *in vivo* (*94*).

Polyphyllin I, a component derived from *Rhizoma Paridis Chonglou*, was proved to suppress proliferation and metastasis of human ovarian cancer cell line HO-8910PM by activating the JNK signaling pathway (*95*).

Collectively, the above saponins fight against cancers by targeting the following pathways: *i*) p38 MAPK pathway; *ii*) JNK pathway; *iii*) mitochondrial pathway; *iv*) AIF pathway; *v*) mTOR pathway; *vi*) ROS dependant pathway; *vii*) p53/p21 pathway; *viii*) β-catenin/Tcf pathway; and *ix*) ERK pathway

2.11. *Steroid*

A steroid is a type of organic compound that contains a characteristic arrangement of four cycloalkane rings joined to one another.

Bufalin is a major bioactive component of Venenum Bufonis, a traditional Chinese medicine obtained from the skin and parotid venomglands of toads. In a EGFR mutant lung cancer cell line, it was proved to reverse HGF-induced EGFR-TKIs resistance by blocking the Met/PI3K/Akt signaling pathway (*96*). In human hepatoma cell lines HCCLM3 and HepG2, bufalin plays a role in suppressing proliferation, migration, invasion and adhesion of hepatoma cells inhibition of the AKT/GSK3β/β-catenin/E-cadherin signaling pathway (*97*). There are a number of research reports on the apoptosis effect of bufalin. In lung cancer cells, breast cancer cells, prostate cancer cells, hepatocellular carcinoma cells, gastric cancer cells, and leukemia cells, bufalin was demonstrated to induce apoptosis through the NF-κB pathway and mitochondrial pathway (*98*). Bufalin was also proved to increase apoptosis of SW620 human

colon cancer cells *via* inhibition of the jak/STAT3 signaling pathway (*99*).

Bufotalin, a major compound in toad venom, was demonstrated to sensitize the death receptor-induced apoptosis of HeLa cells by the STAT1-dependent signaling pathway (*100*).

Bufadienolide, a major class of biologically active compounds derived from the traditional Chinese medicine ChanSu, was proved to be a sensitizer of death receptor TRAIL through inhibition of the STAT3/Mcl-1 pathway (101). Arenobufagin, a natural bufadienolide from toad venom, increases apoptosis and autophagy of HepG2 human hepatocellular carcinoma cells by inhibiting the PI3K/Akt/mTOR signaling pathway (*102*).

Cucurbitacin E, a natural compound derived from the climbing stem of *Cucumis melo* L., was previously shown to have antioxidant and antitumor activities. In MDA-MB-231 and 4T1 human breast cancer cells, cucurbitacin E suppresses breast tumor metastasis *via* inhibition of the Src/FAK/Rac1/MMP pathway (*103*). In PC3 and HUVEC cells, cucurbitacin E restrains tumor angiogenesis *via* inhibition of VEGFR2-mediated Jak/STAT3 and MAPK signaling pathways (*104*).

These steroids are able to suppress proliferation or induce apoptosis of cancer cells by signaling pathways as follows: *i*) Met/PI3K/Akt pathway; *ii*) AKT/GSK3β/β-catenin/E-cadherin pathway; *iii*) NF-κB pathway; *iv*) mitochondrial pathway; *v*) STAT3 pathway; *vi*) STAT1 pathway; *vii*) Src/FAK/Rac1/MMP pathway; and *viii*) MAPK pathway. Based on this research, the main effect of steroids is to induce apoptosis of cancer cells.

2.12. *Polysaccharide*

Polysaccharides are polymeric carbohydrate molecules composed of long chains of monosaccharide units bound together by glycosidic linkages and on hydrolysis give the constituent monosaccharides or oligosaccharides. They range in structure from linear to highly branched.

Laminarin, a storage glucan (a polysaccharide of glucose) found in brown algae *Laminaria digitata*, is used in traditional Chinese medicine, and has been shown to have several biological activities, including anticancer activities. In HT-29 human colon cancer cells, it suppresses tumor cell proliferation through the ErbB signaling pathway (*105*). In human colon cancer LOVO cells, laminarin reveals an effect on induction of apoptosis through the mitochondrial signaling pathway (*106*). In another human colon cell line HT-29, laminarin was proved to induce apoptosis of cancer cells by regulating the insulin-like growth fator-IR (IGF-1R) signaling pathway (*107*). In the same cell line LOVO, laminarin was demonstrated by another research group to increase apoptosis of cancer cells by activating the death receptor (DR) signaling pathway(*108*).

Fucoidan is a sulfated polysaccharide found mainly in various species of brown algae and brown seaweed. In human NSCLC cell lines CL1-5 and A549, fucoidan decreases tumor proliferation *via* the TGFR/Smad7/Smurf2 pathway. Meanwhile, fucoidan reduces tumor size in LLC1-xenograft male C57BL/6 mice (*109*). In mouse hepatocarcinoma Hca-F cells, fucoidan can suppress tumor cell growth, adhesion, invasion, and metastasis through the NF-κB pathway and ERK pathway *in vitro* and *in vivo* (*110*). In 4T1 mouse breast cancer cells, fucoidan was proved to inhibit cancer cell growth by blockage of the Wnt/β-catenin signaling pathway *in vitro* and *in vivo* (*111*).

Blazei polysaccharides, polysaccharides extracted from the fungus *Agaricus blazei*, was demonstrated to induce apoptosis of human leukemia HL-60 cells *via* the mitochondrial signaling pathway (*112*). Another polysaccharide from pomegranate peels also induces apoptosis of U-2 human osteosarcoma cells through the mitochondrial signaling pathway (*113*).

These polysaccharides stand up to cancers by targeting the following pathways: *i*) mitochondrial pathway; *ii*) ErbB pathway; *iii*) IGF-1R pathway; *iv*) DR pathway; *v*) TGFR/Smad7/Smurf2 pathway; *vi*) NF-κB pathway; *vii*) ERK pathway; and *viii*) Wnt/β-catenin pathway. The mitochondrial pathway is the main target for polysaccharides.

2.13. *Glycoside*

Glycoside is a molecule in which a sugar is bound to another functional group *via* a glycosidic bond. Glycosides play numerous important roles in living organisms. Many plants store chemicals in the form of inactive glycosides. These can be activated by enzyme hydrolysis, which causes the sugar part to be broken off, making the chemical available for use.

Salidroside (Rhodioloside) is a glucoside of tyrosol found in the plant *Rhodiola rosea*. In TEU-2 human bladder epithelial cells, salidroside inhibits the growth of cancer cells by the blockage of the mTOR pathway (*114*). In the A549 NSCLC cell line, salidroside decreases tumor cell proliferation *via* inhibition of the ROS/p38 signaling pathway (*115*).

Gastrodin, a natural product isolated from *Gastrodia elata* Blume, was demonstrated to repress the growth of H22 murine ascetic hepatoma cells by inhibiting the NF-κB signaling pathway (*116*). Stevioside, a diterpene glycoside found in the leaf of *Stevia rebaudiana*, was reported to induce ROS-mediated apoptosis of MCF-7 cells *via* the mitochondrial pathway (*117*). Fomitoside-K, a biologically active component isolated from a mushroom *Fomitopsis nigra*, also can increase apoptosis of YD-10B human oral squamous cells through the mitochondrial pathway (*118*). In A549 lung cancer cells, oleifolioside B, a cycloartane-

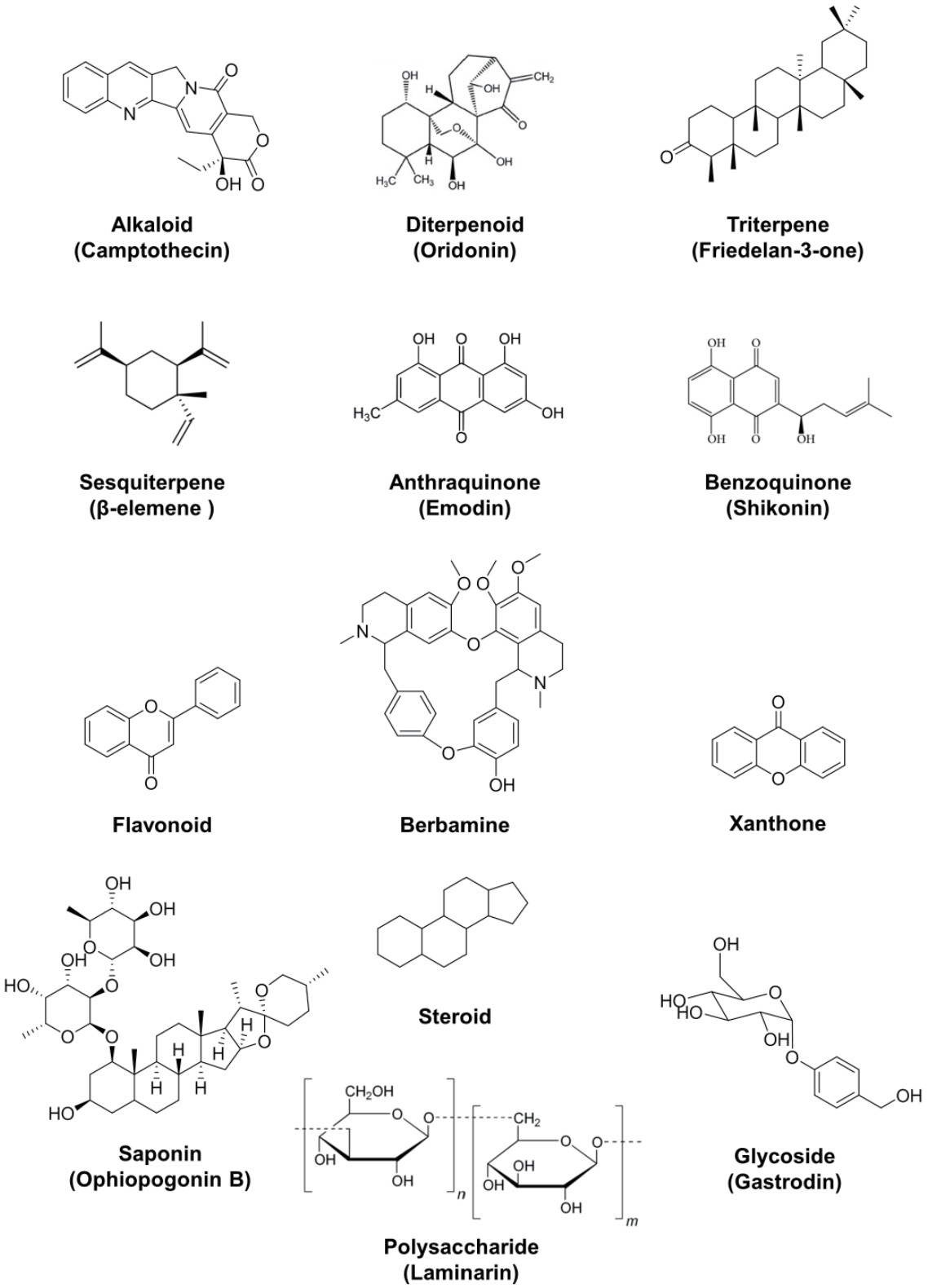

Figure 1. The typical chemical structures of TCM components.

type triterpene glycoside isolated from *Dendropanax morbifera* Leveille, promotes apoptosis through targeting the nuclear factor erythroid 2-related factor 2 (Nrf2) signaling pathway which can antagonize the NF-κB pathway (*119*). Periplocin and icariin which were mentioned above also belong to the glycoside family.

Summarily, these glycosides functions on cancer cells through signaling pathways as follows: *i*) mitochondrial pathway; *ii*) mTOR pathway; *iii*) MAPK pathway; *iv*) ERK pathway; *v*) NF-κB pathway; *vi*) β-catenin pathway; and *vii*) Rac1 pathway. The mitochondrial pathway is more common as a therapeutic target.

2.14. *Planar conformation and cell cycle arrest*

Based on several recent papers, a planar conformation could enhance the potency of the compound to intercalate into free DNA, and subsequently prevent DNA cleavage by DNA topoisomerase I (P1245) (120). For example, camptothecin has a planar pentacyclic ring structure that contains a pyrrolo [3,4-β]-quinoline moiety, conjugated pyridone moiety and one chiral center at position 20 within the alpha-hydroxy lactone ring with (S) configuration. Its planar structure is considered to be one of the most important factors in topoisomerase inhibition (P3,6) (*9*).

Among the TCM components mentioned above, many of them possess a planar conformation: aloe emodin, 2-methyl-1,3,6-trihydroxy-9,10-anthraquinone, shikonin, tanshinone I, 1,3,6,7-tetrahydroxyxanthone, 1,3,5-trihydroxy-13,13- dimethyl-2H-pyran [7,6-b] xanthone, and camptothecin.

3. Conclusion

In recent times, cancers have had the second highest mortality among all diseases. Although chemotherapy is acknowledged as one of the most effective therapeutic methods for cancers, it faces serious side effects and increasing drug resistance. For centuries, traditional Chinese medicine (TCM) was used to treat cardiac disease, diabetes, inflammation, cancer and so on. As the mechanisms of TCM remain poorly understood, more and more studies focus on research of the mechanisms of TCM *in vitro* and *in vivo*. Here, the components isolated from TCM are classified into several groups by their chemical structure (Figure 1) and corresponding cellular

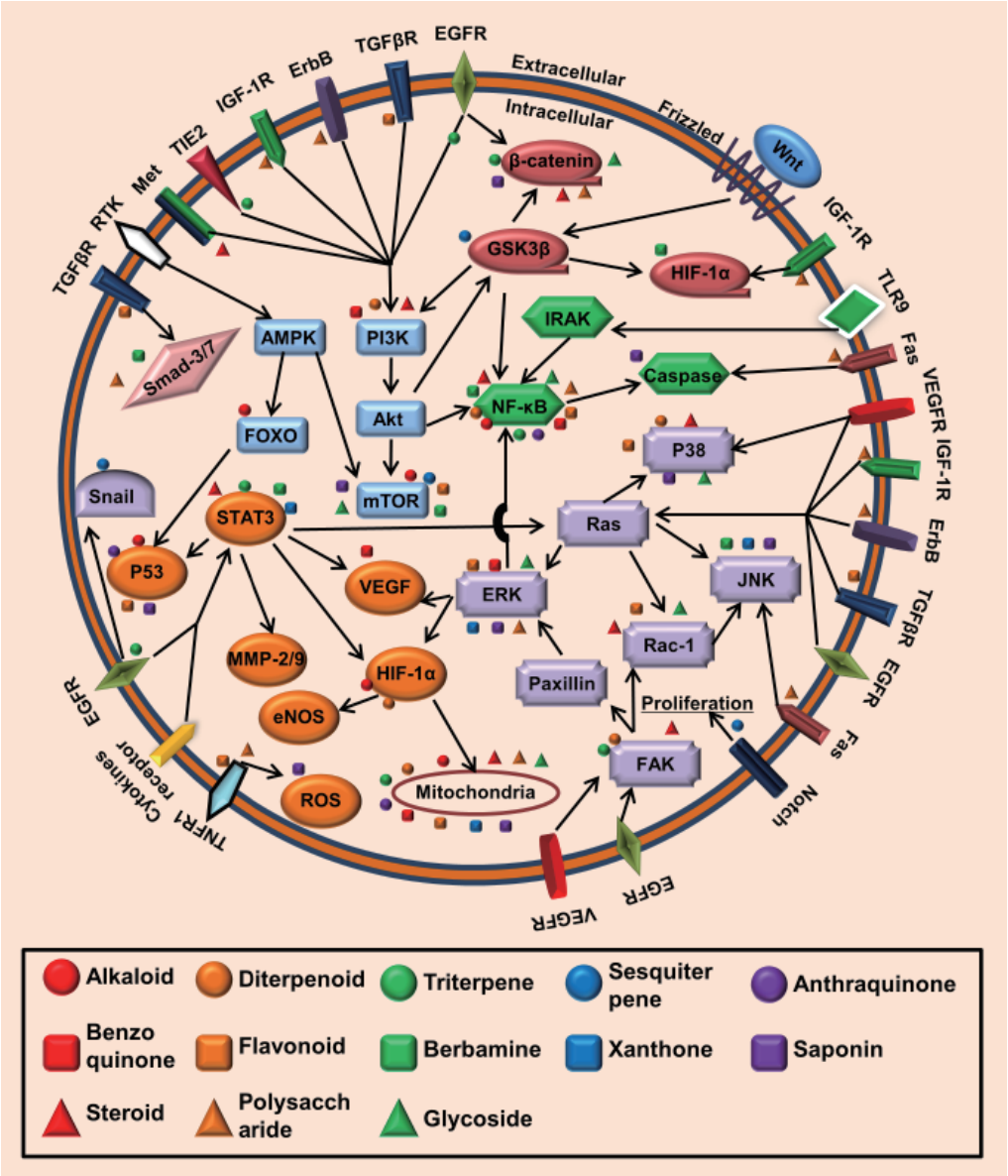

Figure 2. A map of association between TCM components and signaling pathways of cancer cells. In this map, the net of signaling pathways, which were reported to be affected by TCM components, are described and components are put around corresponding elements in the form of particles with various colors and shapes.

signaling pathways are summarized (Figure 2).

Based on the summary above, the veil over some characteristics has been lifted. First, the polysaccharide group mainly targets the cell surface receptors and induces a wider intracellular response, such as the ErbB pathway, IGF-1R pathway, DR pathway, TGF-β pathway, EGFR pathway, and angpt2/tie2 pathway. Second, the mitochondrial pathway and NF-κB pathway are the major targets for almost all of the groups. Targeting these two pathways leads to apoptosis of cancer cells. Meanwhile, apoptosis effects can be induced by other pathways, like the p53 pathway, HIF-1α pathway, ROS pathway, p38 MAPK pathway, FOXO3α pathway, DR pathway and so on. Maybe the combination of these different pathways can avoid drug resistance and make TCM a potential alternative medicine. Third, the mTOR signaling pathway is targeted by half of the component groups to inhibit proliferation, invasion and metastasis of cancer cells. There also are alternative pathways, such as the ERK pathway, β-catenin pathway, FAK pathway, Smad pathway, and so on. Fourth, in several studies, a combination of TCM components and existing chemotherapeutic agents could yield a better antitumor effect, such as vinblastine and nanoliposomal C6-ceramide, androgarpholide and taxifolin, ganoderic acid and cisplatin, β-elemene and cisplatin, shikonin and gemcitabine, quercetin and trichostatin A, and saikosaponin and cisplatin. Fifth, various component groups are oriented towards different pathways. Some of them focus more on apoptosis-related pathways, such as alkaloids, diterpenoids, anthraquinones, berbamines, and xanthones. While some of them concern more proliferation, invasion and metastasis-related pathways, such as triterpenes, sesquiterpenes, polysaccharides, and glycosides. Other components focus on both aspects, such as benzoquinones, flavonoids, saponins, and steroids. The more targets the components can attack, maybe the better antitumor effects they can achieve.

From the information above, it suggests there may be a certain association between some chemical structures and specific signaling pathways. However, there still are some uncertainties. First, although some components share the same core ring structure, various modifications make for different targeting pathways and cellular activity changes. Second, most research groups focus on several major signaling pathways, and association between TCM components and other pathways is short of enough data support. Third, information about chemical structural association between TCM components and targets is in short supply. In spite of this, studies on associations between TCM components and signaling pathways will shed light on future medicine development and administration. In the first place, the research mechanism of components will help identify the mechanisms of TCM. Secondly, associations between TCM components and pathways will provide some clues for target drug development. Third, this will provide a big picture of association between components and pathways for antitumor TCM studies. Finally, this research will provide evidence for combinational therapies using TCM and clinical chemotherapeutic drugs. Based on the advantages above, TCM could be widely used as alternative medicine for cancer therapies.

References

1. Jemal A, Bray F, Center MM, Ferlay J, Ward E, Forman D. Global cancer statistics. CA Cancer J Clin. 2011; 61:69-90.
2. Chou R, Croswell JM, Dana T, Bougatsos C, Blazina I, Fu R, Gleitsmann K, Koenig HC, Lam C, Maltz A, Rugge JB, Lin K. Screening for prostate cancer: a review of the evidence for the U.S. Preventive Services Task Force. Annals of Internal Medicine. 2011; 155:762-771.
3. Kessler DA, Austin RH, Levine H. Resistance to Chemotherapy: Patient Variability and Cellular Heterogeneity. Cancer Res. 2014; 74:4663-4670.
4. Li X, Yang G, Zhang Y, Yang J, Chang J, Sun X, Zhou X, Guo Y, Xu Y, Liu J, Bensoussan A. Traditional Chinese medicine in cancer care: A review of controlled clinical studies published in Chinese. PLoS One. 2013; 8:e60338.
5. Chen X, Hussain S, Parveen S, Zhang S, Yang Y, Zhu C. Sulfonyl group-containing compounds in the design of potential drugs for the treatment of diabetes and its complications. Curr Med Chem. 2012; 19:3578-3604.
6. Heretsch P, Tzagkaroulaki L, Giannis A. Modulators of the hedgehog signaling pathway. Bioorg Med Chem. 2010; 18:6613-6624.
7. Lao Y, Wang X, Xu N, Zhang H, Xu H. Application of proteomics to determine the mechanism of action of traditional Chinese medicine remedies. J Ethnopharmacol. 2014; 155:1-8.
8. Selvarajah J, Nathawat K, Moumen A, Ashcroft M, Carroll VA. Chemotherapy-mediated p53-dependent DNA damage response in clear cell renal cell carcinoma: role of the mTORC1/2 and hypoxia-inducible factor pathways. Cell Death & Disease. 2013; 4:e865.
9. Bertozzi D, Marinello J, Manzo SG, Fornari F, Gramantieri L, Capranico G. The natural inhibitor of DNA topoisomerase I, camptothecin, modulates HIF-1alpha activity by changing miR expression patterns in human cancer cells. Mol Cancer Ther. 2014; 13:239-248.
10. Zhang JW, Zhang SS, Song JR, Sun K, Zong C, Zhao QD, Liu WT, Li R, Wu MC, Wei LX. Autophagy inhibition switches low-dose camptothecin-induced premature senescence to apoptosis in human colorectal cancer cells. Biochem Pharmacol. 2014; 90:265-275.
11. You J, Wan F, de Cui F, Sun Y, Du YZ, Hu FQ. Preparation and characteristic of vinorelbine bitartrate-loaded solid lipid nanoparticles. Int J Pharm. 2007; 343:270-276.
12. Adiseshaiah PP, Clogston JD, McLeland CB, Rodriguez J, Potter TM, Neun BW, Skoczen SL, Shanmugavelandy SS, Kester M, Stern ST, McNeil SE. Synergistic combination therapy with nanoliposomal C6-ceramide and vinblastine is associated with autophagy dysfunction in hepatocarcinoma and colorectal cancer models. Cancer Lett. 2013; 337:254-265.
13. Li W, Hua B, Saud SM, Lin H, Hou W, Matter MS, Jia L, Colburn NH, Young MR. Berberine regulates AMP-activated protein kinase signaling pathways and inhibits

colon tumorigenesis in mice. Mol Carcinog. 2014; [Epub ahead of print]
14. Zheng F, Tang Q, Wu J, Zhao S, Liang Z, Li L, Wu W, Hann S. p38alpha MAPK-mediated induction and interaction of FOXO3a and p53 contribute to the inhibited-growth and induced-apoptosis of human lung adenocarcinoma cells by berberine. J Exp Clin Cancer Res. 2014; 33:36.
15. Zhang Y, Sun S, Chen J, Ren P, Hu Y, Cao Z, Sun H, Ding Y. Oxymatrine induces mitochondria dependent apoptosis in human osteosarcoma MNNG/HOS cells through inhibition of PI3K/Akt pathway. Tumour Biol. 2014; 35:1619-1625.
16. Chen H, Zhang J, Luo J, Lai F, Wang Z, Tong H, Lu D, Bu H, Zhang R, Lin S. Antiangiogenic effects of oxymatrine on pancreatic cancer by inhibition of the NF-kappaB-mediated VEGF signaling pathway. Oncol Rep. 2013; 30:589-595.
17. Jin H, Sun Y, Wang S, Cheng X. Matrine activates PTEN to induce growth inhibition and apoptosis in V600EBRAF harboring melanoma cells. Int J Mol Sci. 2013; 14:16040-16057.
18. Niu H, Zhang Y, Wu B, Jiang H, He P. Matrine induces the apoptosis of lung cancer cells through downregulation of inhibitor of apoptosis proteins and the Akt signaling pathway. Oncol Rep. 2014; 32:1087-1093.
19. Li Y, Zhang ZN, Zhao HM, Tong ZC, Yang J, Wang H, Liang XJ. Matrine inhibits the invasive properties of human osteosarcoma cells by downregulating the ERK-NF-kappaB pathway. Anticancer Drugs. 2014; 25:1035-1043.
20. Yang H, Dou QP. Targeting apoptosis pathway with natural terpenoids: implications for treatment of breast and prostate cancer. Curr Drug Targets. 2010; 11:733-744.
21. Zhang ZR, Al Zaharna M, Wong MM, Chiu SK, Cheung HY. Taxifolin enhances andrographolide-induced mitotic arrest and apoptosis in human prostate cancer cells *via* spindle assembly checkpoint activation. PLoS One. 2013; 8:e54577.
22. Kumar S, Patil HS, Sharma P, Kumar D, Dasari S, Puranik VG, Thulasiram HV, Kundu GC. Andrographolide inhibits osteopontin expression and breast tumor growth through down regulation of PI3 kinase/Akt signaling pathway. Curr Mol Med. 2012; 12:952-966.
23. Lee YC, Lin HH, Hsu CH, Wang CJ, Chiang TA, Chen JH. Inhibitory effects of andrographolide on migration and invasion in human non-small cell lung cancer A549 cells *via* down-regulation of PI3K/Akt signaling pathway. Eur J Pharmacol. 2010; 632:23-32.
24. Lin HH, Tsai CW, Chou FP, Wang CJ, Hsuan SW, Wang CK, Chen JH. Andrographolide down-regulates hypoxia-inducible factor-1alpha in human non-small cell lung cancer A549 cells. Toxicol Appl Pharmacol. 2011; 250:336-345.
25. Zhang QQ, Ding Y, Lei Y, Qi CL, He XD, Lan T, Li JC, Gong P, Yang X, Geng JG, Wang LJ. Andrographolide suppress tumor growth by inhibiting TLR4/NF-kappaB signaling activation in insulinoma. Int J Biol Sci. 2014; 10:404-414.
26. Wong AM, Zhang Y, Kesler K, Deng M, Burhenn L, Wang D, Moro A, Li Z, Heber D. Genomic and *in vivo* evidence of synergy of a herbal extract compared to its most active ingredient: Rabdosia rubescens vs. oridonin. Exp Ther Med. 2010; 1:1013-1017.
27. Bao R, Shu Y, Wu X, *et al*. Oridonin induces apoptosis and cell cycle arrest of gallbladder cancer cells *via* the mitochondrial pathway. BMC Cancer. 2014; 14:217.
28. Wang S, Zhong Z, Wan J, Tan W, Wu G, Chen M, Wang Y. Oridonin induces apoptosis, inhibits migration and invasion on highly-metastatic human breast cancer cells. Am J Chin Med. 2013; 41:177-196.
29. Shen Y, Lu B, Zhang S, Ma ZJ. Diterpenoid C of Radix Curcumae: An inhibitor of proliferation and inducer of apoptosis in human colon adenocarcinoma cells acting *via* inhibiting MAPK signaling pathway. Pharm Biol. 2014; 52:1158-1165.
30. Liu RM, Zhong JJ. Ganoderic acid Mf and S induce mitochondria mediated apoptosis in human cervical carcinoma HeLa cells. Phytomedicine. 2011; 18:349-355.
31. Li F, Wang Y, Wang X, Li J, Cui H, Niu M. Ganoderic acids suppress growth and angiogenesis by modulating the NF-kappaB signaling pathway in breast cancer cells. Int J Clin Pharmacol Ther. 2012; 50:712-721.
32. Yao X, Li G, Xu H, Lu C. Inhibition of the JAK-STAT3 signaling pathway by ganoderic acid A enhances chemosensitivity of HepG2 cells to cisplatin. Planta Medica. 2012; 78:1740-1748.
33. Kim JH, Kim YH, Song GY, Kim DE, Jeong YJ, Liu KH, Chung YH, Oh S. Ursolic acid and its natural derivative corosolic acid suppress the proliferation of APC-mutated colon cancer cells through promotion of beta-catenin degradation. Food Chem Toxicol. 2014; 67:87-95.
34. Saraswati S, Agrawal SS, Alhaider AA. Ursolic acid inhibits tumor angiogenesis and induces apoptosis through mitochondrial-dependent pathway in Ehrlich ascites carcinoma tumor. Chem Biol Interact. 2013; 206:153-165.
35. Gai L, Cai N, Wang L, Xu X, Kong X. Ursolic acid induces apoptosis *via* Akt/NF-kappaB signaling suppression in T24 human bladder cancer cells. Mol Med Rep. 2013; 7:1673-1677.
36. Xavier CP, Lima CF, Pedro DF, Wilson JM, Kristiansen K, Pereira-Wilson C. Ursolic acid induces cell death and modulates autophagy through JNK pathway in apoptosis-resistant colorectal cancer cells. J Nutr Biochem. 2013; 24:706-712.
37. Wu GS, Song YL, Yin ZQ, Guo JJ, Wang SP, Zhao WW, Chen XP, Zhang QW, Lu JJ, Wang YT. Ganoderiol A-enriched extract suppresses migration and adhesion of MDA-MB-231 cells by inhibiting FAK-SRC-paxillin cascade pathway. PLoS One. 2013; 8:e76620.
38. Chung HJ, Park EJ, Pyee Y, Hua Xu G, Lee SH, Kim YS, Lee SK. 25-Methoxyhispidol A, a novel triterpenoid of Poncirus trifoliata, inhibits cell growth *via* the modulation of EGFR/c-Src signaling pathway in MDA-MB-231 human breast cancer cells. Food Chem Toxicol. 2011; 49:2942-2946.
39. He MF, Liu L, Ge W, Shaw PC, Jiang R, Wu LW, But PP. Antiangiogenic activity of Tripterygium wilfordii and its terpenoids. J Ethnopharmacol. 2009; 121: 61-68.
40. Wang CY, Tsai AC, Peng CY, Chang YL, Lee KH, Teng CM, Pan SL. Dehydrocostuslactone suppresses angiogenesis *in vitro* and *in vivo* through inhibition of Akt/GSK-3beta and mTOR signaling pathways. PLoS One. 2012; 7:e31195.
41. Zhang X, Li Y, Zhang Y, Song J, Wang Q, Zheng L, Liu D. Beta-elemene blocks epithelial-mesenchymal transition in human breast cancer cell line MCF-7 through Smad3-mediated down-regulation of nuclear transcription factors. PLoS One. 2013; 8:e58719.
42. Zhang X, Zhang Y, Li Y. beta-elemene decreases cell

invasion by upregulating E-cadherin expression in MCF-7 human breast cancer cells. Oncol Rep. 2013; 30:745-750.
43. Yan B, Zhou Y, Feng S, Lv C, Xiu L, Zhang Y, Shi J, Li Y, Wei P, Qin Z. beta -Elemene-Attenuated Tumor Angiogenesis by Targeting Notch-1 in Gastric Cancer Stem-Like Cells. Evid Based Complement Alternat Med. 2013; 2013:268468.
44. Li QQ, Lee RX, Liang H, Wang G, Li JM, Zhong Y, Reed E. beta-Elemene enhances susceptibility to cisplatin in resistant ovarian carcinoma cells *via* downregulation of ERCC-1 and XIAP and inactivation of JNK. Int J Oncol. 2013; 43:721-728.
45. Sui JQ, Xie KP, Zou W, Xie MJ. Emodin Inhibits Breast Cancer Cell Proliferation through the ERalpha-MAPK/Akt-Cyclin D1/Bcl-2 Signaling Pathway. Asian Pac J Cancer Prev. 2014; 15:6247-6251.
46. Yaoxian W, Hui Y, Yunyan Z, Yanqin L, Xin G, Xiaoke W. Emodin induces apoptosis of human cervical cancer hela cells *via* intrinsic mitochondrial and extrinsic death receptor pathway. Cancer Cell Int. 2013; 13:71.
47. Yu JQ, Bao W, Lei JC. Emodin regulates apoptotic pathway in human liver cancer cells. Phytother Res. 2013; 27:251-257.
48. Ismail S, Haris K, Abdul Ghani AR, Abdullah JM, Johan MF, Mohamed Yusoff AA. Enhanced induction of cell cycle arrest and apoptosis *via* the mitochondrial membrane potential disruption in human U87 malignant glioma cells by aloe emodin. J Asian Nat Prod Res. 2013; 15:1003-1012.
49. Lin ML, Lu YC, Chung JG, Wang SG, Lin HT, Kang SE, Tang CH, Ko JL, Chen SS. Down-regulation of MMP-2 through the p38 MAPK-NF-kappaB-dependent pathway by aloe-emodin leads to inhibition of nasopharyngeal carcinoma cell invasion. Mol Carcinog. 2010; 49:783-797.
50. Zeng GZ, Fan JT, Xu JJ, Li Y, Tan NH. Apoptosis induction and G2/M arrest of 2-methyl-1,3,6-trihydroxy-9,10-anthraquinone from Rubia yunnanensis in human cervical cancer Hela cells. Pharmazie. 2013; 68:293-299.
51. Shi S, Cao H. Shikonin promotes autophagy in BXPC-3 human pancreatic cancer cells through the PI3K/Akt signaling pathway. Oncol Lett. 2014; 8:1087-1089.
52. Wang Y, Zhou Y, Jia G, Han B, Liu J, Teng Y, Lv J, Song Z, Li Y, Ji L, Pan S, Jiang H, Sun B. Shikonin suppresses tumor growth and synergizes with gemcitabine in a pancreatic cancer xenograft model: Involvement of NF-kappaB signaling pathway. Biochem Pharmacol. 2014; 88:322-333.
53. Kim SJ, Kim JM, Shim SH, Chang HI. Shikonin induces cell cycle arrest in human gastric cancer (AGS) by early growth response 1 (Egr1)-mediated p21 gene expression. J Ethnopharmacol. 2014; 151:1064-1071.
54. Wang H, Wu C, Wan S, Zhang H, Zhou S, Liu G. Shikonin attenuates lung cancer cell adhesion to extracellular matrix and metastasis by inhibiting integrin beta1 expression and the ERK1/2 signaling pathway. Toxicology. 2013; 308:104-112.
55. Liu C, Yin L, Chen J. The apoptotic effect of shikonin on human papillary thyroid carcinoma cells through mitochondrial pathway. Tumour Biol. 2014; 35:1791-1798.
56. Tung YT, Chen HL, Lee CY, Chou YC, Lee PY, Tsai HC, Lin YL, Chen CM. Active Component of Danshen (Salvia miltiorrhiza Bunge), Tanshinone I, Attenuates Lung Tumorigenesis *via* Inhibitions of VEGF, Cyclin A, and Cyclin B Expressions. Evid Based Complement Alternat Med. 2013; 2013:319247.
57. Gong Y, Li Y, Lu Y, Li L, Abdolmaleky H, Blackburn GL, Zhou JR. Bioactive tanshinones in Salvia miltiorrhiza inhibit the growth of prostate cancer cells *in vitro* and in mice. Int J Cancer. 2011; 129:1042-1052.
58. Lee CY, Sher HF, Chen HW, Liu CC, Chen CH, Lin CS, Yang PC, Tsay HS, Chen JJ. Anticancer effects of tanshinone I in human non-small cell lung cancer. Mol Cancer Ther. 2008; 7:3527-3538.
59. Chen F, Zhuang M, Peng J, Wang X, Huang T, Li S, Lin M, Lin H, Xu Y, Li J, Chen Z, Huang Y. Baicalein inhibits migration and invasion of gastric cancer cells through suppression of the TGFbeta signaling pathway. Mol Med Rep. 2014; [Epub ahead of print]
60. Aryal P, Kim K, Park PH, Ham S, Cho J, Song K. Baicalein induces autophagic cell death through AMPK/ULK1 activation and downregulation of mTORC1 complex components in human cancer cells. Febs Journal. 2014; [Epub ahead of print]
61. Li HL, Zhang S, Wang Y, Liang RR, Li J, An P, Wang ZM, Yang J, Li ZF. Baicalein induces apoptosis *via* a mitochondrial-dependent caspase activation pathway in T24 bladder cancer cells. Mol Med Rep. 2013; 7:266-270.
62. Wang N, Ren D, Deng S, Yang X. Differential effects of baicalein and its sulfated derivatives in inhibiting proliferation of human breast cancer MCF-7 cells. Chem Biol Interact. 2014; 221C:99-108.
63. Zhang Z, Lv J, Lei X, Li S, Zhang Y, Meng L, Xue R, Li Z. Baicalein reduces the invasion of glioma cells *via* reducing the activity of p38 signaling pathway. PLoS One. 2014; 9:e90318.
64. Chen K, Zhang S, Ji Y, Li J, An P, Ren H, Liang R, Yang J, Li Z. Baicalein inhibits the invasion and metastatic capabilities of hepatocellular carcinoma cells *via* down-regulation of the ERK pathway. PLoS One. 2013; 8:e72927.
65. Kim MC, Lee HJ, Lim B, Ha KT, Kim SY, So I, Kim BJ. Quercetin induces apoptosis by inhibiting MAPKs and TRPM7 channels in AGS cells. Int J Mol Med. 2014; 33:1657-1663.
66. Chan ST, Yang NC, Huang CS, Liao JW, Yeh SL. Quercetin enhances the antitumor activity of trichostatin A through upregulation of p53 protein expression *in vitro* and *in vivo*. PLoS One. 2013; 8:e54255.
67. Pratheeshkumar P, Budhraja A, Son YO, Wang X, Zhang Z, Ding S, Wang L, Hitron A, Lee JC, Xu M, Chen G, Luo J, Shi X. Quercetin inhibits angiogenesis mediated human prostate tumor growth by targeting VEGFR- 2 regulated AKT/mTOR/P70S6K signaling pathways. PLoS One. 2012; 7:e47516.
68. Liu KC, Yen CY, Wu RS, Yang JS, Lu HF, Lu KW, Lo C, Chen HY, Tang NY, Wu CC, Chung JG. The roles of endoplasmic reticulum stress and mitochondrial apoptotic signaling pathway in quercetin-mediated cell death of human prostate cancer PC-3 cells. Environ Toxicol. 2014; 29:428-439.
69. Wu J, Zuo F, Du J, Wong PF, Qin H, Xu J. Icariside II induces apoptosis *via* inhibition of the EGFR pathways in A431 human epidermoid carcinoma cells. Mol Med Rep. 2013; 8:597-602.
70. Ma HR, Wang J, Chen YF, Chen H, Wang WS, Aisa HA. Icariin and icaritin stimulate the proliferation of SKBr3 cells through the GPER1-mediated modulation of the EGFR-MAPK signaling pathway. Int J Mol Med. 2014; 33:1627-1634.

71. Wang Y, Dong H, Zhu M, Ou Y, Zhang J, Luo H, Luo R, Wu J, Mao M, Liu X, Wei L. Icariin exterts negative effects on human gastric cancer cell invasion and migration by vasodilator-stimulated phosphoprotein *via* Rac1 pathway. Eur J Pharmacol. 2010; 635:40-48.
72. Lee HS, Cho HJ, Yu R, Lee KW, Chun HS, Park JH. Mechanisms underlying apoptosis-inducing effects of Kaempferol in HT-29 human colon cancer cells. Int J Mol Sci. 2014; 15:2722-2737.
73. Dang Q, Song W, Xu D, Ma Y, Li F, Zeng J, Zhu G, Wang X, Chang LS, He D, Li L. Kaempferol suppresses bladder cancer tumor growth by inhibiting cell proliferation and inducing apoptosis. Mol Carcinog. 2014; [Epub ahead of print]
74. Luo H, Rankin GO, Juliano N, Jiang BH, Chen YC. Kaempferol inhibits VEGF expression and *in vitro* angiogenesis through a novel ERK-NFkappaB-cMyc-p21 pathway. Food Chem. 2012; 130:321-328.
75. Jin X, Wu Y. Berbamine enhances the antineoplastic activity of gemcitabine in pancreatic cancer cells by activating transforming growth factor-beta/Smad signaling. Anat Rec (Hoboken). 2014; 297:802-809.
76. Nam S, Xie J, Perkins A, Ma Y, Yang F, Wu J, Wang Y, Xu RZ, Huang W, Horne DA, Jove R. Novel synthetic derivatives of the natural product berbamine inhibit Jak2/Stat3 signaling and induce apoptosis of human melanoma cells. Mol Oncol. 2012; 6:484-493.
77. Yang F, Nam S, Brown CE, Zhao R, Starr R, Ma Y, Xie J, Horne DA, Malkas LH, Jove R, Hickey RJ. A novel berbamine derivative inhibits cell viability and induces apoptosis in cancer stem-like cells of human glioblastoma, *via* up-regulation of miRNA-4284 and JNK/AP-1 signaling. PLoS One. 2014; 9:e94443.
78. Du HP, Shen JK, Yang M, Wang YQ, Yuan XQ, Ma QL, Jin J. 4-Chlorobenzoyl berbamine induces apoptosis and G2/M cell cycle arrest through the PI3K/Akt and NF-kappaB signal pathway in lymphoma cells. Oncol Rep. 2010; 23:709-716.
79. Yang Z, Li C, Wang X, Zhai C, Yi Z, Wang L, Liu B, Du B, Wu H, Guo X, Liu M, Li D, Luo J. Dauricine induces apoptosis, inhibits proliferation and invasion through inhibiting NF-kappaB signaling pathway in colon cancer cells. J Cell Physiol. 2010; 225:266-275.
80. Tang XD, Zhou X, Zhou KY. Dauricine inhibits insulin-like growth factor-I-induced hypoxia inducible factor 1alpha protein accumulation and vascular endothelial growth factor expression in human breast cancer cells. Acta Pharmacol Sin. 2009; 30:605-616.
81. Fu WM, Wang WM, Wang H, Zhu X, Liang Y, Kung HF, Zhang JF. 1,3,5-Trihydroxy-13,13-dimethyl-2H-pyran [7,6-b] xanthone directly targets heat shock protein 27 in hepatocellular carcinoma. Cell Biol Int. 2014; 38:272-276.
82. Fu WM, Zhang JF, Wang H, Xi ZC, Wang WM, Zhuang P, Zhu X, Chen SC, Chan TM, Leung KS, Lu G, Xu HX, Kung HF. Heat shock protein 27 mediates the effect of 1,3,5-trihydroxy-13,13-dimethyl-2H-pyran [7,6-b] xanthone on mitochondrial apoptosis in hepatocellular carcinoma. J Proteomics. 2012; 75:4833-4843.
83. Shan T, Cui XJ, Li W, Lin WR, Lu HW, Li YM, Chen X, Wu T. alpha-Mangostin suppresses human gastric adenocarcinoma cells *in vitro via* blockade of Stat3 signaling pathway. Acta Pharmacol Sin. 2014; 35:1065-1073.
84. Hsieh SC, Huang MH, Cheng CW, Hung JH, Yang SF, Hsieh YH. alpha-Mangostin induces mitochondrial dependent apoptosis in human hepatoma SK-Hep-1 cells through inhibition of p38 MAPK pathway. Apoptosis. 2013; 18:1548-1560.
85. Yuan J, Wu Y, Lu G. alpha-Mangostin suppresses lipopolysaccharide-induced invasion by inhibiting matrix metalloproteinase-2/9 and increasing E-cadherin expression through extracellular signal-regulated kinase signaling in pancreatic cancer cells. Oncol Lett. 2013; 5:1958-1964.
86. Hung SH, Shen KH, Wu CH, Liu CL, Shih YW. Alpha-mangostin suppresses PC-3 human prostate carcinoma cell metastasis by inhibiting matrix metalloproteinase-2/9 and urokinase-plasminogen expression through the JNK signaling pathway. J Agric Food Chem. 2009; 57:1291-1298.
87. Wang Y, He QY, Chiu JF. Dioscin induced activation of p38 MAPK and JNK *via* mitochondrial pathway in HL-60 cell line. Eur J Pharmacol. 2014; 735: 52-58.
88. Kim EA, Jang JH, Lee YH, Sung EG, Song IH, Kim JY, Kim S, Sohn HY, Lee TJ. Dioscin induces caspase-independent apoptosis through activation of apoptosis-inducing factor in breast cancer cells. Apoptosis. 2014; 19:1165-1175.
89. Xu QJ, Hou LL, Hu GQ, Xie SQ. [Molecular mechanism of ophiopogonin B induced cellular autophagy of human cervical cancer HeLa cells]. Yao Xue Xue Bao. 2013; 48:855-859.
90. Chen M, Du Y, Qui M, *et al*. Ophiopogonin B-induced autophagy in non-small cell lung cancer cells *via* inhibition of the PI3K/Akt signaling pathway. Oncol Rep. 2013; 29:430-436.
91. Wang Q, Zheng XL, Yang L, Shi F, Gao LB, Zhong YJ, Sun H, He F, Lin Y, Wang X. Reactive oxygen species-mediated apoptosis contributes to chemosensitization effect of saikosaponins on cisplatin-induced cytotoxicity in cancer cells. J Exp Clin Cancer Res. 2010; 29:159.
92. Chen JC, Chang NW, Chung JG, Chen KC. Saikosaponin-A induces apoptotic mechanism in human breast MDA-MB-231 and MCF-7 cancer cells. Am J Chin Med. 2003; 31:363-377.
93. Zhao L, Shan B, Du Y, Wang M, Liu L, Ren FZ. Periplocin from Cortex periplocae inhibits cell growth and down-regulates survivin and c-myc expression in colon cancer *in vitro* and *in vivo via* beta-catenin/TCF signaling. Oncol Rep. 2010; 24:375-383.
94. Lu ZJ, Zhou Y, Song Q, Qin Z, Zhang H, Zhou YJ, Gou LT, Yang JL, Luo F. Periplocin inhibits growth of lung cancer *in vitro* and *in vivo* by blocking AKT/ERK signaling pathways. Cell Physiol Biochem. 2010; 26:609-618.
95. Gu L, Feng J, Xu H, Luo M, Su D. Polyphyllin I inhibits proliferation and metastasis of ovarian cancer cell line HO-8910PM *in vitro*. J Tradit Chin Med. 2013; 33:325-333.
96. Kang XH, Xu ZY, Gong YB, Wang LF, Wang ZQ, Xu L, Cao F, Liao MJ. Bufalin Reverses HGF-Induced Resistance to EGFR-TKIs in EGFR Mutant Lung Cancer Cells *via* Blockage of Met/PI3k/Akt Pathway and Induction of Apoptosis. Evid Based Complement Alternat Med. 2013; 2013:243859.
97. Qiu DZ, Zhang ZJ, Wu WZ, Yang YK. Bufalin, a component in Chansu, inhibits proliferation and invasion of hepatocellular carcinoma cells. BMC Complement Altern Med. 2013; 13:185.
98. Yin PH, Liu X, Qiu YY, Cai JF, Qin JM, Zhu HR, Li Q.

Anti-tumor activity and apoptosis-regulation mechanisms of bufalin in various cancers: new hope for cancer patients. Asian Pac J Cancer Prev. 2012; 13:5339-5343.
99. Zhu Z, Li E, Liu Y, Gao Y, Sun H, Ma G, Wang Z, Liu X, Wang Q, Qu X, Yu Y. Inhibition of Jak-STAT3 pathway enhances bufalin-induced apoptosis in colon cancer SW620 cells. World J Surg Oncol. 2012; 10:228.
100. Waiwut P, Inujima A, Inoue H, Saiki I, Sakurai H. Bufotalin sensitizes death receptor-induced apoptosis *via* Bid- and STAT1-dependent pathways. Int J Oncol. 2012; 40:203-208.
101. Dong Y, Yin S, Li J, Jiang C, Ye M, Hu H. Bufadienolide compounds sensitize human breast cancer cells to TRAIL-induced apoptosis *via* inhibition of STAT3/Mcl-1 pathway. Apoptosis. 2011; 16:394-403.
102. Zhang DM, Liu JS, Deng LJ, Chen MF, Yiu A, Cao HH, Tian HY, Fung KP, Kurihara H, Pan JX, Ye WC. Arenobufagin, a natural bufadienolide from toad venom, induces apoptosis and autophagy in human hepatocellular carcinoma cells through inhibition of PI3K/Akt/mTOR pathway. Carcinogenesis. 2013; 34:1331-1342.
103. Zhang T, Li J, Dong Y, Zhai D, Lai L, Dai F, Deng H, Chen Y, Liu M, Yi Z. Cucurbitacin E inhibits breast tumor metastasis by suppressing cell migration and invasion. Breast Cancer Res Treat. 2012; 135:445-458.
104. Dong Y, Lu B, Zhang X, Zhang J, Lai L, Li D, Wu Y, Song Y, Luo J, Pang X, Yi Z, Liu M. Cucurbitacin E, a tetracyclic triterpenes compound from Chinese medicine, inhibits tumor angiogenesis through VEGFR2-mediated Jak2-STAT3 signaling pathway. Carcinogenesis. 2010; 31:2097-2104.
105. Park HK, Kim IH, Kim J, Nam TJ. Induction of apoptosis and the regulation of ErbB signaling by laminarin in HT-29 human colon cancer cells. Int J Mol Med. 2013; 32:291-295.
106. Ji YB, Ji CF, Zhang H. Laminarin induces apoptosis of human colon cancer LOVO cells through a mitochondrial pathway. Molecules. 2012; 17:9947-9960.
107. Park HK, Kim IH, Kim J, Nam TJ. Induction of apoptosis by laminarin, regulating the insulin-like growth factor-IR signaling pathways in HT-29 human colon cells. Int J Mol Med. 2012; 30:734-738.
108. Ji CF, Ji YB. Laminarin-induced apoptosis in human colon cancer LoVo cells. Oncol Lett. 2014; 7:1728-1732.
109. Hsu HY, Lin TY, Wu YC, Tsao SM, Hwang PA, Shih YW, Hsu J. Fucoidan inhibition of lung cancer *in vivo* and *in vitro* : Role of the Smurf2-dependent ubiquitin proteasome pathway in TGFbeta receptor degradation. Oncotarget. 2014; [Epub ahead of print]
110. Wang P, Liu Z, Liu X, Teng H, Zhang C, Hou L, Zou X. Anti-Metastasis Effect of Fucoidan from Undaria pinnatifida Sporophylls in Mouse Hepatocarcinoma Hca-F Cells. PLoS One. 2014; 9:e106071.
111. Xue M, Ge Y, Zhang J, Liu Y, Wang Q, Hou L, Zheng Z. Fucoidan inhibited 4T1 mouse breast cancer cell growth *in vivo* and *in vitro via* downregulation of Wnt/beta-catenin signaling. Nutr Cancer. 2013; 65:460-468.
112. Li X, Zhao X, Wang H, Han J, Liu L. A polysaccharide from the fruiting bodies of Agaricus blazei Murill induces caspase-dependent apoptosis in human leukemia HL-60 cells. Tumour Biol. 2014; [Epub ahead of print]
113. Li J, Zhang F, Wang S. A polysaccharide from pomegranate peels induces the apoptosis of human osteosarcoma cells *via* the mitochondrial apoptotic pathway. Tumour Biol. 2014; 35:7475-7482.
114. Liu Z, Li X, Simoneau AR, Jafari M, Zi X. Rhodiola rosea extracts and salidroside decrease the growth of bladder cancer cell lines *via* inhibition of the mTOR pathway and induction of autophagy. Mol Carcinog. 2012; 51:257-267.
115. Wang J, Li JZ, Lu AX, Zhang KF, Li BJ. Anticancer effect of salidroside on A549 lung cancer cells through inhibition of oxidative stress and phospho-p38 expression. Oncol Lett. 2014; 7:1159-1164.
116. Shu G, Yang T, Wang C, Su H, Xiang M. Gastrodin stimulates anticancer immune response and represses transplanted H22 hepatic ascitic tumor cell growth: Involvement of NF-kappaB signaling activation in CD4+ T cells. Toxicol Appl Pharmacol. 2013; 269:270-279.
117. Paul S, Sengupta S, Bandyopadhyay TK, Bhattacharyya A. Stevioside induced ROS-mediated apoptosis through mitochondrial pathway in human breast cancer cell line MCF-7. Nutr Cancer. 2012; 64:1087-1094.
118. Bhattarai G, Lee YH, Lee NH, Lee IK, Yun BS, Hwang PH, Yi HK. Fomitoside-K from Fomitopsis nigra induces apoptosis of human oral squamous cell carcinomas (YD-10B) *via* mitochondrial signaling pathway. Biol Pharm Bull. 2012; 35:1711-1719.
119. Jin CY, Yu HY, Park C, *et al*. Oleifolioside B-mediated autophagy promotes apoptosis in A549 human non-small cell lung cancer cells. Int J Oncol. 2013; 43:1943-1950.
120. Woo SH, Sun NJ, Cassady JM, Snapka RM. Topoisomerase II inhibition by aporphine alkaloids. Biochem Pharmacol. 1999; 57:1141-1145.

(Received June 25, 2014; Revised July 29, 2014; Accepted August 5, 2014)

Review

DOI: 10.5582/ddt.2014.01031

Advances in the study of molecularly targeted agents to treat hepatocellular carcinoma

Jialu Chen[1], Jianjun Gao[2,3,*]

[1] *Department of Chemistry, Fudan University, Shanghai, China;*
[2] *Department of Surgery, Graduate School of Medicine, The University of Tokyo, Tokyo, Japan;*
[3] *Department of Pharmacology, School of Pharmaceutical Sciences, Qingdao University, Qingdao, Shandong, China.*

Summary **Hepatocellular carcinoma (HCC) is a severe form of liver cancer that is found worldwide. Treatments such as liver transplantation and surgical resection and local-regional therapies such as transarterial chemoembolization have progressed considerably and play a prominent role in HCC management. After those treatments, though, systematic drug intervention is required to deal with tumor metastasis in its early stages and the high frequency of tumor recurrence and/or metastasis. The approval of sorafenib, an agent that targets receptor tyrosine kinases (RTKs), as the first effective drug for systemic treatment of HCC represents a milestone in the treatment of this disease. In addition to sorafenib, a number of agents that target various RTKs or intracellular signal transduction molecules, such as mTOR, are currently being investigated as monotherapy or combination therapy for HCC. This article reviews advances in the study of molecularly targeted agents to treat HCC.**

Keywords: Hepatocellular carcinoma, molecularly targeted agents; VEGFR, EGFR, c-MET

1. Introduction

Hepatocellular carcinoma (HCC) is the fifth most common cancer in men, the seventh most common cancer in women, and the third most common cause of cancer deaths worldwide. HCC resulted in 696,000 deaths worldwide in 2008 (*1*). The condition has distinct geographical variation, with the vast majority of cases (85%) occurring in countries in East Asia and sub-Saharan Africa and lower incidence rates in Australia, Northern Europe, and the US (*2*). The pathogenesis of HCC is complex and not completely understood. Hepatocarcinogenesis is a multistep process involving inflammation, hyperplasia, and dysplasia that finally leads to malignant transformation. The specific sequence of genetic events that mediate these steps is only partially known (*3*). Chronic hepatitis B (HBV) infection and chronic hepatitis C (HCV) infection play a key role in the onset and development of HCC; HBV is responsible for approximately half of the cases of HCC. HBV is responsible for the majority of cases in China and Africa while HCV is the major cause of HCC in Japan, the US, and parts of Europe. Other risk factors include toxins (aflatoxin B1 and alcohol), metabolic diseases (non-alcoholic fatty liver disease and diabetes), hereditary diseases (hemochromatosis), and immune-related diseases (autoimmune hepatitis and primary biliary cirrhosis) (*4,5*). In addition, cirrhosis is present in 67% to 80% of patients with HCC, making HCC a highly complicated disease (*6,7*).

Treatments for HCC include resection, liver transplantation, percutaneous ethanol injection (PEI), radiofrequency ablation (RF), transcatheter arterial chemoembolization (TACE), and sorafenib depending on the Barcelona Clinic Liver Cancer (BCLC) stage of HCC (*8*). However, the asymptomatic nature of early disease and the limited use of surveillance result in the disease often being diagnosed in its advanced stages in which systemic drug intervention is required. To date, sorafenib (a small-molecule kinase inhibitor) is the only standard drug therapy for patients with advanced HCC, with modest effectiveness at prolonging patients' overall

**Address correspondence to:*
Dr. Jianjun Gao, Department of Surgery, Graduate School of Medicine, The University of Tokyo, 7-3-1 Hongo, Bunkyo-ku, Tokyo, Japan.
E-mail: gao-tky@umin.ac.jp

survival (OS) for around 2-3 months (*9*). However, the mechanism by which sorafenib treats advanced HCC is not well known, and no biomarkers have been identified to predict the effectiveness of sorafenib in patients with HCC. In addition, the tolerance and resistance to sorafenib in some patients with HCC further limit the clinical efficacy of sorafenib.

Given the modest efficacy of sorafenib, there is still a need for a treatment of advanced HCC. The efficacy of systemic chemotherapy therapies is limited in patients with HCC because of their cirrhotic liver, potentially poor hepatic reserve, and the chemoresistance of the tumor (*10*). Recently, molecularly targeted drugs to treat HCC have been extensively studied. Multiple molecular pathways implicated in HCC pathogenesis, including vascular endothelial growth factor receptor (VEGFR), fibroblast growth factor receptor (FGFR), platelet-derived growth factor receptor (PDGFR), epidermal growth factor receptor (EGFR), mesenchymal-epithelial transition factor (c-MET), and the mammalian target of rapamycin (mTOR) pathways, may act as potential targets for therapeutic interventions (Figure 1) (*11*).

This review describes the study of current kinase inhibitors besides sorafenib and their combination with other agents to treat HCC, and preclinical data and clinical data are presented (Table 1, Table S1 and S2) (*http://www.ddtjournal.com/docindex.php?year=2014&kanno=4*). A retrospective analysis of these studies could provide a clearer understanding of the study of kinase inhibitors in HCC and facilitate further progress in the study of new kinase inhibitors.

2. Antiangiogenic agents

HCC is a highly vascularized tumor. VEGF is an angiogenic growth factor and its elevated expression is found in surgical specimens of HCC compared to non-tumoral liver tissue (*12*). Thus, one approach to treatment of HCC is to target angiogenic factors, such as VEGF, PDGFR, and FGFR. Sorafenib has already been approved, but many VEGFR TKIs are also being investigated, such as sunitinib, linifanib, and brivanib. Three multikinase inhibitors (sunitinib, brivanib, and linifanib) have been studied as first-line therapies in comparison to sorafenib, but all failed to achieve their primary endpoints.

2.1. *Sorafenib*

Sorafenib is an oral multi-kinase inhibitor that blocks multiple growth factor pathways including VEGFR-1, -2, -3, PDGFR-β, Raf, RET, and FLT-3 (*13,14*). To date, sorafenib is the only drug approved for the treatment of unresectable HCC, based on the results of the SHARP trial and a parallel phase III trial in the Asia-Pacific region. In the SHARP trial, sorafenib significantly prolonged the median OS of patients with advanced

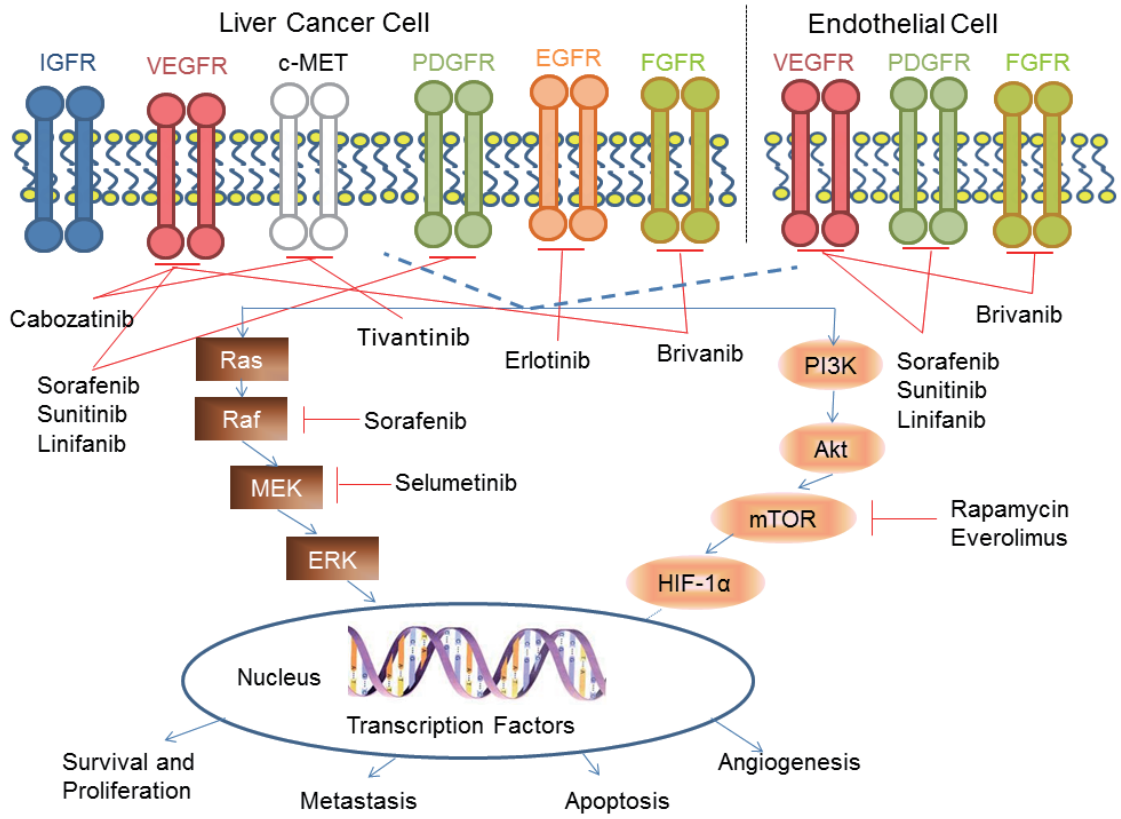

Figure 1. Signal transduction pathways implicated in HCC pathology and molecularly targeted agents that are currently being investigated.

Table 1. The current status of clinical studies of small molecule inhibitors

Agents	Targets	I Ongoing	I Completed	I Terminated	I withdrawan	II Ongoing	II Completed	II Terminated	II unknown	II suspended	III Ongoing	III Completed	III Terminated	III unknown
Sunitinib	VEGFR, PDGFR, c-KIT				1	1*	3	3					1	
Axitinib	VEGFR, PDGFR				1	4								
Dovitinib	VEGFR, PDGFR					1								
Linifanib	VEGFR, PDGFR						1						1	
Brivanib	VEGFR, FGFR		2				1				1	2	1	
Cediranib	VEGFR						1	1						
Pazopanib	VEGFR, PDGFR, c-Kit		2											
Lenalidomide	VEGF	1				1								
Orantinib	VEGFR-2, PDGFR, FGFR		1				1				1			
Cabozantinib	MET, VEGFR2, KIT							1			1			
Tivantinib	c-MET	1	1				1				2			
Foretinib	c-MET, VEGFR-2	1												
Erlotinib	EGFR	1	1			2	4	2			1			
Gefitinib	EGFR						1		1					
Everolimus	mTOR			1		5	1				1	1		
Rapamycin	mTOR	1	1			1								1
Temsirolimus	mTOR	1				1		1	1					
Refametinib	MEK					2								
Selumetinib	MEK						1							

*, Continuation Study

(Table 1. Continued)

Agents	Targets	II/III unknown	II/III completed	I/II ongoing	I/II completed	I/II terminated	I/II withdrawan	I/II unknown	IV ongoing
Sunitinib	VEGFR, PDGFR, c-KIT	1							
Axitinib	VEGFR, PDGFR								
Dovitinib	VEGFR, PDGFR								
Linifanib	VEGFR, PDGFR								
Brivanib	VEGFR, FGFR								
Cediranib	VEGFR								
Pazopanib	VEGFR, PDGFR, c-Kit								
Lenalidomide	VEGF								
Orantinib	VEGFR-2, PDGFR, FGFR				1				
Cabozantinib	MET, VEGFR2, KIT								
Tivantinib	c-MET								
Foretinib	c-MET, VEGFR-2								
Erlotinib	EGFR					1	1		
Gefitinib	EGFR								
Everolimus	mTOR			1	1	1			1
Rapamycin	mTOR		1						
Temsirolimus	mTOR			1				1	
Refametinib	MEK								
Selumetinib	MEK			1					

HCC from 7.9 months to 10.7 months ($p < 0.001$) and the median time to progression (TTP) from 2.8 months to 5.5 months ($p < 0.001$) (*9*). In the Asia-Pacific trial, the median OS and TTP were prolonged from 4.2 months to 6.5 months ($p = 0.014$) and from 1.4 months to 2.8 months ($p = 0.0005$), respectively. In both trials, the median OS of patients with advanced HCC was prolonged, but the shorter median OS in the Asia-Pacific trial may be due to differences in the state of the liver of patients in varied regions. In the Asia-Pacific trial, 73.0% of patients had baseline HBV infection compared to 12.0% in the SHARP study, whereas 8.4% of patients in the Asia-Pacific trial had baseline HCV infection compared to 30% in the SHARP trial (*15*).

However, the mechanism of sorafenib is still unclear and no biomarker has been identified to predict suitable patients for sorafenib treatment or the prognosis of those patients.

2.2. *Sunitinib*

Sunitinib is a multi-targeted receptor tyrosine kinase inhibitor of VEGFR, PDGFR, and c-KIT that was already approved for the treatment of renal cell carcinoma (RCC) and imatinib-resistant gastrointestinal stromal tumors (GIST) (*16,17*). In comparison to sorafenib, sunitinib has no activity against Raf but is about 10 times more active against most receptor tyrosine kinases present on the cell surface (including VEGFRs and PDGFR-β) (*18*). In two phase II studies of sunitinib in patients with advanced HCC, patients received 50 mg/d of sunitinib orally, 4 weeks on and 2 weeks off (*19,20*). Both studies found that sunitinib had a high toxicity, with treatment-related deaths occurring in 10% of patients (4, $n = 37$) in one study and grade 3/4 adverse effects (AEs) occurring in 80% of patients in the other study. The fact that sunitinib targets many different receptors may explain the high incidence of severe adverse events (SAEs) such as the classic hand-foot syndrome, stomatitis, and other dermatologic toxicities. In addition, a phase II study with continuous sunitinib treatment (37.5 mg daily) yielded promising results, with a progression-free survival at 12 weeks (PFS-12) of 33.3% (*21*). However, a phase III study of sunitinib malate versus sorafenib in patients with advanced HCC (patients were given 37.5 mg of sunitinib orally once a day or 400 mg of sorafenib twice a day) was terminated in 2010 because of a higher incidence of SAEs in the sunitinib arm and the fact that sunitinib did not prove to be either superior or non-inferior to sorafenib in terms of the OS of patients with advanced HCC (*22*). Due to the failure of the phase III trial, sunitinib is not considered as a therapeutic option for HCC anymore. Nevertheless, it may have anti-angiogenic and anti-fibrotic properties that may occasion its reuse at a lower dose to treat cirrhosis or advanced fibrosis (*23*).

2.3. *Brivanib*

Brivanib is the alanine ester of BMS-540215 and is hydrolyzed to the active moiety BMS-540215 *in vivo*. BMS-540215 has potent and selective inhibition of VEGFR and FGFR, with a high selectivity for VEGFR-2 and -3 (*24*). Preclinical studies have shown that brivanib has broad-spectrum *in vivo* antitumor activity at multiple dose levels (*25*).

A number of studies on brivanib to treat HCC have recently been conducted, and 3 relevant phase III studies yielded negative results. The phase III BRISK-PS Study involved 395 patients with advanced HCC whose condition progressed after sorafenib or who were intolerant to sorafenib (*26*). The patients were randomly assigned (2:1) to receive 800 mg of brivanib orally once a day plus best supportive care (BSC) or a placebo plus BSC. The median OS was 9.4 months for patients given brivanib and 8.2 months for those given the placebo ($p = 0.3307$), so there was little difference. Exploratory analyses revealed some differences between the two arms in terms of the median TTP (4.2 months for patients given brivanib *vs.* 2.7 months for patients given the placebo) and overall response rate (ORR, 10% for patients given brivanib *vs.* 2% for patients given the placebo). Notably, hyponatremia, an AE that was frequently reported in this study (occurring in 11% of patients as a grade 3 to 4 AE), has not been reported with other targeted agents, suggesting that this AE may be relatively specific to brivanib.

The phase III BRISK-FL Study tested the efficacy of brivanib versus sorafenib (*27*). In the study, patients with advanced HCC who had no prior systemic therapy were randomly assigned (1:1) to receive 400 mg of sorafenib orally twice a day ($n = 578$) or 800 mg of brivanib orally once a day ($n = 577$). The study did not meet its primary endpoint of OS noninferiority for brivanib versus sorafenib, with a median OS of 9.9 months for patients given sorafenib and 9.5 months for patients given brivanib. The two arms had a similar TTP and ORR. The incidence of SAEs (sorafenib:brivanib = 11.7%:11.3%) indicates that brivanib is less well-tolerated than sorafenib.

In these two phase III trials, brivanib failed to improve the OS for patients with advanced HCC but it did improve TTP and ORR, indicating that brivanib does have potential antitumor activity. Why it failed to improve the OS in both trials warrants further investigation.

In addition, the phase III Trans-Arterial Chemo-Embolization (TACE) Adjuvant HCC (BRISK TA) trial was terminated when 2 other phase III studies of brivanib in patients with advanced HCC failed to meet their OS objectives (*28*). In the trial, 502 patients were randomized to receive TACE + 800 mg of brivanib daily ($n = 249$, brivanib was stopped 2 days before a TACE session and restarted between day 3 and day 21 following

TACE) or TACE + a placebo (n = 253). However, the OS of both groups did not differ (26.4 months for patients given brivanib *vs.* 26.1 for patients given the placebo).

2.4. *Linifanib*

Linifanib is a multi-targeted receptor tyrosine kinase inhibitor that can inhibit members of VEGFR and PDGFR families with minimal activity against unrelated kinases (*29,30*). In a phase II trial of linifanib, 44 patients with advanced HCC who had received ≤ 1 prior systemic therapy were given linifanib orally at a dose of 0.25 mg/kg (*31*). The progression-free rate at 16 weeks (PFR-16) was 31.8%, with secondary endpoints of an ORR of 9.1%, TPP of 3.7 months, and OS of 9.7 months. The incidence of grade 3/4 AEs was 59.1%, with fatigue (13.6%) and hypertension (25.0%) being the most common. Results indicated that single-agent linifanib was clinically active in patients with advanced HCC with an acceptable safety profile. However, a phase III study of the efficacy and tolerance of linifanib versus sorafenib in advanced HCC was terminated in 2012 for unexplained reasons (*32*).

2.5. *Other kinase inhibitors*

Antiangiogenic agents have been described thus far, though other kinase inhibitors that target VEGFR are also being tested to treat advanced HCC. Cediranib, a VEGFR inhibitor, has completed a phase II trial involving advanced HCC, with results shown in Table S1 (*http://www.ddtjournal.com/docindex.php?year=2014&kanno=4*) (*33*). Pazopanib, an inhibitor that targets VEGFR and PDGFR and that has already been approved by the FDA to treat advanced RCC and advanced soft tissue sarcomas, has completed a phase I trial involving patients with HCC (Table S1) (*http://www.ddtjournal.com/docindex.php?year=2014&kanno=4*) (*34*). Orantinib, a receptor kinase inhibitor that targets VEGFR, PDGFR, and FGFR, has finished a phase I/II trial involving patients with advanced HCC and a phase II trial where it was combined with TACE and displayed promising antitumor ability (Table S1) (*http://www.ddtjournal.com/docindex.php?year=2014&kanno=4*) (*35,36*).

3. c-Met inhibitors

The hepatocyte growth factor (HGF)/c-MET signaling pathway plays a pivotal role in the development of several solid tumors, including HCC. Stimulation of the HGF/c-MET signaling pathway leads to the cascade reaction of Ras/Raf/MEK/ERK and PI3K/AKT, promoting tumor cell growth and invasion (*37*). In HCC, activation of the HGF/c-MET pathway is associated with an aggressive phenotype and poor prognosis (*38*).

3.1. *Tivantinib (ARQ 197)*

Tivantinib (ARQ 197) is a selective, non-ATP competitive, small-molecule c-MET inhibitor that inhibits growth and induces apoptosis in human tumor cell lines expressing c-MET (*39*). In a phase II study of tivantinib as a second-line treatment for advanced HCC, patients with advanced HCC and Child-Pugh class A cirrhosis who had progressed on or were unable to tolerate first-line systemic therapy were treated with tivantinib or a placebo (*40*). In the study, 71 patients were randomly assigned to receive tivantinib and 36 patients were randomly assigned to receive a placebo. Patients with tumors expressing high levels of c-MET (≥ 2+ in ≥ 50% of tumor cells) had a longer median TTP when given tivantinib than when given a placebo (2.7 months for 22 patients with high levels of c-MET given tivantinib *vs.* 1.4 months for 15 patients with high levels of c-MET given a placebo). The encouraging results indicated that tivantinib is effective as a second-line treatment for patients with HCC expressing high levels of c-MET. Furthermore, c-MET expression may be a promising biomarker in patients with HCC. A pivotal phase III study of patients with advanced HCC expressing high levels of c-MET after sorafenib failure is currently underway (*41*). However, some researchers have, based on *in-vitro* studies, suggested that tivantinib is not only a c-MET inhibitor but also an antimitotic agent that kills tumor cells independently of c-MET, contradicting the results of other studies (*42,43*). Further studies to clarify the mechanisms of the anti-HCC action of tivantinib are warranted.

3.2. *Cabozantinib (XL184)*

Cabozantinib (XL184) is an oral small-molecule tyrosine kinase inhibitor that blocks phosphorylation of c-MET and VEGFR-2 and that also has activity against AXL, RET, and KIT (*44*). Recently, HCC cell and mouse xenograft experiments measuring total MET and phosphorylated MET (p-MET) have indicated that high levels of p-MET are associated with resistance to adjuvant sorafenib treatment and that cabozantinib has significant antitumor activity against HCC (*45*). In a phase II randomized discontinuation trial, 41 patients with Child-Pugh class A advanced HCC received up to one round of prior systemic treatment before being treated with cabozantinib at a dosage of 100 mg/day for 12 weeks. The median PFS was 4.4 months, median OS was 15.1 months, and AFP response was 35% (reduction of ≥ 50%). In the trial, cabozantinib had encouraging clinical activity against HCC (*46*).

4. mTOR inhibitors

Over the past few years, several molecular pathways have been identified as contributing to the molecular

pathogenesis of HCC; the PI3K/AKT/mTOR pathway in particular plays a critical role (*47,48*). Upregulation of mTOR signalling has been observed in 40-45% of patients with HCC and a cell experiment indicated that elevated levels of phosphorylated mTOR were correlated with increased cell proliferation (*49,50*). Preclinical studies have demonstrated that mTOR inhibitors were effective at inhibiting cell proliferation, tumor growth, and metastasis in HCC tumor models (*51,52*).

4.1. *Rapamycin (sirolimus)*

Rapamycin (sirolimus) is an immunosuppressant and is used to prevent rejection in organ transplants, and especially in kidney transplants. Recently, the drug has been found to be effective at inhibiting mTOR and is being studied as a treatment for HCC (*52*). In a phase II study of sirolimus in treatment-naive patients with advanced HCC, 25 patients were treated with sirolimus 20 mg/week for 1 month and then 30 mg/week (*53*). The median TTP was 3.8 months, the OS was 6.6 months, and the ORR was 8%. These data suggest that sirolimus has antitumor action against advanced HCC, and further study is needed to investigate the efficacy of rapamycin in patients with advanced HCC.

4.2. *Everolimus*

Everolimus is a derivative of rapamycin and is also an mTOR inhibitor. Preclinical studies have indicated that everolimus inhibits tumour growth in xenograft models of human HCC (*54*). A phase I/II study of everolimus in advanced HCC has tested the toxicity and efficacy of everolimus in patients with advanced HCC and adequate hematologic, hepatic, and renal function (*55*). In the study, 3 patients were treated with everolimus at 5 mg/d and 25 patients were treated with everolimus at 10 mg/d. The median PFS and OS for the latter group were 3.8 months and 8.4 months, respectively. The estimated PFS at 24 weeks was 28.6%. A phase III study named the EVOLVE-1 study tested the effect of everolimus on survival in patients with advanced HCC after failure of sorafenib (*56*). In the study, 362 patients were randomized to receive everolimus 7.5 mg/d and 184 patients received a placebo. Both groups also received BSC. Results indicated that everolimus did not improve OS in patients with advanced HCC whose disease progressed during or after receiving sorafenib or who were intolerant of sorafenib. Despite preemptive antiviral therapy in the EVOLVE-1 study, HBV reactivation based on central laboratory findings occurred in 37.0% of patients given everolimus and 22.7% of patients given the placebo who were HBV-DNA or HBsAg-positive (or both) at the baseline. The limitation of the EVOLVE-1 study was believed to be because the study was not designed to identify a molecularly or clinically selected population that would potentially benefited from everolimus. Furthermore, mTOR inhibitors have immunosuppressive and antitumor actions, so the potential benefits of this class of agents in the adjuvant setting are being assessed in a phase III trial of sirolimus for patients with HCC after liver transplantation (*57*).

5. MEK inhibitors

The Ras/Raf/MEK/ERK signaling pathway plays a pivotal role in the regulation of many cellular processes, including proliferation, survival, differentiation, apoptosis, motility, and metabolism (*58*). A study noted activation of this pathway in half of patients with HCC; this pathway may be involved in multistep hepatocarcinogenesis, and especially in the progression of HCC (*59*). MEK inhibitors can inhibit the mitogen-activated protein kinase enzymes MEK1 and/or MEK2. Hence, MEK inhibitors have potential as a treatment for HCC.

Selumetinib is a selective, non-ATP-competitive small-molecule inhibitor of MEK1/2 (*60*). A phase II study of selumetinib administered 100 mg of selumetinib to 19 patients twice a day for 21 days, but the study was terminated midway through since no response was radiographically evident in this group. The short TTP and no ORR indicated the minimal effectiveness of selumetinib in treating advanced HCC (*61*).

6. Combined therapy

Drug resistance frequently occurs with molecularly targeted cancer therapy. An important mechanism of resistance is the compensatory activation of related signaling pathways (*62*). To date, several molecular pathways have been identified as contributing to the molecular pathogenesis of HCC. Of these, the PI3K/AKT/mTOR and Ras/Raf/MEK/ERK pathways have been studied the most extensively. These two pathways may be activated by multiple upstream receptors (*e.g.*, VEGFR and c-MET) and inhibition of specific upstream receptors may lead to compensatory activation *via* other pathways. Various inhibitors must be combined with other therapies to more effectively treat HCC.

6.1. *Combination of sorafenib and TACE*

Combinational therapies with sorafenib have the potential to further improve therapeutic options for patients suffering from advanced HCC. TACE is the standard therapy for patients with HCC who are not eligible for surgery (*63*). The hepatic artery is embolized by selectively injecting small embolic particles coated with chemotherapeutic agents. Molecular biology studies have shown that plasma VEGF levels usually increase after TACE treatment, providing a rationale for the combination of TACE and sorafenib (*64*).

In a trial involving patients with HCV-related intermediate-stage HCC, 62 patients with Child-Pugh class A disease were randomized (1:1) to receive 400 mg of sorafenib twice a day or a placebo 30 days after TACE (30 mg of doxorubicin and 10 mg of mitomycin C with 10 mL of iodinated nonionic contrast media and 20 mL of iodinated oil) (*65*). The median TTP was 9.2 months in the sorafenib group and 4.9 months in the placebo group ($p < 0.001$). Results indicated that a conventional TACE procedure followed by sorafenib treatment resulted in a significantly longer TTP for patients with intermediate-stage HCV-related HCC.

However, another study revealed conflicting results. In a phase III study of sorafenib after TACE in Japanese and Korean patients, 458 patients with unresectable HCC, Child-Pugh class A cirrhosis, and ≥ 25% tumor necrosis/shrinkage 1-3 months after 1 or 2 TACE sessions were randomized at a ratio of 1:1 to receive 400 mg sorafenib twice a day or a placebo (> 50% of patients started sorafenib > 9 weeks after TACE) (*66*). The median TTP was 5.4 versus 3.7 months ($p = 0.252$), and the 1-year and 2-year survival rates were 94.6% *vs.* 94.1% and 72.1% *vs.* 73.8%, respectively. This trial found that sorafenib did not significantly prolong TTP in patients who responded to TACE. Moreover, the researchers attributed their findings to the delay in starting sorafenib after TACE and/or low daily sorafenib doses.

In a propensity score matching study involving Chinese patients with advanced HCC, 198 patients were treated with TACE alone (1:1 ratio of cisplatin and iodized oil), and 82 were treated with a combination therapy of TACE and sorafenib (combined therapy group) (*67*). In addition, the 82 patients were matched using propensity-score matching at a 1:2 ratio with 164 patients who received TACE monotherapy. The median OS and TTP were 7.0 months *vs.* 4.9 months ($p = 0.003$) and 2.6 months *vs.* 1.9 months ($p = 0.001$), respectively. In a phase II, prospective single-arm multinational study, 192 patients with intermediate-stage, unresectable HCC received doxorubicin-based TACE (an emulsion of lipiodol 5-20 mL and doxorubicin 30-60 mg) with interrupted dosing of sorafenib (sorafenib discontinued for 3 days before and 4-7 days after TACE) and TACE/sorafenib cycles were repeated every 6-8 weeks (*68*). Combined TACE/sorafenib was well-tolerated, with SAEs occurring in 27.1% of patients. Median PFS and TTP were 12.8 and 13.8 months, respectively. These two studies showed that the combination of TACE and sorafenib is well-tolerated and more effective than TACE monotherapy.

Overall, the combination of TACE and sorafenib seems to be more effective than TACE monotherapy (Table S2) (*http://www.ddtjournal.com/docindex.php?year=2014&kanno=4*) (69-71). Randomized controlled trials are still needed to further confirm this effectiveness, characterize the optimal schedule of sorafenib administration and TACE, and determine which patients are most likely to benefit from this treatment. Moreover, similar combinational strategies could be investigated with other locoregional treatments (*e.g.* radioembolization plus sorafenib and radiofrequency ablation plus sorafenib).

6.2. *Combination of bevacizumab and erlotinib*

EGFR is a member of the RTK family and a potent regulator of the activity of the Ras/Raf/MEK/ERK cascade (*72*). EGFR is highly expressed in human hepatoma cell lines, and the high expression of EGFR is associated with higher cell proliferation (*73*). Erlotinib is an EGFR inhibitor that inhibits the formation of phosphotyrosine residues in EGFR and the initiation of signal cascades by binding to the ATP binding site of the receptor in a reversible fashion (*74*). However, several phase II trials of erlotinib to treat advanced HCC have indicated that single agent erlotinib provided a modest clinical benefit (*75,76*), and a phase III trial of erlotinib monotherapy to treat HCC was not conducted.

As a matter of fact, the multiplicity and complexity of molecular aberrations in HCC necessitate a multi-targeted approach combined with EGFR inhibitors. Recently, several trials of erlotinib plus bevacizumab, a recombinant humanized monoclonal antibody that binds to VEGF in patients with advanced HCC, have yielded results, although some are controversial.

A phase II trial of the combination of bevacizumab and erlotinib involved 40 patients with advanced HCC who received bevacizumab 10 mg/kg every 14 days and 150 mg of oral erlotinib daily in a 28-day cycle (*77*). The primary endpoint of PFS at 16 weeks was 62.5%. The median PFS was 9.0 months and OS was 15.65 months. Another phase II trial of bevacizumab and erlotinib involving 59 patients with unresectable HCC administered 150 mg of oral erlotinib daily and 10 mg/kg of bevacizumab every 14 days in a 28-day cycle. The PFS at 16 weeks was 64% and SAEs occurred in 30.51% of patients (*78*). Both trials showed that the combination of bevacizumab and erlotinib had significant antitumor activity in patients who had advanced HCC.

However, other trials had conflicting results. A phase II study of bevacizumab plus erlotinib in patients with advanced HCC has been conducted (*79*). In 27 patients treated with 150 mg of erlotinib daily and 10 mg/kg of bevacizumab on days 1 and 15 every 28 days, one patient had a confirmed partial response and 11 (48%) had stable disease. Median TTP was 3.0 months and OS was 9.5 months. In addition, a phase II study of bevacizumab and erlotinib in the treatment of patients with advanced HCC not responding to sorafenib administered 10 mg/kg of bevacizumab every 2 weeks and 150 mg of erlotinib daily for a maximum of 6 cycles (*80*). With 10 patients recruited, the trial was halted in the first stage according to

pre-set statistical criteria. Of these 10 patients, none responded or had stable disease. The median TTP was 1.81 months and OS was 4.37 months. A phase II trial of 21 patients with metastatic or inoperable HCC who had not received local or systemic therapy administered 15 mg/kg of bevacizumab every 3 weeks and 150 mg of oral erlotinib daily. The PFS at 27 weeks was 23.8% (*73*). These trials showed that erlotinib combined with bevacizumab had minimal activity in patients with advanced HCC or in an unselected population with sorafenib-refractory advanced HCC.

Furthermore, a phase III trial is underway to evaluate the clinical benefit of 400 mg of sorafenib twice a day and 150 mg of erlotinib once a day versus 400 mg of sorafenib twice a day and a placebo once a day in patients with advanced HCC (*81*). The combination of bevacizumab and erlotinib warrants additional evaluation in randomized controlled trials.

In addition to the studies discussed thus far, some *in-vitro* studies have provided a rationale for the combination of EGFR TKIs and IGF-1R TKIs. In terms of its mechanism of action, anti-IGF-1R therapy may cause acquired resistance *via* the activation of HER3, which EGFR TKIs may inhibit (*82,83*).

7. Conclusion and prospects for the future

Up to now, sorafenib has been the only standard therapy for advanced HCC, with most phase III trials failing to reach their primary endpoints. The failure of other molecularly targeted drugs may be due to several reasons.

First, HCC is quite complex with a pathogenesis including hepatitis B and C, and HCC is always associated with liver cirrhosis. The heterogeneity of hepatoma cells makes therapy much more complicated and affects the performance of targeted drugs to treat HCC. Therefore, effective treatment of HCC would require the simultaneous treatment of three distinct diseases: hepatitis, cirrhosis, and cancer. In addition, many carcinogenic pathways are activated as HCC develops, but no single pathway has been identified as the most important (*84*). Second, most phase III trials have shown that surrogate endpoints such as TTP, PFS, and ORR inconsistently predict OS. Both the selection of eligible patients and determination of primary endpoints may affect the outcome of trials. However, there are no yet known biomarkers that can predict whether patients are sensitive to sorafenib or other molecularly targeted drugs. In the absence of well-characterized and validated predictive biomarkers, targeted agents will likely continue to have a high risk of failure if phase III trials are conducted in unselected populations. Relevant biomarkers that may predict clinical outcome in patients receiving everolimus are being assessed in the EVOLVE-1 population (*56*). Third, the existing TKIs used in trials to treat HCC are primarily agents optimized for the treatment of other cancers and thus may not exhibit the best kinase inhibitory profile to counteract the signaling abnormalities that are characteristic of HCC. This limitation, coupled with the likely involvement of multi-genic lesions in HCC, may affect the performance of targeted therapies in treating HCC (*85*). Future studies of targeted agents to treat HCC should focus on answering these questions and particularly on identifying patient populations based on molecular classification and predictive biomarkers.

References

1. Schutte K, Bornschein J, Malfertheiner P. HCC: Epidemiological trends and risk factors. Dig Dis. 2009; 27:80-92.
2. Ferlay J, Shin HR, Bray F, Forman D, Mathers C, Parkin DM. Estimates of worldwide burden of cancer in 2008: GLOBOCAN 2008. Int J Cancer. 2010; 127:2893-2917.
3. Feitelson MA, Sun B, Satiroglu Tufan NL, Liu J, Pan J, Lian Z. Genetic mechanisms of hepatocarcinogenesis. Oncogene. 2002; 21:2593-2604.
4. Gomaa AI, Khan SA, Toledano MB, Waked I, Taylor-Robinson SD. Hepatocellular carcinoma: Epidemiology, risk factors and pathogenesis. World J Gastroenterol. 2008; 14:4300-4308.
5. El-Serag HB, Rudolph KL. Hepatocellular Carcinoma: Epidemiology and molecular carcinogenesis. Gastroenterology. 2007; 132:2557-2576.
6. Simonetti RG, Cammà C, Fiorello F, Politi F, D'Amico G, Pagliaro L. Hepatocellular carcinoma. A worldwide problem and the major risk factors. Dig Dis Sci. 1991; 36:962-972.
7. Unoura M, Kaneko S, Matsushita E, Shimoda A, Takeuchi M, Adachi H, Kawai H, Urabe T, Yanagi M, Matsui O. High-risk groups and screening strategies for early detection of hepatocellular carcinoma in patients with chronic liver disease. Hepatogastroenterology. 1993; 40:305-310.
8. Villanueva A, Hernandez-Gea V, Llovet JM. Medical therapies for hepatocellular carcinoma: A critical view of the evidence. Nat Rev Gastroenterol Hepatol. 2012; 10:34-42.
9. Llovet JM, Ricci S, Mazzaferro V, Hilgard P, Gane E, Blanc JF, Bruix J. Sorafenib in advanced hepatocellular carcinoma. N Engl J Med. 2008; 359:378-390.
10. Marin JJG, Castaño B, Martinez-Becerra P, Rosales R, Monte MJ. Chemotherapy in the treatment of primary liver tumours. Cancer Ther. 2008; 6:711-728.
11. Moeini A, Cornellà H, Villanueva A. Emerging signaling pathways in hepatocellular carcinoma. Liver Cancer. 2012; 1:83-93.
12. An FQ, Matsuda M, Fujii H, Matsumoto Y. Expression of vascular endothelial growth factor in surgical specimens of hepatocellular carcinoma. J Cancer Res Clin. 2000; 126:153-160.
13. McDermott U, Sharma SV, Dowell L, *et al*. Identification of genotype-correlated sensitivity to selective kinase inhibitors by using high-throughput tumor cell line profiling. Proc Natl Acad Sci USA. 2007; 104:19936-19941.
14. Tai WT, Cheng AL, Shiau CW, Huang HP, Huang JW, Chen PJ, Chen KF. Signal transducer and activator of transcription 3 is a major kinase-independent target of

sorafenib in hepatocellular carcinoma. J Hepatol. 2011; 55:1041-1048.
15. Cheng AL, Kang YK, Chen Z, *et al*. Efficacy and safety of sorafenib in patients in the Asia-Pacific region with advanced hepatocellular carcinoma: A phase III randomised, double-blind, placebo-controlled trial. Lancet Oncol. 2009; 10:25-34.
16. Motzer RJ, Hutson TE, Tomczak P, *et al*. Sunitinib versus interferon α in metastatic renal-cell carcinoma. N Engl J Med. 2007; 356:115-124.
17. Demetri GD, van Oosterom AT, Garrett CR, *et al*. Efficacy and safety of sunitinib in patients with advanced gastrointestinal stromal tumour after failure of imatinib: A randomised controlled trial. Lancet. 2006; 368:1329-1338.
18. Zhu AX, Raymond E. Early development of sunitinib in hepatocellular carcinoma. Expert Rev Anticanc. 2009; 9:143-150.
19. Faivre S, Raymond E, Boucher E, Douillard J, Lim HY, Kim JS, Zappa M, Lanzalone S, Lin X, Deprimo S, Harmon C, Ruiz-Garcia A, Lechuga MJ, Cheng AL. Safety and efficacy of sunitinib in patients with advanced hepatocellular carcinoma: An open-label, multicentre, phase II study. Lancet Oncol. 2009; 10:794-800.
20. Barone C, Basso M, Biolato M, Pompili M, Rufini V, Miele L, Basso M, De Gaetano AM, Castaldi P, Iaculli A, Leccisotti L, Riccardi L, Grieco A. A phase II study of sunitinib in advanced hepatocellular carcinoma. Dig Liver Dis. 2013; 45:692-698.
21. Koeberle D, Montemurro M, Samaras P, Majno P, Simcock M, Limacher A, Lerch S, Kovàcs K, Inauen R, Hess V, Saletti P, Borner M, Roth A, Bodoky G. Continuous sunitinib treatment in patients with advanced hepatocellular carcinoma: A Swiss Group for Clinical Cancer Research (SAKK) and Swiss Association for the Study of the Liver (SASL) multicenter phase II trial (SAKK 77/06). The Oncologist. 2010; 15: 285-292.
22. Cheng AL, Kang YK, Lin DY, Park JW, Kudo M, Qin S, Chung HC, Song X, Xu J, Poggi G, Omata M, Pitman Lowenthal S, Lanzalone S, Yang L, Lechuga MJ, Raymond E. Sunitinib versus sorafenib in advanced hepatocellular cancer: Results of a randomized phase III trial. J Clin Oncol. 2013; 31:4067-4075.
23. Majumder S, Piguet AC, Dufour JF, Chatterjee S. Study of the cellular mechanism of Sunitinib mediated inactivation of activated hepatic stellate cells and its implications in angiogenesis. Eur J Pharmacol. 2013; 705: 86-95.
24. Bhide R, Cai ZW, Zhang YZ, *et al*. Discovery and preclinical studies of (R)-1-(4-(4-fluoro-2-methyl-1H-indol-5-yloxy)-5-methylpyrrolo[2,1-f][1,2,4]triaazin-6-yloxy)propan- 2-ol (BMS-540215), an *in vivo* active potent VEGFR-2 inhibitor. J Med Chem. 2006; 49:2143-2146.
25. Huynh H, Ngo VC, Fargnoli J, Ayers M, Soo KC, Koong HN, Thng CH, Ong HS, Chung A, Chow P, Pollock P, Byron S, Tran E. Brivanib alaninate, a dual inhibitor of vascular endothelial growth factor receptor and fibroblast growth factor receptor tyrosine kinases, induces growth inhibition in mouse models of human hepatocellular carcinoma. Clin Cancer Res. 2008; 14:6146-6153.
26. Llovet J M, Decaens T, Raoul J L, *et al*. Brivanib in patients with advanced hepatocellular carcinoma who were intolerant to sorafenib or for whom sorafenib failed: results from the randomized phase III BRISK-PS study. J Clin Oncol. 2013; 31:3509-3516.
27. Johnson P J, Qin S, Park J W, *et al*. Brivanib versus sorafenib as first-line therapy in patients with unresectable, advanced hepatocellular carcinoma: Results from the randomized phase III BRISK-FL study. J Clin Oncol. 2013; 31:3517-3524.
28. Kudo M, Han G, Finn R S, *et al*. Brivanib as adjuvant therapy to transarterial chemoembolization in patients with hepatocellular carcinoma: A randomized phase 3 trial. Hepatolog. 2014; [Epub ahead of print]
29. Albert DH, Tapang P, Magoc TJ, *et al*. Preclinical activity of ABT-869, a multitargeted receptor tyrosine kinase inhibitor. Mol Cancer Ther. 2006; 5:995-1006.
30. Guo J, Marcotte PA, McCall JO, Dai Y, Pease LJ, Michaelides MR, Davidsen SK, Glaser KB. Inhibition of phosphorylation of the colony-stimulating factor-1 receptor (c-Fms) tyrosine kinase in transfected cells by ABT-869 and other tyrosine kinase inhibitors. Mol Cancer Ther. 2006; 5:1007-1013.
31. Toh HC, Chen PJ, Carr BI, Knox JJ, Gill S, Ansell P, McKeegan EM, Dowell B, Pedersen M, Qin Q, Qian J, Scappaticci FA, Ricker JL, Carlson DM, Yong WP. Phase 2 trial of linifanib (ABT-869) in patients with unresectable or metastatic hepatocellular carcinoma. Cancer. 2013; 119:380-387.
32. Efficacy and Tolerability of ABT-869 Versus Sorafenib in Advanced Hepatocellular Carcinoma (HCC) *http://clinicaltrials.gov/ct2/show/NCT01009593?term=Linifanib%2C+hepatocellular+carcinoma&rank=1* (accessed July 25, 2014)
33. Alberts S1, Fitch TR, Kim GP, Morlan BW, Dakhil SR, Gross HM, Nair S. Cediranib (AZD2171) in Patients with Advanced Hepatocellular Carcinoma: A Phase II North Central Cancer Treatment Group (NCCTG) Clinical Trial. Am J Clin Oncol. 2012; 35:329.
34. Yau T, Chen PJ, Chan P, Curtis CM, Murphy PS, Suttle AB, Gauvin J, Hodge JP, Dar MM, Poon RT. Phase I dose-finding study of pazopanib in hepatocellular carcinoma: evaluation of early efficacy, pharmacokinetics, and pharmacodynamics. Clin Cancer Res. 2011; 17:6914-6923.
35. Kanai F, Yoshida H, Tateishi R, *et al*. A phase I/II trial of the oral antiangiogenic agent TSU-68 in patients with advanced hepatocellular carcinoma. Cancer Chemother Pharmacol, 2011; 67:315-324.
36. Inaba Y, Kanai F, Aramaki T, Yamamoto T, Tanaka T, Yamakado K, Kaneko S, Kudo M, Imanaka K, Kora S, Nishida N, Kawai N, Seki H, Matsui O, Arioka H, Arai Y. A randomised phase II study of TSU-68 in patients with hepatocellular carcinoma treated by transarterial chemoembolisation. Eur J Cancer. 2013; 49:2832-2840.
37. Comoglio P M, Giordano S, Trusolino L. Drug development of MET inhibitors: targeting oncogene addiction and expedience. Nat Rev Dreg Discov. 2008; 7:504-516.
38. Kaposi-Novak P, Lee JS, Gòmez-Quiroz L, Coulouarn C, Factor VM, Thorgeirsson SS. Met-regulated expression signature defines a subset of human hepatocellular carcinomas with poor prognosis and aggressive phenotype. J Clin Invest. 2006; 116:1582-1595.
39. Eathiraj S, Palma R, Volckova E, Hirschi M, France DS, Ashwell MA, Chan TC. Discovery of a novel mode of protein kinase inhibition characterized by the mechanism of inhibition of human mesenchymal-epithelial transition factor (c-Met) protein autophosphorylation by ARQ 197.

J Biol Chem. 2011; 286:20666-20676.
40. Santoro A, Rimassa L, Borbath I, *et al*. Tivantinib for second-line treatment of advanced hepatocellular carcinoma: A randomised, placebo-controlled phase 2 study. Lancet Oncol. 2013; 14:55-63.
41. A Randomized Double-blind, Placebo-controlled Japanese Phase III Trial of ARQ 197 in Hepatocellular Carcinoma (HCC) (JET-HCC). *http://clinicaltrials.gov/ct2/show/NCT02029157?term=Tivantinib%2C+hepatocellular+carcinoma&rank=5* (accessed July 25,2014).
42. Katayama R, Aoyama A, Yamori T, Qi J, Oh-hara T, Song Y, Engelman JA, Fujita N. Cytotoxic activity of tivantinib (ARQ 197) is not due solely to c-MET inhibition. Cancer Res. 2013; 73:3087-3096.
43. Basilico C1, Pennacchietti S, Vigna E, Chiriaco C, Arena S, Bardelli A, Valdembri D, Serini G, Michieli P. Tivantinib (ARQ197) displays cytotoxic activity that is independent of its ability to bind MET. Clin Cancer Res. 2013; 19:2381-2392.
44. Yakes FM, Chen J, Tan J, *et al*. Cabozantinib (XL184), a novel MET and VEGFR2 inhibitor, simultaneously suppresses metastasis, angiogenesis, and tumor growth. Mol Cancer Ther. 2011; 10:2298-2308.
45. Xiang Q, Chen W, Ren M, Wang J, Zhang H, Deng DY, Zhang L, Shang C, Chen Y. Cabozantinib suppresses tumor growth and metastasis in hepatocellular carcinoma by a dual blockade of VEGFR2 and MET. Clin Cancer Res. 2014; 20:2959-2970.
46. Verslype C, Cohn A L, Kelley R K, *et al*. Activity of cabozantinib (XL184) in hepatocellular carcinoma: Results from a phase II randomized discontinuation trial (RDT). J Clin Oncol. 2012; 30:4007.
47. Bjornsti M-A, Houghton PJ. The TOR pathway: a target for cancer therapy. Nat Rev Cancer. 2004; 4:335-348.
48. Hay N, Sonenberg N. Upstream and downstream of mTOR. Genes Dev. 2004; 18:1926-1945.
49. Sahin F, Kannangai R, Adegbola O, Wang J, Su G, Torbenson M. mTOR and P70 S6 kinase expression in primary liver neoplasms. Clin Cancer Res. 2004; 10:8421-8425.
50. Sieghart W, Fuereder T, Schmid K, Cejka D, Werzowa J, Wrba F, Wang X, Gruber D, Rasoul-Rockenschaub S, Peck-Radosavljevic M, Wacheck V. Mammalian target of rapamycin pathway activity in hepatocellular carcinomas of patients undergoing liver transplantation. Transplantation. 2007; 83:425-432.
51. Varma S, Khandelwal RL. Effects of rapamycin on cell proliferation and phosphorylation of mTOR and p70(S6K) in HepG2 and HepG2 cells overexpressing constitutively active Akt/PKB. Biochim Biophys Acta. 2007; 1770:71-78.
52. Huynh H, Chow KH, Soo KC, Toh HC, Choo SP, Foo KF, Poon D, Ngo VC, Tran E. RAD001 (everolimus) inhibits tumour growth in xenograft models of human hepatocellular carcinoma. J Cell Mol Med. 2009; 13:1371-1380.
53. Decaens T, Luciani A, Itti E, Hulin A, Roudot-Thoraval F, Laurent A, Zafrani ES, Mallat A, Duvoux C. Phase II study of sirolimus in treatment-naive patients with advanced hepatocellular carcinoma. Dig Liver Dis. 2012; 44:610-616.
54. Huynh H, Chow KH, Soo KC, Toh HC, Choo SP, Foo KF, Poon D, Ngo VC, Tran E. RAD001 (everolimus) inhibits tumour growth in xenograft models of human hepatocellular carcinoma. J Cell Mol Med. 2009; 13:1371-1380.
55. Zhu A X, Abrams T A, Miksad R, *et al*. Phase 1/2 study of everolimus in advanced hepatocellular carcinoma. Cancer. 2011; 117:5094-5102.
56. Zhu A X, Kudo M, Assenat E, *et al*. Effect of everolimus on survival in advanced hepatocellular carcinoma after failure of sorafenib: The EVOLVE-1 Randomized Clinical Trial. JAMA. 2014; 312:57-67.
57. Immunosuppression in Patients Undergoing Liver Transplantation for Hepatocellular Carcinoma. *http://clinicaltrials.gov/ct2/show/NCT00355862?term=NCT00355862&rank=1* (accessed July 25,2014)
58. Blum R, Cox AD, Kloog Y. Inhibitors of chronically active RAS: Potential for treatment of human malignancies. Recent Pat Anticancer Drug Discov. 2008; 3:31-47.
59. Ito Y, Sasaki Y, Horimoto M, Wada S, Tanaka Y, Kasahara A, Ueki T, Hirano T, Yamamoto H, Fujimoto J, Okamoto E, Hayashi N, Hori M. Activation of mitogen-activated protein kinases/extracellular signal-regulated kinases in human hepatocellular carcinoma. Hepatology. 1998; 27:951-958.
60. Davies BR, Logie A, McKay JS, Martin P, Steele S, Jenkins R, Cockerill M, Cartlidge S, Smith PD. AZD6244 (ARRY-142886), a potent inhibitor of mitogen-activated protein kinase/extracellular signal regulated kinase kinase 1/2 kinases: Mechanism of action *in vivo*, pharmacokinetic/pharmacodynamics relationship, and potential for combination in preclinical models. Mol Cancer Ther. 2007; 6:2209-2219.
61. O'Neil BH, Goff LW, Kauh JS, Strosberg JR, Bekaii-Saab TS, Lee RM, Kazi A, Moore DT, Learoyd M, Lush RM, Sebti SM, Sullivan DM. Phase II study of the mitogen-activated protein kinase 1/2 inhibitor selumetinib in patients with advanced hepatocellular carcinoma. J Clin Oncol. 2011; 29:2350-2356.
62. Ou DL, Lee BS, Chang YC, Lin LI, Liou JY, Hsu C, Cheng AL. Potentiating the efficacy of molecular targeted therapy for hepatocellular carcinoma by inhibiting the insulin-like growth factor pathway. PloS one. 2013; 8: e66589.
63. Bruix J, Sala M, Llovet J M. Chemoembolization for hepatocellular carcinoma. Gastroenterology, 2004; 127:S179-S188.
64. Wilhelm SM, Adnane L, Newell P, Villanueva A, Llovet JM, Lynch M. Preclinical overview of sorafenib, a multikinase inhibitor that targets both Raf and VEGF and PDGF receptor tyrosine kinase signaling. Mol Cancer Ther. 2008; 7:3129-3140.
65. Sansonno D, Lauletta G, Russi S, Conteduca V, Sansonno L, Dammacco F.Transarterial chemoembolization plus sorafenib: a sequential therapeutic scheme for HCV-related intermediate-stage hepatocellular carcinoma: a randomized clinical trial. The oncologist. 2012; 17:359-366.
66. Kudo M, Imanaka K, Chida N, *et al*. Phase III study of sorafenib after transarterial chemoembolisation in Japanese and Korean patients with unresectable hepatocellular carcinoma. Eur J Cancer. 2011; 47:2117-2127.
67. Hu H, Duan Z, Long X, Hertzanu Y, Shi H, Liu S, Yang Z. Sorafenib Combined with Transarterial Chemoembolization versus Transarterial Chemoembolization Alone for Advanced-Stage Hepatocellular Carcinoma: A Propensity Score Matching Study. PloS one. 2014; 9:e96620.
68. Chao Y, Chung YH, Han G, Yoon JH, Yang J, Wang J, Shao GL, Kim BI, Lee TY. The combination of TACE

(transcatheter arterial chemombolization) and sorafenib is well-tolerated and effective in Asian Patients with hepatocellular carcinoma: Final results of the START trial. Int J Cancer. 2014; [Epub ahead of print]
69. Pawlik TM, Reyes DK, Cosgrove D, Kamel IR, Bhagat N, Geschwind JF. Phase II trial of sorafenib combined with concurrent transarterial chemoembolization with drug-eluting beads for hepatocellular carcinoma. J Clin Oncol. 2011; 29:3960-3967.
70. Park JW, Koh YH, Kim HB, Kim HY, An S, Choi JI, Woo SM, Nam BH. Phase II study of concurrent transarterial chemoembolization and sorafenib in patients with unresectable hepatocellular carcinoma. J Hepatol. 2012; 56:1336-1342.
71. Zhao Y, Wang WJ, Guan S, Li HL, Xu RC, Wu JB, Liu JS, Li HP, Bai W, Yin ZX, Fan DM, Zhang ZL, Han GH. Sorafenib combined with transarterial chemoembolization for the treatment of advanced hepatocellular carcinoma: A large-scale multicenter study of 222 patients. Ann Oncol. 2013; 24:1786-1792.
72. Bublil EM, Yarden Y. The EGF receptor family: spearheading a merger of signaling and therapeutics. Curr Opin Cell Biol. 2007; 19:124-134.
73. Govindarajan R, Siegel E, Makhoul I, Williamson S. Bevacizumab and erlotinib in previously untreated inoperable and metastatic hepatocellular carcinoma. Am J Clin Oncol. 2013; 36:254-257.
74. Raymond E, Faivre S, Armand J P. Epidermal growth factor receptor tyrosine kinase as a target for anticancer therapy. Drugs. 2000; 60:15-23.
75. Philip PA, Mahoney MR, Allmer C, Thomas J, Pitot HC, Kim G, Donehower RC, Fitch T, Picus J, Erlichman C. Phase II study of Erlotinib (OSI-774) in patients with advanced hepatocellular cancer. J Clin Oncol. 2005; 23:6657-6663.
76. Thomas MB, Chadha R, Glover K, Wang X, Morris J, Brown T, Rashid A, Dancey J, Abbruzzese JL. Phase 2 study of erlotinib in patients with unresectable hepatocellular carcinoma. Cancer. 2007; 110:1059-1067.
77. Thomas MB, Morris JS, Chadha R, Iwasaki M, Kaur H, Lin E, Kaseb A, Glover K, Davila M, Abbruzzese J. Phase II trial of the combination of bevacizumab and erlotinib in patients who have advanced hepatocellular carcinoma. J Clin Oncol. 2009; 27:843-850.
78. Efficacy and Safety Study of Bevacizumab and Erlotinib to Treat Primary Liver Cancer That Cannot be Removed By Surgery. *http://clinicaltrials.gov/ct2/show/NCT00242502?term=NCT00242502&rank=1* (accessed July 25,2014).
79. Philip PA, Mahoney MR, Holen KD, Northfelt DW, Pitot HC, Picus J, Flynn PJ, Erlichman C. Phase 2 study of bevacizumab plus erlotinib in patients with advanced hepatocellular cancer. Cancer. 2012; 118:2424-2430.
80. Yau T, Wong H, Chan P, Yao TJ, Pang R, Cheung TT, Fan ST, Poon RT. Phase II study of bevacizumab and erlotinib in the treatment of advanced hepatocellular carcinoma patients with sorafenib-refractory disease. Invest New Drug. 2012; 30:2384-2390.
81. Nexavar-Tarceva Combination Therapy for First Line Treatment of Patients Diagnosed With Hepatocellular Carcinoma (SEARCH). *http://clinicaltrials.gov/ct2/show/NCT00901901?term=erlotinib%2C+hepatocellular+carcinoma&rank=6* (accessed July 25,2014).
82. Desbois-Mouthon C, Baron A, Blivet-Van Eggelpoël MJ, Fartoux L, Venot C, Bladt F, Housset C, Rosmorduc O. Insulin-like growth factor-1 receptor inhibition induces a resistance mechanism *via* the epidermal growth factor receptor/HER3/AKT signaling pathway: rational basis for cotargeting insulin-like growth factor-1 receptor and epidermal growth factor receptor in hepatocellular carcinoma. Clin Cancer Res. 2009; 15:5445-5456.
83. Ou DL, Lee BS, Chang YC, Lin LI, Liou JY, Hsu C, Cheng AL. Potentiating the efficacy of molecular targeted therapy for hepatocellular carcinoma by inhibiting the insulin-like growth factor pathway. PloS one. 2013; 8:e66589.
84. Bagi C M, Gebhard D F, Andresen C J. Antitumor effect of vascular endothelial growth factor inhibitor sunitinib in preclinical models of hepatocellular carcinoma. Eur J Gastroen Hepat. 2012; 24:563-574.
85. Ho HK, Chua BT, Wong W, Lim KS, Teo V, Ong HT, Chen X, Zhang W, Hui KM, Go ML, Ullrich A. Benzylidene-indolinones are effective as multi-targeted kinase inhibitor therapeutics against hepatocellular carcinoma. Mol Oncol. 2014; [Epub ahead of print]

(Received July 8, 2014; Received August 20, 2014; Accepted August 23, 2014)

Original Article

DOI: 10.5582/ddt.2014.01029

Design of amphiphilic oligopeptides as models for fine tuning peptide assembly with plasmid DNA

Geetha N. Goparaju, Pardeep K. Gupta*

Department of Pharmaceutical Sciences, University of the Sciences in Philadelphia, Philadelphia, PA, USA.

Summary **We discuss the design of novel amphiphilic oligopeptides with hydrophobic and cationic amino acids to serve as models to understand peptide-DNA assembly. Biophysical and thermodynamic characterization of interaction of these amphiphilic peptides with plasmid DNA is presented. Peptides with at least +4 charges favor stable complex formation. Surface potential is dependent on the type of hydrophobic amino acid for a certain charge. Thermodynamically it is a spontaneous interaction between most of the peptides and plasmid DNA. Lys_7 and Tyr peptides with +4/+5 charges indicate cooperative binding with pDNA without saturation of interaction while Val_2-Gly-Lys_4, Val-Gly-Lys_5, and Phe-Gly-Lys_5 lead to saturation of interaction indicating condensed pDNA within the range of N/Ps studied. We show that the biophysical properties of DNA-peptide complexes could be modulated by design and the peptides presented here could be used as building blocks for creating DNA-peptide complexes for various biomedical applications, mainly nucleic acid delivery.**

Keywords: Plasmid DNA, amphiphilic peptides, hydrodynamics, thermodynamics, zeta potential

1. Introduction

Cationic peptides for non-viral gene delivery are being explored for a long time (*1-4*). Planck *et al*. (*5*), showed that the short-chain oligolysines - DNA complexes rather than polylysine is a better choice for receptor-mediated gene delivery due to minimal activation of the complement system. It was also shown that the compacting ability of arginyl (Arg) peptides > lysine (Lys) peptides > ornithyl peptides. However, complement activation by octaarginyl peptides was stronger than that induced by an octalysyl peptide. *In-vitro* gene delivery studies suggested that a minimum chain length of six to eight cationic amino acids is required to compact DNA into structures active in receptor-mediated gene delivery (*5,6*). Our studies showed that amphiphilic peptides with smaller hydrophobic domain form smaller complexes and their stability in solution depends on the nature of the hydrophobic amino acid (*7*). A short hydrophobic N-terminal of the peptide showed better condensing abilities compared with the peptides with larger hydrophobic N-terminal (*8*). In a recent study, factors like the presence of tryptophan and the overall hydrophobicity of the peptides as well as colloidal stability of the peptide-DNA complexes was analyzed (*9*). Such studies highlight the importance of understanding structure-stability relationships in development of novel nucleic acid delivery vectors. This work presents rational design of amphiphilic oligopeptides with distinct hydrophilic and hydrophobic domains that can confer confinement of interaction and bring different hydrodynamic properties and thermodynamics upon interaction with plasmid DNA.

2. Materials and Methods

2.1. *Materials*

Plasmid DNA (pDNA) used in this study was the 5.757 kb gWiZ GFP plasmid (obtained from Genlantis, San Diego, CA, USA). Reagents and protected amino acid residues for peptide synthesis were purchased from American Peptide Company (Sunnyvale, CA, USA). All the other materials such as ethidium bromide, monobasic sodium phosphate, sodium hydroxide, *N*,*N*-diisopropylcarbodiimide (DIC), 1-hydroxybenzotriazole

**Address correspondence to:*
Dr. Pardeep K. Gupta, Department of Pharmaceutical Sciences, University of the Sciences in Philadelphia, 600 S 43rd Street, Philadelphia, PA 19104, USA.
E-mail: p.gupta@usp.edu

hydrate (HOBT), piperidine, dichloromethane (DCM), methanol, hexane, trifluoroacetic acid (TFA), thianisole (TIS), dimethylformamide (DMF) and ether were obtained from Fisher Scientific Co (Fair Lawn, NJ, USA) or Sigma Chemical Co (St Louis, MO, USA) and were used without further purification.

2.2. *Peptide synthesis*

All the peptides used in the study were synthesized by solid phase peptide synthesis (*10*). The starting material was 1.653 g of Lys-wang resin with a resin load of 0.6 mEq/g. Lysine was deprotected with 20% piperidine solution in DMF. Fmoc amino acids (three equivalents excess relative to the resin) were activated using HOBt and DIC. The activated amino acids were then added to the deprotected resin and stirred for 1.5 h. 1.396, 0.884, and 1.009 g of lysine (Lys), glycine (Gly), and valine (Val) were activated for peptides containing valine. 1.173, 0.743, and 0.848 g of lysine, glycine and phenylalanine (Phe) were activated for peptides containing phenylalanine. The activated amino acids were then added to the deprotected resin and stirred for 1.5 h. Following the reaction, the peptide-resin slurry was drained and washed five times with DMF. After this step, the final peptide was recovered or the next amino acid was added after deprotection. After addition of the last amino acid, the resin was finally washed with DMF, DCM, methanol and hexane and dried. The peptides from the dry resins were cleaved by adding TFA/TIS (thioanisole)/water (95 mL/2.5 mL/2.5 mL) and stirring for 2 h. The peptides were collected and purified by repetitive washing and precipitation in cold ether until a white precipitate was obtained (*24*). The molecular weight of the peptides was determined by mass spectroscopy by direct injection of a 10 µL peptide solution (20 µg/mL) in methanol using 1,200 L Quadrupole MS/MS system (Varian Inc., Weston Parkway, Cary, NC, USA). Peptide solutions were dialyzed overnight against 10 mM phosphate buffer using dialysis membranes of MWCO 500.

2.3. *Dynamic light scattering (DLS)*

Hydrodynamic size and zeta potential of the complexes was determined by DLS. All peptide solutions and DNA were pre dialyzed using 500 and 3500 MWCO dialysis membranes respectively against 10 mM phosphate buffer for 12-8 h prior to preparing the complexes. DNA and peptide working solutions were mixed in predetermined proportions to obtain complexes at various N/P or +/- (*i.e.*, the ratio of positive charges from nitrogen of peptides to negative charges from the phosphate groups of DNA). The final concentration of DNA was maintained at 50 µg/mL for all the samples. The concentration of the peptides in these samples varied from 12.5 µg/mL to 500 µg/mL depending on the N/P ratio of the sample. These samples were vortexed for 10-15 sec and were kept at room temperature for 30 min for the complexes to be completely formed. Ten mM phosphate buffer of pH 7.4 that was used for this analysis was filtered through 0.45-micron filters. The size and zeta potential of peptide-DNA complexes as a function of N/P ratio were analyzed by DLS using Zeta Sizer Nano (Malvern Instruments, Westborough, MA, USA). The instrument was initially validated using the standards for size and zeta potential (ZP) provided by the manufacturer. Standard of 60 nm for size and −15mV for zeta potential were used for validation. Size and zeta potential of pDNA were also determined. Refractive index for these measurements was set at 1.335. Polydispersity index (PDI) of the samples was also estimated during size analysis. The size data from cumulant analysis and volume distribution has been compared to make final conclusions about size. Z-average diameter for peptide-DNA complexes has been reported in this study. The zeta potential was measured from the electrophoretic mobility of the samples. All the data has been expressed as mean ± standard deviation. Size analysis of peptide solutions (1 mg/mL) without pDNA was performed under similar conditions.

2.4. *Isothermal titration calorimetry (ITC)*

Thermodynamic analysis of complexation was performed by ITC (Microcal, Westborough, MA, USA). Plasmid DNA solution was diluted to get a concentration of 0.1 mg/mL using the dialysate (10 mM phosphate buffer, pH 7.4). Peptide solutions were dialyzed against 10 mM phosphate buffer, pH 7.4. Both DNA and peptide solutions were degassed before use. The buffer solution used for dilution was filtered through 0.45 micron filter. The sample cell of ITC was carefully washed with detergent solution and water. It was further rinsed with the dialysate buffer. A blank titration was performed for each peptide with the buffer in the sample cell and the peptide solution in the syringe. Final titrations were performed with DNA solution in the sample cell and the peptide solution in the syringe. Each titration was done thrice using the following ITC parameters – 20-25 injections were performed with 10 µL of peptide solution per injection. The injection duration was 12 sec and the time between injections was 120 sec. The stirring speed was set at 400 rpm. Two hundred and fifty µL syringe was used and the experiment was performed at 25°C (*11*). Data were analyzed to obtain the stoichiometry of binding, binding constant and change in enthalpy using the ITC software (MCS Origin 3.1) provided by Microcal.

3. Results and Discussion

This study involves analysis of interaction of DNA

and amphiphilic oligopeptides. Amphiphilicity was introduced by replacing some of the lysines with hydrophobic aminoacids so that the basic design of these peptides is $X_{(3-1)}$–Gly-$Lys_{(3-5)}$ where X is valine/phenylalanine/tyrosine. The presence of glycine between the charged and the hydrophobic domains gives flexibility to the peptide. Attaching neutral hydrophobic amino acids will preserve the existing positive charge of the peptide while altering the hydrophobicity. The hydrophobicity index values of valine, phenylalanine and tyrosine are 4.2, 2.8, and –1.3 kcal/mole respectively (*12*). The net charge on the peptides is +1/+3/+5. Lys_7 is the basic cationic peptide that served as a control. The peptide sequences, molecular weight, net charge are shown in Table 1. Based upon the hydrophobic nature of the attached amino acids, these peptides can be arranged in decreasing order of hydrophobicity, as shown below: Val_3-Gly-Lys_3 > Phe_3-Gly-Lys_3 > Val_2-Gly-Lys_4 > Phe_2-Gly-Lys_4 > Val-Gly-Lys_5 > Tyr_3-Gly-Lys_3 > Phe-Gly-Lys_5 > Tyr_2-Gly-Lys_4 > Tyr-Gly-Lys_5 > Lys_7.

Hydrodynamic size analysis of peptides by DLS indicates both monomodal and bimodal distribution depending on the peptide composition. Lys_7 that lacks hydrophobic amino acids forms smaller aggregates of 1.03 nm. It is very interesting to see that all the peptides with a single hydrophobic amino acid such as Val-Gly-Lys_5, Phe-Gly-Lys_5, Tyr-Gly-Lys_5, show a monomodal distribution of 219.0, 257.0, and 224.0 nm respectively. Val_3-Gly-Lys_3, which is the most hydrophobic peptide, also shows a monomodal distribution of size of 11.8 nm. All the other peptides show bimodal distribution. We believe that the propensity to form aggregates depends on the amino acid composition. The size and type of aggregates formed are the result of interplay between interactions within a single chain and interaction between different chains. The simultaneous presence of distinct interactions (*e.g.*, hydrogen bonding, electrostatic, and hydrophobic interactions) in the system leads to rich and subtle molecular self-assembly. In this study, it is important to understand the aggregation of these peptides, as it influences their interaction with pDNA and the colloidal stability of the complexes.

Some peptide-pDNA complexes show precipitation or turbidity at certain N/P (nitrogens from peptide/phosphates from pDNA) ratios. The time taken to precipitate and turbidity are discussed here along with the hydrodynamic size and zeta potential. Samples that were turbid or precipitated were not suitable for DLS measurements. In such cases, the supernatant solution of such samples was used to measure zeta potential. The hydrodynamic size and zeta potential of pDNA under the studied conditions are approximately 20 nm and –55 mV respectively.

DNA complexes of $Val_{(3-1)}$–Gly-$Lys_{(3-5)}$ type peptides exhibit a similar trend in change in size and PDI (Figure 1A-1C). DNA-(Val_3-Gly-Lys_3) complexes show a maximum size of 312.9 nm and a PDI of 0.9 at N/P 0.65 and 0.98 respectively (Figure 1A). Both size and PDI decrease gradually at higher N/P values. At N/P > 5.23 the solution of these complexes shows precipitation. At N/P 10.46 and 13.08 the sample looks turbid when prepared. The turbidity disappears when shaken and reappears with time. DNA complexes of (Val_2-Gly-Lys_4) (Figure 1B) show maximum PDI of 0.7 at N/P 3.36 and decreases drastically to 0.14 at N/P 6.72. The size increases gradually from N/P 1.26 to N/P 6.72. Precipitation is seen at N/P 10.0. These complexes do not show precipitation or visible aggregation between N/P 10.8 and16.8. However they are not stable in solution. The size of DNA-(Val–Gly-Lys_5) complexes remain almost stable between 100-150nm between N/P of 0.51 and 2.02 (Figure 1C). Then there is a drastic increase in the size to 320 nm at N/P 4.05. PDI of these complexes falls down from 0.59 to 0.39. Precipitation occurs at N/P 4.4. Val-Gly-Lys_5–DNA complexes show aggregation and precipitation within 15 min after preparation at N/P 16 and 20.5. Figure 2A shows zeta potential of DNA-Valine based peptides. At low N/P upto 4.0 the change in zeta potential is proportional to the charge of peptide. However, after the N/P at which the complexes show precipitation or turbidity, the clear supernatant was studied for zeta potential. At N/P > 5, ZP of DNA complexes of Lys_7 > (Val-Gly-Lys_5) > (Val_2-Gly-Lys_4) > (Val_3-Gly-Lys_3). We can say that for $Val_{(3-1)}$–Gly-$Lys_{(3-5)}$

Table 1. Properties of oligopeptides used in the study

Oligopeptides	Molecular weight (Calculated)	Net charge	Hydrodynamic Size (nm)	Molecular weight peak from mass spectroscopy
Val_3-Gly-Lys_3	757	+3	11.8 (99.0%)	756
Val_2-Gly-Lys_4	786	+4	42.9 (42.8%), 317.0 (57.2%)	786
Val-Gly-Lys_5	815	+5	219.0 (100%)	814
Phe_3-Gly-Lys_3	901	+3	149.0 (12.1%), 880.0 (73.0%)	900
Phe_2-Gly-Lys_4	882	+4	85.0 (19.3%), 391.0 (73.6%)	881
Phe-Gly-Lys_5	863	+5	257.0 (92.1%)	862
Tyr_3-Gly-Lys_3	949	+3	267.0 (25.3%), 26.1 (70.0%)	948
Tyr_2-Gly-Lys_4	914	+4	95.7 (30.9%), 341.0 (62.9%)	913
Tyr-Gly-Lys_5	879	+5	224.0 (100%)	878
Lys_7	914	+7	1.0 (99.00%)	913

Numbers indicated in the parenthesis for hydrodynamic size are the % volume distribution.

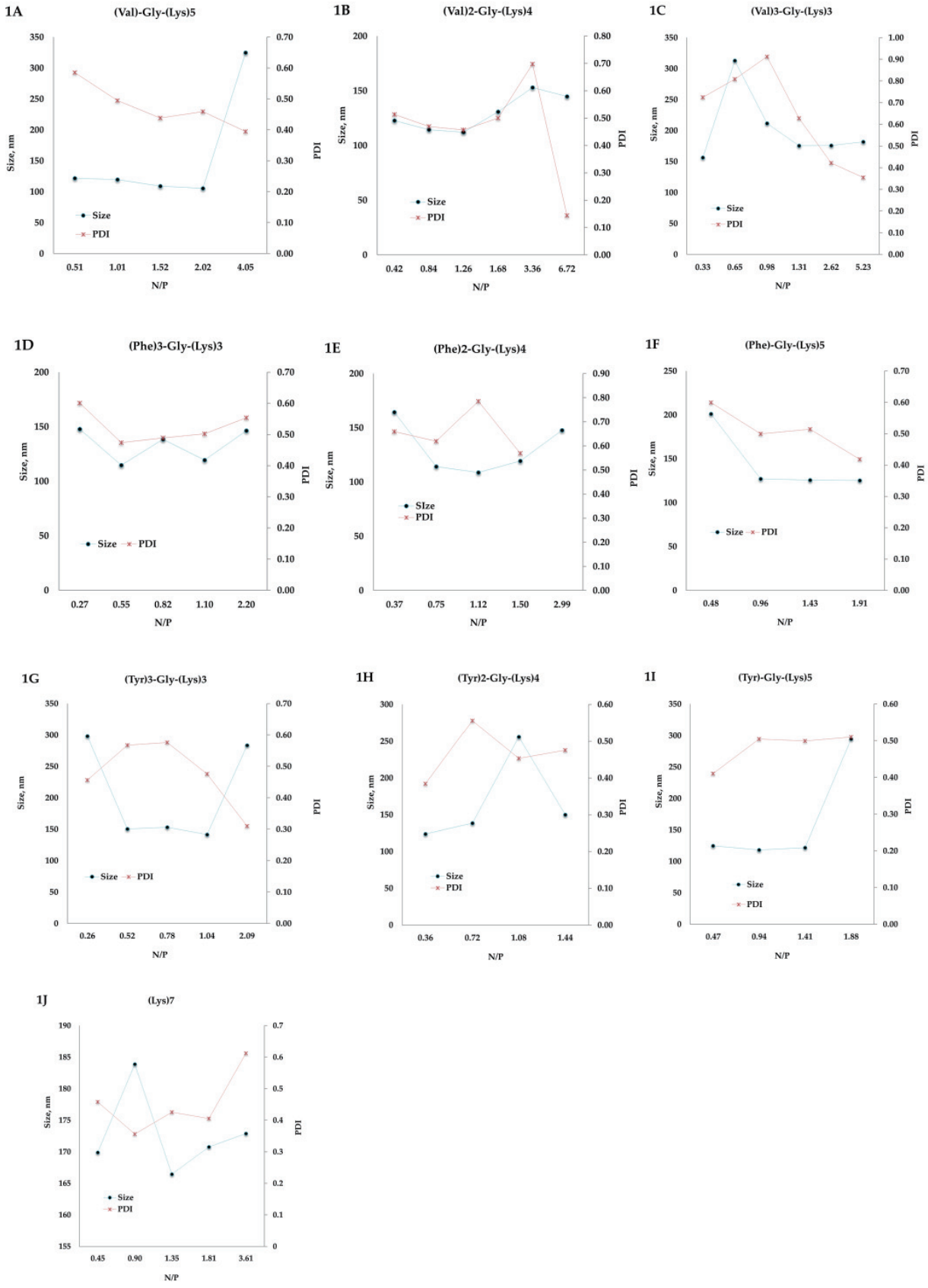

Figure 1. Hydrodynamic size and polydispersity index of plasmid DNA-peptide complexes as a function of charge.

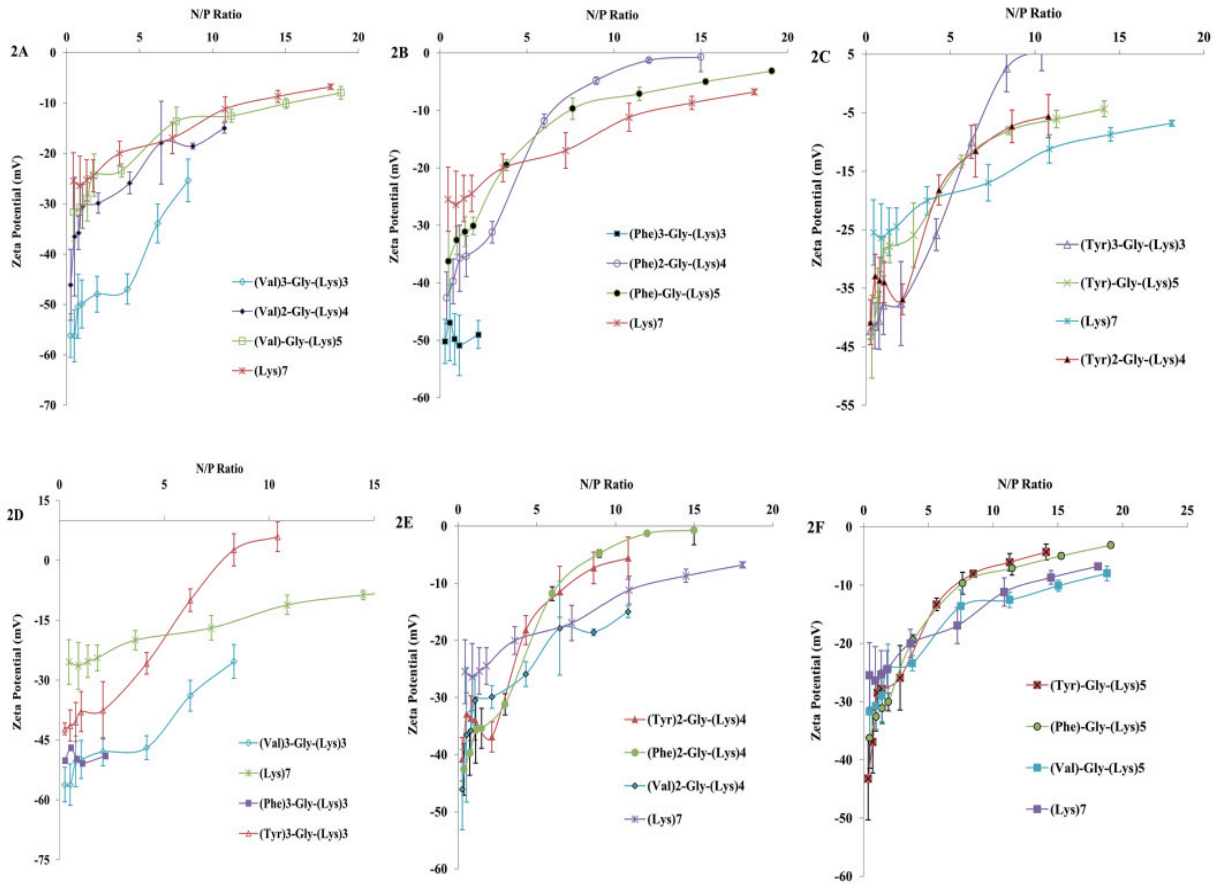

Figure 2. Change in zeta potential of plasmid DNA–peptide complexes as a function of charge.

type peptides, the size of the complexes is predominantly influenced by composition and the surface charge by charge of the peptide.

Phe_3-Gly-Lys_3–DNA complexes (Figure 1D) show a similar trend in size (100-150 nm) and PDI (0.5-0.65) between N/P 0.27 and 2.20. DLS measurements could not be made after N/P 2.20 due to turbidity that disappears by mixing but eventually returns. Precipitation is seen when the samples are left standing overnight. ΔH of 21.39 ± 6.04 cal/mole of Phe_3-Gly-Lys_3-DNA indicates predominance of hydrophobic interactions. Phe_2-Gly-Lys_4-DNA complexes (Figure 1E) show a size between 100-200 nm from N/P 0.37 to 2.99. PDI ranges between 0.5-0.7. The PDI was very high after N/P 1.50 making the sample unsuitable for DLS measurements indicating heterogenous sample. At higher N/P values, immediate precipitation of the complexes is seen. Phe-Gly-Lys_5–DNA complexes (Figure 1F) show a size between 100-200 nm from N/P 0.48 to 1.91. PDI ranges between 0.4-0.6 within the studied N/P. At N/P > 2, the samples are very turbid making DLS measurements impossible. Figure 2B shows zeta potential of DNA and $Phe_{(3-1)}$–Gly-$Lys_{(3-5)}$ type peptide complexes. Again, at low N/P the change in zeta potential is directly proportional to the charge of the peptide. DNA complexes of Phe_3-Gly-Lys_3 precipitate completely at N/P 2.0 and the solution is unsuitable for any further study. Though the net charge of Phe_2-Gly-Lys_4 is only +4, DNA-Phe2-Gly-Lys4 complexes reach near 0 zeta potential but this does not happen with Lys_7. This indicates that the surface charge and size of the DNA complexes depends on both the charge and composition of $Phe_{(3-1)}$–Gly-$Lys_{(3-5)}$ type peptides.

DNA complexes of 290 nm are formed at N/P 0.26 with Tyr_3-Gly-Lys_3 (Figure 1G) and it decreases to 141 nm at N/P 0.52 and then increases to 300 nm at N/P 2.09. The PDI increases from 0.46 to 0.6 and falls down at N/P 2.09. Samples show immediate precipitation at higher N/P values. DNA-Tyr_2-Gly-Lys_4 complexes show a maximum size at N/P 1.08 (Figure 1H). The PDI varies between 0.3 and 0.6 within the range studied. Tyr_2-Gly-Lys_4–DNA complexes, precipitate very slowly. Complete precipitation is seen after 60-75 min. Tyr-Gly-Lys_4–DNA complexes (Figure 1I) show a size of 100-150 nm between N/P 0.47 and 1.41 and drastically increase to 300 nm at N/P 1.88. The PDI also remains almost similar within N/P 0.47 and 1.88 and the complexes precipitate thereafter. DNA-Tyr_3-Gly-Lys_3 complexes even show a positive ZP after N/P 10.43. Figure 2C shows ZP of DNA and $Tyr_{(3-1)}$–Gly-$Lys_{(3-5)}$ type peptides. At very low N/P between 0.025 and 0.25, the zeta potential of DNA complexes of Lys_7 > (Tyr_3-Gly-Lys_3) = (Tyr_2-Gly-Lys_4) > (Tyr-Gly-Lys_5). A similar trend is seen until N/P 6.0 and thereafter, the

zeta potential of DNA complexes of (Tyr_3-Gly-Lys_3) > (Tyr_2-Gly-Lys_4) = (Tyr-Gly-Lys_5) > Lys_7. We can say that though the charge of the peptide influences ZP at lower concentrations of peptides, but the overall composition takes over at somepoint. This also suggests that peptide-peptide interactions play a very importnt role in modulating the properties of the complexes.

Lys_7-DNA complexes have a size bwteen 150-200 nm and PDI between 0.4 and 0.65 within the studies N/P values. Lys_7-DNA complexes (Figure 1J) show turbidity at N/P 7.22 immediately after preparation and precipitation is seen within 15-20 min after preparation between N/P 10 and 20. This indicates, that the presence of the hydrophobic aminoacids aids in keeping the complexes in solution as soluble aggregates due to peptide aggregates that might serve as surfactant micelles. This probably is the reason why there are soluble aggregates with peptides having hydrophobic amino acids. Zeta potential measurements serve as good starting point to understand this phenomenon. These differences in zeta potential combined with size analysis, of different peptides at different charge ratios suggest differing morphologies and composition of the complexes. At a very low concentration of the peptide, the complexes formed are not compact and are very heterogeneous. As the peptide concentration increases, the surfaces charge of the complexes increases, but at the expense of colloidal stability. There is an interplay between electrostatic repulsive forces and vander Waals attractive forces in colloidal stability. Assuming the attractive forces stay constant, if the electric repulsive forces are minimized by neutralization of charges on the surface of the particle, then the balance shifts in favor of net attraction and aggregation results (*13*). At low concentration of the peptide (when +/- charge ratio is less than 1), water soluble nonstoichiometric complexes form in which the content of the peptide units is lower than that of the DNA units, and that contain a net negative charge. Under these conditions the peptide chains are usually distributed among the DNA molecules. Initial ΔH of interaction of all the peptides with DNA (except Phe_3-Gly-Lys_3) is negative indicating electrostatic interaction. ΔH of interaction of most of the peptides is negative and ranges between -186.3 and -65.38 cal/mole indicating the predominance of electrostatic interactions (Table 2). The charge of the complex elevates with an increase in the peptide content, which in turn results in the amount of hydrophobic sites. At some point the complex reaches a critical composition, and the hydrophobicity increases to such an extent that further binding of the peptide should lead to precipitation of the complex. Under these conditions uneven distribution of the peptide molecules among DNA molecules occurs. This is called the disproportionation phenomenon. There is simultaneous formation of two types of complexes (non-stoichiometric and stoichiometric) that differ in the composition and solubility. At this stage, the surface charge is dependent on the interplay of the hydrophobic interactions due to Tyr/Phe/Val among peptides and with DNA. The non-stoichiometric complexes with a favorable charge composition remain in solution and the stoichiometric complex becomes insoluble because of higher content of the peptide in composition. This is evident from the precipitation seen in the peptide-DNA complexes. In the stoichiometry complex, the negative charge of the DNA is completely compensated (*14,15*). As the concentration of the peptide further increases, the portion of the stoichiometry complex grows, while the non-stoichiometric complex falls down. This is evident from precipitation and possibility of zeta potential measurement in the supernatant of the same sample for complexes at higher ratios. At higher N/P > 6.0, (Figure 2D-2F), Tyr peptides with +3/+5 charge have greater effect on zeta potential than Lys7 while those possessing +4 charge do not have a similar effect. Among peptides having +4 charges, Phe and Val containing peptides show greater impact than Lys_7 followed by Tyr peptide (Figure 2D-2F). Change in zeta potential is mainly related to neutralization of negative charges on pDNA. Zeta potential data shows that the interaction of the peptides with pDNA is dependent on both the charged and hydrophobic residues after a certain DNA-peptide composition is reached. At low concentration of the Tyr peptides, +3/+4 charges are favorable in neutralizing the positive charge on pDNA while at higher concentration of the peptides +3/+5 charge seems to be favorable. For peptides with +5 charges, presence of Phe and Val seems to be more favorable in neutralizing the charge on pDNA. This could be due to the differences in interaction of the hydrophobic amino acids with pDNA. This leads to an important conclusion that the though initial interaction of the peptide with pDNA is cationic charge dependent, eventually the orientation and interaction of the hydrophobic part of the peptide with pDNA controls the complex formation and its stability in solution.

Zeta potential was also studied at very low N/P between 0.025 and 0.25 (data not presented here). At a very low concentration of peptides, the interaction is mostly guided by the positive charge of the peptide. Lys_7-DNA complexes show maximum increase in zeta potential compared to all the other peptides. At

Table 2. Change in enthalpy for plasmid DNA-peptide interaction in pH 7.4 phosphate buffer.

Peptide	ΔH Cal/ mole
$(Val)_3$-Gly-$(Lys)_3$	-157.88 ± 14.02
$(Val)_2$-Gly-$(Lys)_4$	-279.00 ± 29.07
(Val)-Gly-$(Lys)_5$	-148.83 ± 6.46
$(Tyr)_3$-Gly-$(Lys)_3$	-65.38 ± 2.52
$(Phe)_3$-Gly-$(Lys)_3$	21.39 ± 6.04
$(Phe)_2$-Gly-$(Lys)_4$	-115.44 ± 8.18
(Phe)-Gly-$(Lys)_5$	-186.30 ± 5.09

Table 3. Thermodynamic parameters of peptide-pDNA interaction

Thermodynamic parameters	$(Val)_2$-Gly-$(Lys)_4$	(Val)-Gly-$(Lys)_5$	(Phe)-Gly-$(Lys)_5$
N	1.22 ± 0.23 (12.98)	1.67 ± 0.23 (13.91)	1.39 ± 0.04 (3.05)
K (M^{-1})	2.88×10^4 ± 2042.06 (7.09)	2.12×10^4 ± 251.66 (1.18)	2.01×10^4 ± 3394.1 (16.87)
ΔH ($Cal \cdot Mole^{-1}$)	-2.79×10^2 ± 2.07 (10.43)	-1.48×10^2 ± 6.46 (4.34)	-1.86×10^2 ± 5.09 (2.73)
ΔG ($Cal \cdot Mole^{-1}$)	-6.08×10^3 ± 41.38 (0.68)	-5.90×10^3 ± 7.05 (0.12)	-5.87×10^3 ± 100.46 (1.71)
ΔS ($Cal \cdot Mole^{-1} \cdot K^{-1}$)	19.5 ± 0.202 (1.039)	19.3 ± 0.035 (0.182)	19.1 ± 0.354 (1.86)

Standard deviations given in parenthesis.

such low N/P values, when compared to peptides with similar charges, DNA complexes show the following trend in zeta potential: Lys_7 > Tyr_3-Gly-Lys_3 > Phe_3-Gly-Lys_3 > Val_3-Gly-Lys_3; Lys_7 > Tyr_2-Gly-Lys_4 > Val_2-Gly-Lys_4 > Phe_2-Gly-Lys_4; Lys_7 > Val-Gly-Lys_5 = Phe-Gly-Lys_5 > Tyr-Gly-Lys_5. Below N/P 0.25, it can be seen that Lys7 dominates all the other peptides due to maximum cationic charge density. Among peptides having +3/+4 charges, Tyr peptides show the maximum effect on zeta potential while the presence of Tyr in +5 charged peptides leads to minimal effect on zeta potential. This indicates that the initial interaction of Tyr peptides possessing +3/+4 charges with pDNA is highly electrostatic and is favorable in neutralizing the charge.

ITC performed below the N/P of precipitation of Val_3-Gly-Lys_3, Phe_3-Gly-Lys_3, Phe_2-Gly-Lys_4, Tyr_3-Gly-Lys_3 do not show any indication of saturation of interaction with DNA. Titration of Tyr_2-Gly-Lys_4, Tyr-Gly-Lys_5 and Lys_7, into pDNA solution, shows varying binding heats indicating probability of cooperative binding. A further increase in peptide concentration results in involvement of most of the nucleic acid chains in complex formation. The ΔG values of interaction are negative indicating spontaneity of interaction and is similar for all the three peptides. The binding affinity (K) of Val_2-Gly-Lys_4 > Val-Gly-Lys_5 > Phe-Gly-Lys_5. The binding constants were found to be in the order of 10^4. This value represents moderate binding affinity. The stoichiometry for this interaction ranges from 1.22-1.67 amino group/phosphate. The change in entropy is positive. ΔS of interaction of these peptides with DNA is around 19 $cal \cdot mole^{-1}K^{-1}$ (Table 3). Stoichiometry (N) of interaction, binding constant (K), ΔG of interaction and ΔS were calculated for Val_2-Gly-Lys_4, Val-Gly-Lys_5 and Phe-Gly-Lys_5 (Table 3). Stoichiometry (N) ranges between 1.22 and 1.67. Negative ΔH and positive ΔS indicate a significant contribution of enthalpy and entropy towards free energy indicating the significance of both electrostatic and hydrophobic interactions in condensation of pDNA. Binding constants (K) of these peptides with pDNA are in the order of 2.01 to 2.88 × 10^4 indicating moderate interaction.

Conclusions

Amphiphilic peptides studied interact with pDNA to form complexes of 100-300 nm with varied stability in solution. Val and Phe peptides with +4 charges and Tyr peptides with +3/+5 charges could modulate surface potential of the peptide-pDNA complexes much better than Lys_7. Thermodynamic analysis shows spontaneous interaction between all the peptides and pDNA. Lys_7 and Tyr peptides with +4/+5 charges indicate cooperative binding with pDNA without condensation while Val_2-Gly-Lys_4, Val-Gly-Lys_5, and Phe-Gly-Lys_5 showed condensation of pDNA within the range of N/Ps studied. This study shows that separation of cationic and hydrophobic domains with a spacer amino acid can be used as a design strategy to modulate and fine-tune the hydrodynamic and thermodynamic properties of the resultant DNA complexes.

Acknowledgements

Authors would like to thanks Dr. Satishchandran, Dr. Michael Bruist and Dr. Russel DiGate for their valuable suggestions during the course of this work.

References

1. Tokunaga M, Nagao MM, Nagata M, Hazemoto N, Yotsuyanagi TJ. Pharm Sci Technol Japan. 2003; 63:71-78.
2. Tokunaga M, Hazemoto N, Yotsuyanagi T. Effect of oligopeptides on gene expression: Comparison of DNA/peptide and DNA/peptide/liposome complexes, Int J Pharm. 2004; 269:71-80.
3. Niidome T, Ohmori N, Ichinose A, Wada A, Mihara H, Hayama T, Aoyagi H. Binding of cationic α-helical peptides to plasmid DNA and their gene transfer abilities into cells. J Bio Chem. 1997; 272:15307-15312.
4. Choi HS, Kim HH, Yang JM, Shin S. An insight into the gene delivery mechanism of the arginine peptide system: Role of the peptide/DNA complex size. Biochim Biophys Acta. 2006; 1760:1604-1612.
5. Planck C, Tang MX, Wolfe AR, Szoka FC Jr. Branched cationic peptides for gene delivery: Role of type and number of cationic residues in formation and in vitro activity of DNA polyplexes. Hum Gene Ther. 1999; 10:319-332.
6. Felgner PL, Heller MJ, Lehn P, Behr JP, Szoka FC Jr. Artificial self-assembling systems for gene delivery. Conference Proceeding Series, ACS, Washington DC, USA, 1996.
7. Goparaju GN, Satishchandran C, Gupta PK. The effect of the structure of small cationic peptides on the characteristics of peptide-DNA complexes. Int J Pharm.

2008; 369:162-169.
8. Goparaju GN, Bruist MF, Satishchandran C, Gupta PK. Influence of N-terminal hydrophobicity of cationic peptides on thermodynamics of their interaction with plasmid DNA. Chem Biol Drug Des. 2009; 73:502-510.
9. Sharma R, Shivpuri S, Anand A, Kulshreshtha A, Ganguli M. Insight into the role of physicochemical parameters in a novel series of amphipathic peptides for efficient DNA delivery. Mol Pharm. 2013; 10:2588-2560.
10. Chan WC, White PD. Fmoc Solid Phase Peptide Synthesis: A practical approach. Oxford University Press, New York, USA, 2000; pp. 41-74.
11. Pierce MM, Raman CS, Nall BT. Isothermal titration calorimetry of protein-protein interactions. Methods. 1999; 19:213-221.
12. Kyte J, Doolittle RF. A simple method for displaying the hydropathic character of a protein. J Mol Biol. 1982; 157:105-132.
13. Weithoff CM, Middaugh CR. Light Scattering Techniques for Characterization of Synthetic Gene Therapy Vectors. Methods in Molecular Medicine: Non-Viral Vectors for Gene Therapy Methods and Protocols. 2001; 349-376.
14. Kabanov AV, Astafieva IV, Chikindas ML, Rosenblat GF, Kiselev VI, Severin, ES, Kabanov VA. DNA interpolyelectrolyte complexes as a tool for efficient cell transformation. Biopolymers. 1991; 31:1437-1443.
15. Kennedy MT, Pozharski EV, Rakhmanova VA, MacDonald RC. Factors governing the assembly of cationic phospholipid-DNA complexes. Biophysical J. 2000; 78:1620-1633.

(Received August 8, 2014; Revised August 20, 2014; Accepted August 24, 2014)

Original Article

DOI: 10.5582/ddt.2014.01027

Subcellular localization of KL-6 mucin in intraductal papillary mucinous neoplasm of the pancreas

Yoshinori Inagaki[1,*], Yasuji Seyama[1,2], Kiyoshi Hasegawa[1], Wei Tang[1], Norihiro Kokudo[1]

[1] *Hepato-Biliary-Pancreatic Surgery Division, Department of Surgery, Graduate School of Medicine, the University of Tokyo, Tokyo, Japan;*
[2] *Department of Surgery, Tokyo Metropolitan Bokutoh Hospital, Tokyo, Japan.*

Summary **This study aimed to clarify the expression profile of KL-6 mucin in intraductal papillary mucinous neoplasm (IPMN) and its relation to tumor malignancy. Expression of KL-6 mucin in 38 IPMNs (intraductal papillary mucinous adenoma (IPMA), 24 cases; minimally invasive intraductal papillary mucinous carcinoma (MI-IPMC), 8 cases; invasive carcinoma originating from IPMC (IC-IPMC), 6 cases) and 66 pancreatic ductal adenocarcinomas (PDACs) was evaluated immunohistochemically. IC-IPMCs and MI-IPMCs had positive staining of KL-6 mucin whereas 58% of IPMAs tested negative. Subcellular localization of KL-6 mucin varied among IPMNs whereas all of the PDAC had positive expression in the circumferential membrane and cytoplasm of cancer cells. IC-IPMCs and MI-IPMCs had a higher frequency of circumferential membrane and cytoplasmic localization of KL-6 mucin than did IPMAs. These results suggest that localization of KL-6 mucin could be used to predict the malignancy of IPMN.**

Keywords: KL-6 mucin, intraductal papillary mucinous neoplasm, invasion

1. Introduction

A dramatic change in sialoglycoconjugate expression on the surface of cancer cells is considered to play an important role in tumor progression (*1,2*). In particular, overexpression of MUC1 mucin, a transmembrane mucin glycoprotein with sialo-oligosaccharides in its extracellular tandem repeat domain (*3*), was frequently detected in various gastrointestinal cancers and suggested an association with the invasive and metastatic capacity of those adenocarcinomas (*4-7*). MUC1 mucin is also frequently detected in pancreatic ductal adenocarcinoma (PDAC) and may be related to its aggressive behavior and poor outcomes (*8,9*). However, MUC1 comes in many forms because of the variation of its carbohydrate components, and each form may have a different effect on cancer progression (*9*).

Aberrant expression or localization of KL-6 mucin, a MUC1 detected by KL-6 monoclonal antibody (mAb), was observed in various cancers of the digestive organs (*10-12*). Clinicopathological analyses suggested that subcellular localization of KL-6 mucin in the circumferential membrane and/or cytoplasm of cancer cells was significantly related to the malignant behavior of cancer, such as the presence of cancer cell invasion and metastasis. In pancreatic cancer tissue, positive KL-6 staining was detected in the cytoplasm and luminal surface of cancer cells in all tested cases (*13*). In addition, that study also noted positive KL-6 staining in 1 of 5 intraductal papillary mucinous neoplasms (IPMNs). However, IPMNs have several stages of malignancy based on the morphology and invasive characteristics of tumor cells, and subcellular localization of KL-6 mucin in IPMNs and its relation to tumor malignancy are still unclear because of the small number of patient in the previous study. In the present study, the subcellular localization of KL-6 mucin was evaluated in several histological types of IPMNs and PDACs.

Released online in J-STAGE as advance publication July 20, 2014.

**Address correspondence to:*
Dr. Yoshinori Inagaki, Hepato-Biliary-Pancreatic Surgery Division, Department of Surgery, Graduate School of Medicine, the University of Tokyo, 7-3-1 Hongo, Bunkyo-ku, Tokyo 113-8655, Japan.
E-mail: yinagaki-tky@umin.ac.jp

2. Patients and Methods

2.1. *Patients*

Tissue samples of IPMNs and PDACs were respectively collected from 38 and 66 patients who underwent pancreatoduodenectomy or distal pancreatectomy from 1994 to 2007 at the Department of Surgery of the University of Tokyo Hospital (Table 1). Patients consisted of 24 men and 14 women ages 42 to 77 years (mean ± SD, 65.9 ± 7.8). Pathological diagnosis of IPMN was classified as intraductal papillary mucinous adenoma (IPMA, $n = 24$), minimally invasive intraductal papillary mucinous carcinoma (MI-IPMC, $n = 8$), or invasive carcinoma originating from IPMC (IC-IPMC, $n = 6$). Pathological characteristics were evaluated according to the Japanese classification of pancreatic cancer from the Japan Pancreatic Society (*14*).

2.2. *Immunohistochemistry*

Sections (5 μm thick) were cut from archival formalin-fixed paraffin-embedded tissue blocks, deparaffinized, and rehydrated through a graded series of ethanol. Endogenous peroxidase activity was quenched with 0.3% hydrogen peroxidase/methanol. After incubation with 5% normal goat serum for 30 min at room temperature, the sections were then incubated with KL-6 mAb (1:200 dilution; Eisai, Tokyo, Japan) for 60 min at room temperature. After the sections were incubated with biotin-conjugated secondary antibody, the biotin-streptavidin-peroxidase complex method was performed using a commercial kit per the manufacturer's instructions (Nichirei Corp., Tokyo, Japan). 3,3'-Diaminobenzidine was used as the chromogen and haematoxylin was used as a counterstain. Negative control sections were treated without the primary antibody. Staining of KL-6 mucin in 10 random microscopic fields (or in the whole section if the slide contained < 10 fields) was observed, and tumor tissues in which > 10% of the cells displayed brown granules in subcellular structures were defined as positive. Subcellular staining patterns of KL-6 mucin were evaluated using the apical membrane, surrounding membrane, and cytoplasm, as described elsewhere (*12,15*).

Table 1. Characteristics of patients with IPMNs

Characteristics	*n* (%)
Age	
≥ 65	22 (58)
< 65	16 (42)
Gender	
Male	24 (63)
Female	14 (37)
Location of IPMN	
Pancreatic head	22 (58)
Pancreatic body/tail	16 (42)
Pathological diagnosis of IPMN	
Adenoma (IPMA)	24 (63)
Minimally invasive carcinoma (MI-IPMC)	8 (21)
Invasive carcinoma (IC-IPMC)	6 (16)

2.3. *Statistical analysis*

A χ^2 test was used to evaluate the relationship between the expression of KL-6 mucin and clinicopathological parameters. Differences of $P < 0.05$ were considered significant. StatView 5.0J (Abacus Concepts, Berkeley, CA) statistical software was used for data analyses.

3. Results

3.1. *Subcellular localization of KL-6 mucin in pancreatic tumor tissue*

Positive staining with KL-6 mAb was observed in 24 IPMNs (63%) and 66 PDACs (100%) (Figure 1). As previously noted, the expression of KL-6 mucin was categorized on the basis of subcellular localization. This varied subcellular localization of KL-6 mucin was observed in IPMNs (Figure 2). Twenty two IPMNs (58%) had positive staining in the apical surface

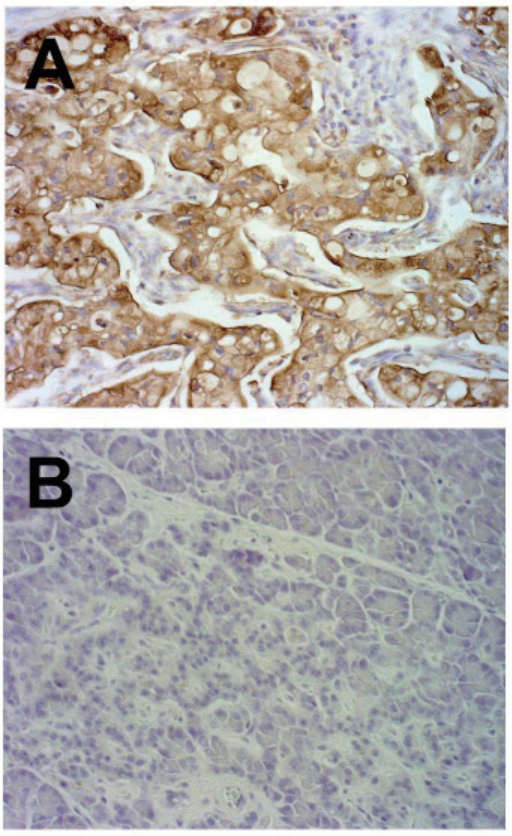

Figure 1. Typical examples of the expression profile of KL-6 mucin in PDACs (A) and non-malignant pancreatic tissue (B). Circumferential membrane and cytoplasmic localization of KL-6 mucin was frequently detected in cancer cells but not in normal pancreatic tissue. Original magnification: ×100.

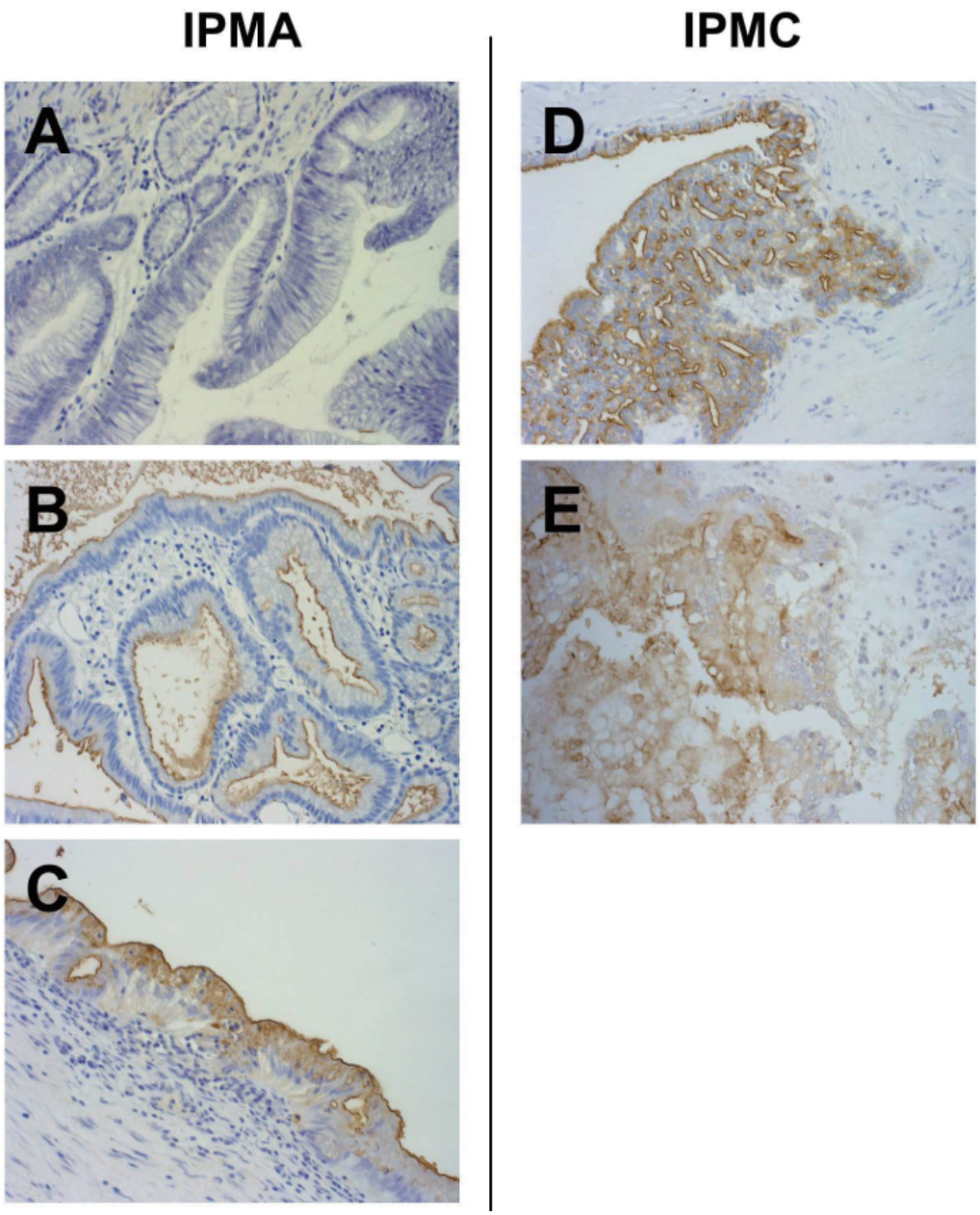

Figure 2. Typical examples of the expression profile of KΛ–6 **mucin in non-invasive and invasive types of IPMN.** IPMAs tested negative for subcellular localization of KΛ–6 mucin (**A**), the apical surface of the membrane tested positive (**B**), and the apical membrane and cytoplasm tested positive (**C**). In IPMNs in the form of carcinoma, the apical surface of the membrane, circumferential membrane and/or cytoplasm in cancer cells tested positive (**D, E**) but the extent varied among tissue. Original magnification: ×100.

of membrane, 9 (24%) had positive staining in the circumferential membrane, and 13 (34%) had positive staining in the cytoplasm of tumor cells. All PDACs had positive staining in the circumferential membrane and cytoplasm of cancer cells (Figure 1).

3.2. *Pathological significance of subcellular localization of KL-6 mucin in IPMNs*

The relationship between subcellular localization of KL-6 mucin and pathological diagnosis of IPMN is summarized in Table 2. All IC-IPMCs and MI-IPMCs had positive staining of KL-6 mucin. All 6 IC-IPMCs and 7 MI-IPMCs (88%) had positive staining in the apical surface of tumor cells. Six IPMAs (40%) had positive staining in the apical surface of tumor cells. Five

Table 2. Subcellular localization of KL-6 mucin in IPMNs

Subcellular localization of KL-6 mucin	IPMA (n = 24)	MI-IPMC (n = 8)	IC-IPMC (n = 6)
Negative	14 (58%)	0 (0%)	0 (0%)
Apical surface	9 (38%)	7 (88%)	6 (100%)
Circumferential membrane	1 (4%)	3 (38%)	5 (83%)
Cytoplasm	2 (8%)	5 (63%)	6 (100%)

IC-IPMC, invasive carcinoma originating from intraductal papillary mucinous carcinoma; IPMA, intraductal papillary mucinous adenoma; MI-IPMC, minimally invasive intraductal papillary mucinous carcinoma.

IC-IPMCs (83%) and 3 MI-IPMCs (38%) had positive staining in the circumferential membrane of tumor cells but only 1 IPMA (4%) tested positive. All 6 IC-IPMCs and 5 MI-IPMCs (63%) had positive staining in the cytoplasm of tumor cells but only 2 IPMAs (8%) tested positive. The rate of positive KL-6 mucin localization in the circumferential membrane or cytoplasm of tumor cells gradually increased in accordance with the invasive malignancy of the IPMN, and the rate of positive KL-6 mucin localization was significantly higher in IC-IPMC and MI-IPMC compared to IPMA (Table 2, $p < 0.0001$). In addition, 2 IC-IPMCs were positive for lymph node metastasis. Staining of KL-6 mucin in the circumferential membrane and cytoplasm of tumor cells was particularly intense. Age, gender, and location of IPMN were not significantly related to the subcellular localization of KL-6 mucin.

4. Discussion

This study focused on the subcellular localization of KL-6 mucin in IPMNs and PDACs and it found that MI-IPMC and IC-IPMC frequently had positive KL-6 mucin expression in the circumferential membrane or cytoplasm of tumor cells. In addition, all PDACs tested positive for KL-6 mucin expression in the circumferential membrane and/or cytoplasm of cancer cells. These results suggested that aberrant expression of KL-6 mucin is associated with the malignancy of IPMN.

KL-6 mAb was originally established from BALB/c mouse splenocytes immunized with a human pulmonary adenocarcinoma cell line, and the overexpression of KL-6 mucin has frequently been detected in this type of cancer tissue (*16*). Recent studies have also noted the aberrant expression of KL-6 mucin in various gastrointestinal cancer tissues and demonstrated its usefulness in clinicopathological diagnosis (*12*). Subcellular localization of KL-6 mucin in the circumferential membrane and/or cytoplasm of cancer cells is significantly associated with deeper invasion, lymphatic invasion, venous invasion, and lymph node metastasis (*11,17*). Therefore, KL-6 mucin may serve as a predictable marker of worse tumor behavior. Furthermore, overexpression of KL-6 mucin in the circumferential membrane and/or cytoplasm of cancer cells at the invasive front of gastric cancer tissue is significantly related to a higher incidence of metastasis and worse survival for patients (*18*). These studies suggested that aberrant localization of KL-6 mucin in the circumferential membrane and/or cytoplasm of cancer cells plays a significant role in cancer cell invasion. In the present study, localization of KL-6 mucin in the circumferential membrane and cytoplasm of tumor cells was frequently detected in MI-IPMCs or IC-IPMCs but not in IPMAs (Table 2). In addition, all PDACs that had highly invasive and metastatic characteristics had this localization of KL-6 mucin. These results suggest that localization of KL-6 mucin in tumor cells is associated with progression of IPMN.

The relationship between the expression of MUC1 and pancreatic tumor behavior has been investigated. Expression of MUC1 was clarified to depict different profiles based on the pathology of pancreatic tumors and the glycoform of MUC1 (*9*). Although PDACs had frequent expression of various forms of MUC1, hyperglycosylated or sialylated MUC1 was detected in the tissue of IPMNs but hypoglycosylated MUC1 was not (*19*). Furthermore, MUC1 expression was detected in invasive areas of IPMNs but not in non-invasive areas (*20*). Expression of specific types of MUC1 may be related to the invasive characteristics of IPMN. Therefore, the detection of MUC1 is considered to be an effective way to diagnose the behavior of IPMN, but there is little evidence on IPMNs based on invasive properties and KL-6 mucin. The present study is the first to show that the rate of detection of malignant KL-6 mucin localization increased gradually in accordance with the invasive characteristics of tumor cells in IPMNs. IC-IPMCs with lymph node metastasis had particularly strong recognition by KL-6 mAb. These results suggest a relationship between the invasive properties of pancreatic tumor cells and expression of MUC1 detected by KL-6 mAb. Cell lines derived from Muc1-null tumors had diminished invasion *in vitro* (*21*), but the role for glycoforms of MUC1 in cancer cell behavior is still unclear. Further studies should clarify the molecular biological importance of KL-6 mucin expression in IPMN cells.

In conclusion, all MI-IPMCs and IC-IPMCs had malignant localization of KL-6 mucin while 58% of IPMAs tested negative. The frequency of positive localization of KL-6 mucin gradually increased in accordance with the invasiveness of IPMNs. The surgical outcomes for IPMNs reportedly depend on their invasive characteristics (*22,23*). Precise evaluation of the invasive malignancy of IPMN is therefore crucial to a better prognosis for patients and determination of surgical strategy. Although further studies should include a larger number of patient, KL-6 mucin could help to distinguish an invasive type of IPMN from a noninvasive or minimally invasive type of IPMN.

Acknowledgements

This study was supported by Grants-in-Aid from the Japan Society for the Promotion of Science (JSPS) and the Ministry of Education, Science, Sports, and Culture of Japan. The authors also wish to thank Atsuko Takeuchi for her valuable technical assistance.

References

1. Singhal A, Hakomori S. Molecular changes in carbohydrate antigens associated with cancer. Bioessays.

1990; 12:223-230.
2 Fogel M, Altevogt P, Schirrmacher V. Metastatic potential severely altered by changes in tumor cell adhesiveness and cell-surface sialylation. J Exp Med. 1983; 157:371-376.
3 Gendler SJ, Lancaster CA, Taylor-Papadimitriou J, Duhig T, Peat N, Burchell J, Pemberton L, Lalani EN, Wilson D. Molecular cloning and expression of human tumor-associated polymorphic epithelial mucin. J Biol Chem. 1990; 265:15286-15293.
4 Nakamori S, Ota DM, Cleary KR, Shirotani K, Irimura T. MUC1 mucin expression as a marker of progression and metastasis of human colorectal carcinoma. Gastroenterology. 1994; 106:353-361.
5 Kashiwagi H, Kijima H, Dowaki S, Ohtani Y, Tobita K, Tsukui M, Tanaka Y, Matsubayasi H, Tsuchida T, Yamazaki H, Nakamura M, Ueyama Y, Tanaka M, Tajima T, Makuuchi H. DF3 expression in human gallbladder carcinoma: significance for lymphatic invasion. Int J Oncol. 2000; 16:455-459.
6 Luttges J, Feyerabend B, Buchelt T, Pacena M, Kloppel G. The mucin profile of noninvasive and invasive mucinous cystic neoplasms of the pancreas. Am J Surg Pathol. 2002; 26:466-471.
7 Zhang HK, Zhang QM, Zhao TH, Li YY, Yi YF. Expression of mucins and E-cadherin in gastric carcinoma and their clinical significance. World J Gastroenterol. 2004; 10:3044-3047.
8 Osako M, Yonezawa S, Siddiki B, Huang J, Ho JJ, Kim YS, Sato E. Immunohistochemical study of mucin carbohydrates and core proteins in human pancreatic tumors. Cancer. 1993; 71:2191-2199.
9 Yonezawa S, Higashi M, Yamada N, Yokoyama S, Goto M. Significance of mucin expression in pancreatobiliary neoplasms. J Hepatobiliary Pancreat Sci. 2010; 17:108-124.
10 Tang W, Inagaki Y, Kokudo N, Guo Q, Seyama Y, Nakata M, Imamura H, Sano K, Sugawara Y, Makuuchi M. KL-6 mucin expression in carcinoma of the ampulla of Vater: association with cancer progression. World J Gastroenterol. 2005; 11:5450-5454.
11 Guo Q, Tang W, Inagaki Y, Midorikawa Y, Kokudo N, Sugawara Y, Nakata M, Konishi T, Nagawa H, Makuuchi M. Clinical significance of subcellular localization of KL-6 mucin in primary colorectal adenocarcinoma and metastatic tissues. World J Gastroenterol. 2006; 12:54-59.
12 Inagaki Y, Xu H, Nakata M, Seyama Y, Hasegawa K, Sugawara Y, Tang W, Kokudo N. Clinicopathology of sialomucin: MUC1, particularly KL-6 mucin, in gastrointestinal, hepatic and pancreatic cancers. Biosci Trends. 2009; 3:220-232.
13 Xu H, Inagaki Y, Seyama Y, Du G, Wang F, Kokudo N, Tang W. Expression of KL-6/MUC1 in pancreatic cancer tissues and its potential involvement in tumor metastasis. Oncol Rep. 2011; 26:371-376.
14 Japan Pancreatic Society Classification of Pancreatic Carcinoma. 1st English ed. Kanehara & Co Ltd. 1996.
15 Rahn JJ, Dabbagh L, Pasdar M, Hugh JC. The importance of MUC1 cellular localization in patients with breast carcinoma: an immunohistologic study of 71 patients and review of the literature. Cancer. 2001; 91:1973-1982.
16 Kohno N, Akiyama M, Kyoizumi S, Hakoda M, Kobuke K, Yamakido M. Detection of soluble tumor-associated antigens in sera and effusions using novel monoclonal antibodies, KL-3 and KL-6, against lung adenocarcinoma. Jpn J Clin Oncol. 1988; 18:203-216.
17 Xu HL, Inagaki Y, Wang FS, Kokudo N, Nakata M, Tang W. Effect of benzyl-*N*-acetyl-alpha-galactosaminide on KL-6 mucin expression and invasive properties of a human pancreatic carcinoma cell line. Drug Discov Ther. 2008; 2:282-285.
18 Inagaki Y, Tang W, Xu H, Nakata M, Mafune K, Konishi T, Seto Y, Kokudo N. Sustained aberrant localization of KL-6 mucin and beta-catenin at the invasion front of human gastric cancer cells. Anticancer Res. 2011; 31:535-542.
19 Horinouchi M, Nagata K, Nakamura A, Goto M, Takao S, Sakamoto M, Fukushima N, Miwa A, Irimura T, Imai K, Sato E, Yonezawa S. Expression of different glycoforms of membrane mucin (MUC1) and secretory mucin (MUC2, MUC5AC and MUC6) in pancreatic neoplasms. Acta Histochem Cytochem. 2003; 36:443-453.
20 Yonezawa S, Taira M, Osako M, Kubo M, Tanaka S, Sakoda K, Takao S, Aiko T, Yamamoto M, Irimura T, Kim YS, Sato E. MUC-1 mucin expression in invasive areas of intraductal papillary mucinous tumors of the pancreas. Pathol Int. 1998; 48:319-322.
21 Besmer DM, Curry JM, Roy LD, Tinder TL, Sahraei M, Schettini J, Hwang SI, Lee YY, Gendler SJ, Mukherjee P. Pancreatic ductal adenocarcinoma mice lacking mucin 1 have a profound defect in tumor growth and metastasis. Cancer research. 2011; 71:4432-4442.
22 Suzuki Y, Atomi Y, Sugiyama M, Isaji S, Inui K, Kimura W, Sunamura M, Furukawa T, Yanagisawa A, Ariyama J, Takada T, Watanabe H, Suda K. Cystic neoplasm of the pancreas: a Japanese multiinstitutional study of intraductal papillary mucinous tumor and mucinous cystic tumor. Pancreas. 2004; 28:241-246.
23 Nara S, Onaya H, Hiraoka N, Shimada K, Sano T, Sakamoto Y, Esaki M, Kosuge T. Preoperative evaluation of invasive and noninvasive intraductal papillary-mucinous neoplasms of the pancreas: clinical, radiological, and pathological analysis of 123 cases. Pancreas. 2009; 38:8-16.

(Received June 30, 2014; Revised July 18, 2014; Accepted July 19, 2014)

Original Article

DOI: 10.5582/ddt.2014.01019

Enhancement of solubility of dexibuprofen applying mixed hydrotropic solubilization technique

Boushra Mohamed El-Houssieny[1], Esmat Zein El-Dein[2], Hussien Mohamed El-Messiry[1,*]

[1] *Department of Pharmaceutics, National Organization of Drug Control and Research, Giza, Egypt;*
[2] *Department of Pharmaceutical Technology, Faculty of Pharmacy, Tanta University, Tanta, Egypt.*

Summary **Dexibuprofen, is a practically water-insoluble nonsterodial anti-inflammatory drug which has a better anti-inflammatory effect than ibuprofen. A mixed hydrotropic solubilization technique was applied in order to improve the aqueous solubility and dissolution rate of dexibuprofen. Nine formulae were prepared using different concentrations of hydrotropic agents (sodium citrate dihydrate and urea). The prepared formulae were inspected visually for color and odor. Hygroscopicity, micromeretic properties, solubility, and pH for 1% aqueous solutions were determined. *In-vitro* dissolution studies of the different prepared formulae were performed adopting the USP XXII dissolution method type I basket apparatus method. The prepared formulae were characterized by infrared (IR) spectroscopy and differential scanning calorimetry (DSC). The prepared formulae were a white color, odorless, slightly hygroscopic and exhibited good flow properties. Formulae containing higher amounts of hydrotropic agents exhibited an increase in the pH, solubility, rate and amount of dexibuprofen released from the dissolution medium. The highest dissolution rate was achieved from the F9 formula at drug:sodium citrate dihydrate:urea ratio (1:3:7.5). IR and DSC thermograph of dexibuprofen, hydrotropic agents and prepared formulae indicated the presence of intermolecular interaction between drug and hydrotropic agents which increased solubility and dissolution rate of drug, also, there is no chemical interaction confirming the stability of the drug with hydrotropic agents.**

Keywords: Solubility, dexibuprofen, hydrotropic agents, formulae

1. Introduction

Dexibuprofen ((S)-(+)-ibuprofen), which has better anti-inflammatory effects than ibuprofen and less gastric damage belongs to class II of the Biopharmaceutical Classification System (BCS) having low water solubility which is the rate limiting step in absorption of drug (*1,2*).

Poor solubility manifests many *in vivo* limitations like incomplete release, poor bioavailability, food effects, and higher inter-subject variability. However, different efforts have been demonstrated to improve bioavailability by increasing dissolution rate, for example: formulation of solid dispersions, solid solutions, micronization, nanosuspension, cocrystal molecular encapsulation with cyclodextrin, co-solvency, hydrotropy, spray drying, solubilization with surfactant, microemulsion, salt formation, polymorphism and combinations of effects (*3*).

Hydrotropy is the term originally put forward by Neuberg (*4*), to describe the increase in the solubility of a solute by the addition of fairly high concentrations of alkali metal salts of various organic acids. However, the term has been used in the literature to designate non-micelle-forming substances, either liquids or solids, organic or inorganic, capable of solubilizing insoluble compounds. The hydrotropic solubilization process involves cooperative intermolecular interaction with several balancing molecular forces, rather than either a specific complexation event or a process dominated by a medium effect, such as co-solvency or salting-in. Hydrotropic agents have been observed to enhance the aqueous solubility of poorly water-soluble drugs

**Address correspondence to:*
Dr. Hussien Mohamed El Messiry, Department of Pharmaceutics, National Organization of Drug Control and Research, 51Wezaret El-Zeraa street, Dokki, Giza, Egypt.
E-mail: hussienelmessiry@hotmail.com

(*5,6*). The aim of our work is to prepare a soluble form of dexibuprofen which can be used in various dosage forms.

2. Materials and Methods

2.1. *Materials*

Dexibuprofen ((S)-(+)-ibuprofen) standard was purchased from Sigma-Aldrich (St. Louis, MO, USA). Dexibuprofen raw material was a gift from Future Pharmaceutical Industries (FPI) (Badr city, Cairo, Egypt). Distilled water was prepared in Central Nervous System (CNS) lab, National Organization of Drug Control and Research (NODCAR) (Dokki, Giza, Egypt). Methanol was purchased from Sigma-Aldrich (Taufkirchen, Germany). Sodium citrate dihydrate and urea were purchased from Medex (Medical Export Co Ltd, Near Naseby, Northamptonshire, UK).

2.2. *Equipment*

Analytical balance (Sartorius AG, Goettingen, Germany). Dissolution Test Station (Hanson Research, SR8 Plus, Chatsworth, USA). Drying Oven Digit (Raypa - R. Espinar, S.L., Barcelona, Spain). Differential scanning calorimetry (DSC) calorimeter (Shimadzu DSC-50, Nakagyo-ku, Kyoto, Japan). Hot plate and stirrer (Jenway, Dunmow, Essex, UK). Infrared spectrophotometer (IR Prestige-21, Shimadzu, Nakagyo-ku, Kyoto, Japan). pH meter (Jenway, Dunmow, Essex, UK). Ultrasonic water bath (Crest Ultrasonics Shanghai Ltd., Song Jiang, Shanghai, China). UV-VIS spectrophotometer (UV-2450, Shimadzu, Nakagyo-ku, Kyoto, Japan).

2.3. *Preparation of formulae*

Nine formulae were prepared using different concentrations of hydrotropic agents (sodium citrate dihydrate and urea) (Table 1). Urea and sodium citrate were accurately weighed. A minimum (possible) quantity of distilled water at 80-85^{o}C contained in a 250 mL beaker was used to dissolve the urea and sodium citrate for quick dissolution. Then, dexibuprofen was added at 30-40^{o}C and a teflon coated magnetic bead was dropped in it. Stirring of magnetic bead in beaker was started using a magnetic stirrer, maintaining the temperature at 30-40^{o}C. Dexibuprofen was completely solubilized. Stirring was continued until a semisolid mass was obtained in the beaker (after evaporation of a large quantity of water). The semisolid mass obtained was spread on several watch glasses in thin layers for quick drying. The watch glasses were kept in an oven, maintained at 40^{o}C for drying. When the mass became pulverizable, it was triturated with the help of mortar and pestle and again kept in oven for drying. After almost complete drying, the powder of the solid dispersion was passed through sieve #100 and was kept for 6 days in a desiccator containing silica gel and stored in air-tight containers.

Table 1. Composition of the prepared formulae

Formula	Dexibuprofen:Sodium citrate:Urea
F1	1:1:2.5
F2	1:2:2.5
F3	1:3:2.5
F4	1:1:5
F5	1:2:5
F6	1:3:5
F7	1:1:7.5
F8	1:2:7.5
F9	1:3 :7.5

2.4. *Evaluation of the prepared formulae*

2.4.1. *Visual inspection*

The prepared formulae were inspected visually for color and odor.

2.4.2. *Determination of loading efficacy*

A weighed amount of each of the prepared formulae equivalent to a theoretical content of 100 mg drug was accurately weighed and allowed to disintegrate completely in 100 mL distilled water, by sonicating for 20 min so as to dissolve drug and hydrotropic agents. One mL of each solution was diluted to 100 mL with distilled water, the absorbance of the solution was measured spectrophotometrically at λ_{max} 222 nm using distilled water as blank. The concentration of the drug was calculated. Each sample was assayed in triplicate and an average of three determinations was calculated.

2.4.3. *Solubility and pH*

Solubility was determined by taking an excess quantity of prepared formulae in fixed volumes of solvent (distilled water). The resulting solution was placed on a water bath sonicator for 24 h. After equilibrium the samples were centrifuged and then supernatant was filtered through a 0.45 µm filter membrane and the concentration of drug in the saturated solution in formulae under investigation was determined spectrophotometrically at λ_{max} 222 nm after appropriate dilution of the filtrate using distilled water as a blank (*3*). Each experiment was done in triplicateand an average of three determinations was calculated. The pH for 1% aqueous solution was determined.

2.3.4. *Hygroscopicity*

Hygroscopicity was measured for 10 g powder (m_1)

stored on a watch glass at 25°C, 80% R.H. for 24 h and the mass gain (m_2) was recorded (*7*). The percent mass gain (% m/m) was calculated from the following equation: $(m_2/m_1) \times 100$.

2.3.5. *In vitro dissolution studies*

In vitro dissolution studies of the different prepared formulae were performed adopting the USP XXII dissolution method type I basket apparatus method. The samples were separately encapsulated in transparent hard gelatin capsules. Five hundred mL of distilled water was used as dissolution media at 37 ± 0.5°C maintaining stirring speed at 50 rpm. The samples were withdrawn at specified time intervals and replaced with an equivalent volume of fresh dissolution medium at different time intervals to keep the volume constant and estimated spectrophotometrically at λ_{max} 222 nm for dissolving drug using distilled water as a blank (*8*). All dissolution tests were performed in triplicate and an average of three determinations was calculated.

2.3.6. *Micromeritic properties*

The prepared formulae were characterized by their micromeretic properties such as bulk and tapped densities, Hausner ratio, % compressability and angle of repose.

Determination of bulk and tapped densities: Five grams powder (*m)* in 250 mL graduated cylinder and the volume occupied (bulk volume v_b) recorded. The graduated cylinder was tapped till constant volume was obtained and the volume of powder (true or tapped volume v_t) was then recorded. The bulk density (P_b) and tapped density (P_t) were calculated in g/mL by dividing the weight over the corresponding volume. Hausner ratio and % compressability (Carr's index) were calculated using measured values for bulk density (P_b) and tapped density (P_t) according to the following equations (*9*): Hausner ratio = P_t/P_b, Ci % = $[(P_t - P_b)/P_t] \times 100$. Ci% is the % compressability of the powder. Each value reported is an average of three determinations. Determination of powder flowability: The fixed highet cone method was adopted. A cut-stem glass funnel having an internal diameter of 0.6 cm was used. The funnel was held at 2.5 cm height (h) over a flat surface. The powder sample (prepared formulae) was allowed to flow gently through the funnel until the cone was formed and reached the funnel surface orifice, powder flow was stopped and the average diameter of the formed cone (D) was determined. The area of base of cone was taken as a measure of internal friction between particles. The angle of repose was calculated by the equation (*10*): tan (α) = 2h/D. The micromeritic properties were done in triplicate and an average of three determinations was calculated.

2.3.7. *Fourier transform infrared spectroscopy (FTIR)*

An amount of 2-3 mg of dexibuprofen, sodium citrate dihydrate, urea, and prepared formulae were mixed separately with 400 mg of dry potassium bromide powder, compressed into transparent discs and their IR spectra was recorded in the wave length region of 4,000-400 cm^{-1}.

2.3.8. *DSC*

DSC was used to evaluate changes of dexibuprofen characteristic peak and heat enthalpy that might occur after mixing with hydrotropic agents. Thermograms of dexibuprofen, sodium citrate dihydrate, urea, and best formula that showed highest dissolution were recorded using Shimadzu DSC-50 calorimeter. The instrument was calibrated using purified indium (99.99%). Samples of (2-4 mg) of each substances as well as the best formula were heated under a nitrogen atmosphere as a carrier gas on an aluminum pan at a flow rate 25 mL/min and a heating rate of 10°C/min over a temperature range of 20 to 300°C.

3. Results and Discussion

3.1. *Visual inspection*

The prepared formulae were white in color and odorless.

3.2. *Determination of loading efficacy*

The entrapment efficacy (EE) of drug loading in the prepared formulae are presented in Table 2. It ranged from 96.67 to 99.79% indicating that there is no effect of hydrotropic agents on the drug.

3.3. *Solubility and pH*

Table 3 shows the phase solubility study and pH for 1% aqueous solution of the prepared formulae. It was noticed that increasing the amount of sodium citrate dihydrate and urea lead to increasing the solubility.

Table 2. Entrapment efficiency of the prepared formulae

Formula	Theoretical percent of dexibuprofen (%)	Entrapment efficiency (%)
F1	22.22	96.67
F2	18.18	94.61
F3	15.38	98.31
F4	14.28	98.67
F5	12.5	97.76
F6	11.11	96.49
F7	10.53	99.62
F8	9.52	99.79
F9	8.69	99.42

Table 3. Phase solubility, pH (1% solution) and percent mass gain of the prepared formulae

Formula	Solubility (g/100mL) for dexibuprofen in the prepared formulae	pH (1% solution)	Percent mass gain (%m/m)
F1	0.287	6.4	0.328%
F2	0.598	6.8	0.568%
F3	0.619	7.0	0.357%
F4	0.753	6.5	0.161%
F5	1.885	6.9	0.346%
F6	2.247	7.1	0.421%
F7	2.354	6.5	0.344%
F8	3.091	6.8	0.293%
F9	4.182	7.8	0.431%

This is due to increasing the concentrations of alkali metal salts of various acids (*4*), and it is concluded that the solubility of dexibuprofen increases synergistically by mixed hydrotropy. The improvement of solubility may be due to changing the crystal forms, different habit, structure and surface modification (*11*). The pH for 1% aqueous solution ranges from 6.4 to 7.8 and that increasing the amount of sodium citrate and urea lead to increasing the pH. The solubility of dexibuprofen increases slightly with an increase in pH, which may be due to the acidic nature of dexibuprofen. Thus, it can be said that, the solubility enhancement of drug by hydrotropes is not entirely due to a pH effect, but it is largely due to hydrotropy (*12*).

3.4. *Hygroscopicity*

The % mass gain of the prepared formulae is presented in Table 3. It ranges from 0.161 to 0.568 so the prepared formulae are described as slightly hygroscopic (*7*).

3.5. *In vitro dissolution studies*

The dissolution profiles of dexibuprofen from the prepared formulae were done and graphically represented in Figures 1, 2, and 3. Table 4 shows the percent dexibuprofen dissolved from different formulae. Dissolution of drug depends on physicochemical and physicotechnical properties of drug particle. These forms directly affect the absorption kinetics of drug and bioavailability of formulae. This assumes greater importance for a drug exhibiting low solubility that makes absorption to be dissolution rate limited. It is established that the modification of the polymorphic state of a compound can bring an increase in solubility (*13*). It is obvious that the percent drug dissolved from the prepared formulae containing higher amounts of sodium citrate dihydrate and urea (F7, F8, and F9) (92.46, 92.67, and 97.57% after 10 min) which is higher than the percent drug dissolved from the prepared formulae containing lower amounts of sodium citrate dihydrate and urea (F1, F2, and F3) (53.47, 54.83, and 65.97% after 20 min). The improvement of dissolution

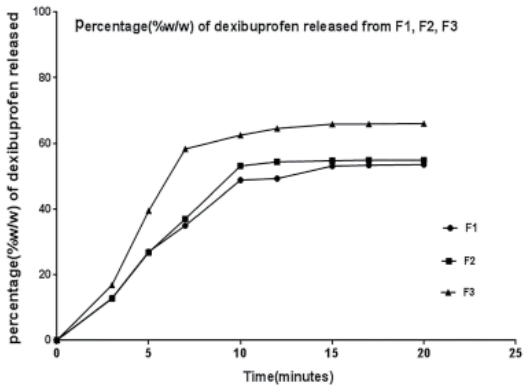

Figure 1. *In vitro* release profile of dexibuprofen from F1, F2, and F3 formulae. 500 mL distilled water was used as dissolution media at 37 ± 0.5°C while maintaining stirring speed at 50 rpm. Samples were estimated spectrophotometrically at λ_{max} 222 nm for dissolving drug in triplicate and an average of three determinations was calculated.

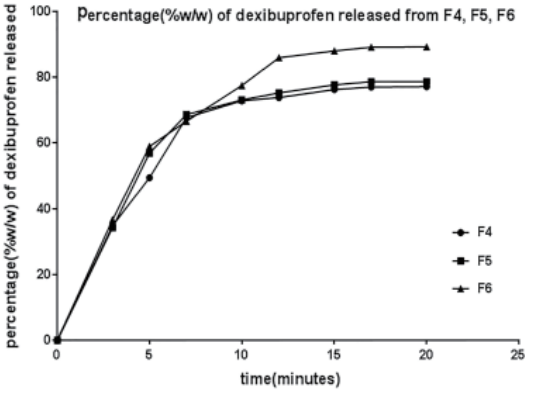

Figure 2. *In vitro* release profile of dexibuprofen from F4, F5, and F6 formulae. 500 mL distilled water was used as dissolution media at 37 ± 0.5°C while maintaining stirring speed at 50 rpm. Samples were estimated spectrophotometrically at λ_{max} 222 nm for dissolving drug in triplicate and an average of three determinations was calculated.

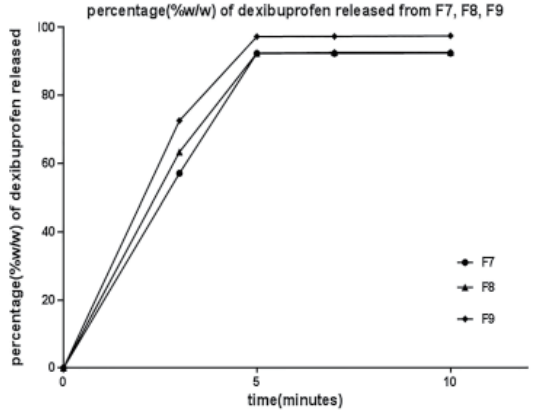

Figure 3. *In vitro* release profile of dexibuprofen from F7, F8, and F9 formulae. 500 mL distilled water was used as dissolution media at 37 ± 0.5°C while maintaining stirring speed at 50 rpm. Samples were estimated spectrophotometrically at λ_{max} 222 nm for dissolving drug in triplicate and an average of three determinations was calculated.

Table 4. *In-vitro* release of dexibuprofen from the prepared formulae

	Percentage (% w/w) of dexibuprofen released after the following time intervals in minutes							
Formula	3	5	7	10	12	15	17	20
F1	12.82	26.97	34.95	48.75	49.23	53.04	53.3	53.47
F2	12.70	26.8	36.99	53.1	54.39	54.64	54.83	54.83
F3	16.82	39.45	58.24	62.46	64.49	65.81	65.85	65.97
F4	34.85	49.49	67.74	72.86	73.83	76.28	77.02	77.19
F5	34.22	56.93	68.66	73.12	75.26	77.72	78.68	78.71
F6	36.64	59	66.64	77.52	85.98	88.03	89.14	89.24
F7	57.14	92.36	92.38	92.46				
F8	63.4	92.43	92.6	92.67				
F9	72.63	97.33	97.36	97.57				

Table 5. Micromeritic properties of the prepared formulae

Formula	Bulk volume (mL)	Tapped volume (mL)	Bulk density (g/mL)	Tapped density (g/mL)	Hausner ratio	Compressibility (%)	Tan θ	Angle of repose (degrees)
F1	228	202	0.44	0.50	1.13	11.40	0.50	31.30
F2	227	198	0.44	0.51	1.15	12.78	0.54	34.42
F3	223	197	0.45	0.51	1.13	11.66	0.50	31.30
F4	233	207	0.43	0.48	1.13	11.16	0.51	32.27
F5	235	208	0.43	0.48	1.13	11.49	0.53	33.26
F6	224	199	0.45	0.50	1.13	11.16	0.51	32.27
F7	229	203	0.44	0.49	1.13	11.35	0.50	31.30
F8	222	196	0.45	0.51	1.13	11.71	0.51	32.27
F9	225.5	200.5	0.44	0.50	1.12	11.09	0.50	31.30

behavior could be attributed to solubilization of the drug using hydrotropic agents (*8*). The faster dissolution could be due to better solubility of the prepared formulae that contains higher amounts of hydrotropic agents because increasing the amount of hydrotropic agents in the formulae leads to increased solubility and dissolution rate.

3.6. *Micromeritic properties*

The results of micromeretic properties of the prepared formulae are shown in Table 5. Bulk densities ranged from 0.43 to 0.45 g/mL and tapped densities ranged from 0.48 to 0.51 g/mL. Hausner ratio values ranged from 1.13 to 1.15 indicating low to moderate inter-particle friction and thus good flow properties (*14*). They showed good flow with respect to average % compressibility which ranged from (11.09 to 11.71%). Also, the angle of repose ranged from 31.30^0 to 34.42^0 indicating good flow properties (*15*).

3.7. *Fourier transform infrared spectroscopy (FTIR)*

The collected FTIR of plain dexibuprofen drug, sodium citrate dihydrate, urea and the prepared formulae are shown in (Figure 4). The main peaks characteristic of the drug are identical and well identified in the prepared formulae. This can be summarized: prominent peaks at 3,087, 1,707, 1,406, 1,050 cm^{-1} corresponding to O-H stretching, C=O stretching, C-C stretching, O-H bending respectively. The FTIR showed no changes occurred in the chemical nature of drug indicating absence of chemical interaction between drug and hydrotropic agents and so, confirming drug stability. From these results, it can be speculated that a drug-hydrotropic agent hydrogen bond existed in this formula and caused reduced drug recrystallization (*16*), also intermolecular interaction between drug and hydrotropic agents occurred (*5,6*).

3.8. *DSC*

DSC pattern of plain dexibuprofen, sodium citrate dihydrate, urea and the F9 formula are recorded in Figure 5. It is clear that, the DSC of plain dexibuprofen drug showed an endothermic peak at onset of 47.25°C reaching a peak at 56.51°C, an endset of 66.49°C and the enthalpy was 210.40 J/g while hydrotropic agents; sodium citrate and urea showed an endothermic peak at 169.8°C and 138.53°C, respectively. The endothermic peak of drug is related to its melting point. There was a slight difference in melting endotherms of selected formulae as well as decreasing intensity and loss of sharpness compared to that of pure drug (drug = 62.52°C, sodium citrate dehydrate = 143.65°C, urea = 103.05°C). These results might be explained in terms of a presence of intermolecular interaction between drug and hydrotropic agents. Basically the thermal process of any mixture is the sum of individual components. However, there was invariably very little

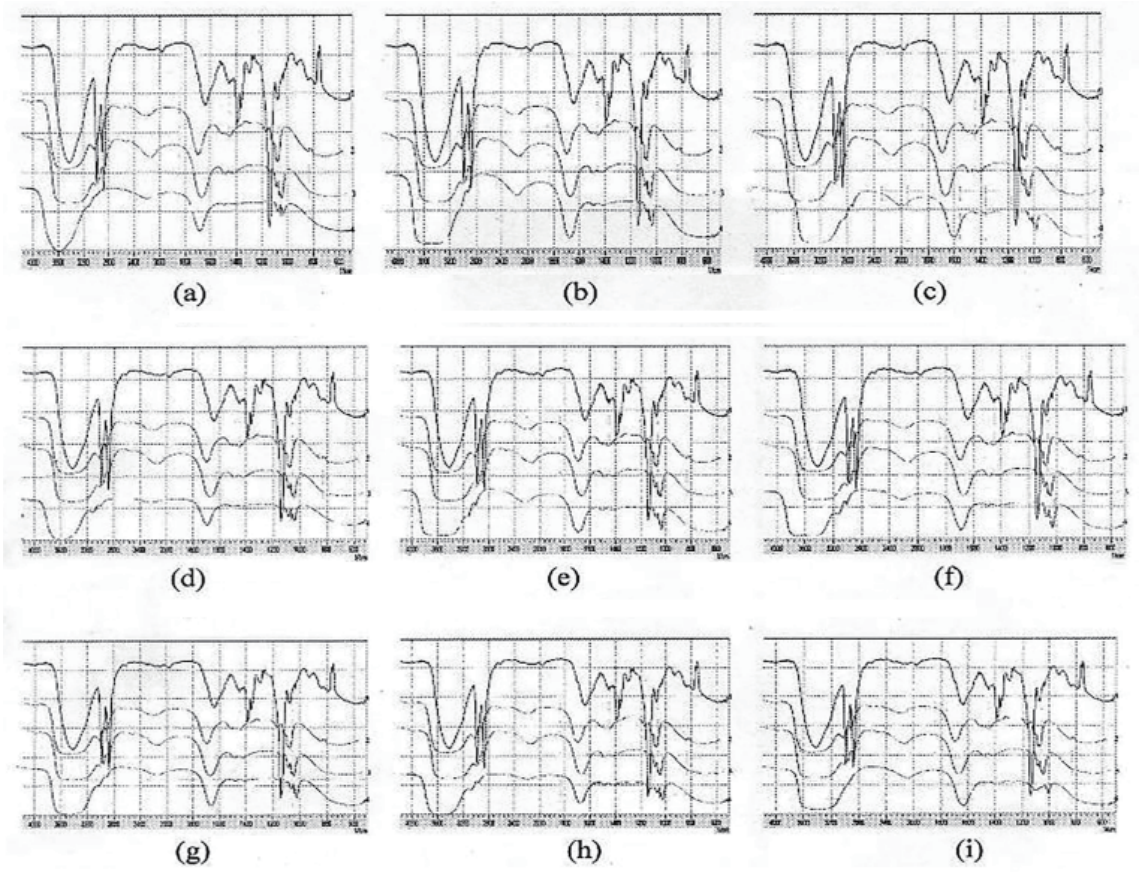

Figure 4. IR spectroscopy for dexibuprofen (1), sodium citrate dihydrate (2), urea (3) and formulae (4). An amount of 2-3 mg of dexibuprofen, sodium citrate dihydrate, urea, and prepared formulae were mixed separately with 400 mg of dry potassium bromide powder, compressed into transparent discs and their IR spectra was recorded in the wave length region of 4,000-400 cm^{-1}. **(a)** IR spectroscopy for dexibuprofen, sodium citrate dihydrate, urea, and F1. **(b)** IR spectroscopy for dexibuprofen, sodium citrate dihydrate, urea and F2. **(c)** IR spectroscopy for dexibuprofen, sodium citrate dihydrate, urea, and F3. **(d)** IR spectroscopy for dexibuprofen, sodium citrate dihydrate, urea, and F4. **(e)** IR spectroscopy for dexibuprofen, sodium citrate dihydrate, urea, and F5. **(f)** IR spectroscopy for dexibuprofen, sodium citrate dihydrate, urea and F6. **(g)** IR spectroscopy for dexibuprofen, sodium citrate dihydrate, urea, and F7. **(h)** IR spectroscopy for dexibuprofen, sodium citrate dihydrate, urea, and F8. **(i)** IR spectroscopy for dexibuprofen, sodium citrate dihydrate, urea, and F9.

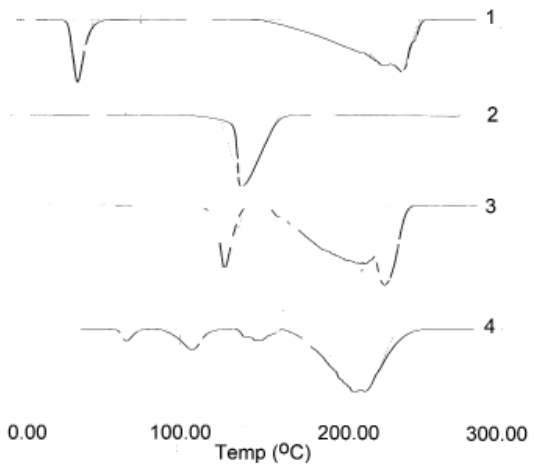

Figure 5. DSC for dexibuprofen, sodium citrate dihydrate, urea, and F9 formula. (1) dexibuprofen, **(2)** sodium citrate dihydrate, **(3)** urea, **(4)** F9. The instrument was calibrated using purified indium (99.99%). Samples of (2-4 mg) of each substance as well as the best formula were heated under a nitrogen atmosphere as a carrier gas on an aluminum pan at flow rate 25 mL/min and a heating rate of 10°C/min over a temperature range of 20 to 300°C.

change in transition temperature when mixing two or more components. When two substances are mixed, the purity of each may be reduced and generally very slight lower melting endotherms may result (*17*). This explains the very slight shift drug hydrotropic agent peak. Previous work (*18*), accepts small events and considers them to not represent any determinable interaction. This could be due to differences in moisture content of samples (*19*). Also, some changes in the peak shape and height to width ratio can be seen because of possible differences in the mixture sample geometry (*20*). The observed change in enthalpy indicates a change in crystallinity of the drug (*21*), resulting in an increase in dissolution rate.

In conclusion, the mixed hydrotropic solubilization technique significantly influenced solubilization of dexibuprofen which is practically insoluble thus contributing to dissolution improvement. Increasing the amount of hydrotropic agents leads to an increase in pH, solubility, rate and amount of dexibuprofen release from the dissolution medium. The highest dissolution

rate was achieved from F9 formula at drug: hydrotropic agent ratio 1:3:7.5. The prepared formulae are slightly hygroscopic and show good flow properties. Drug stability with hydrotropic agents and intermolecular interaction between them has been confirmed by FTIR and DSC results.

Acknowledgements

This work was supported by a grant from National Organization of Drug Control and Research and Department of Pharmaceutical Technology, Faculty of Pharmacy, Tanta University.

References

1. Adams SS, Bresloff P, Mason CG. Pharmacological differences between the optical isomers of ibuprofen evidence for metabolic inversion of the (-) isomer. J Pharm Pharmacol. 2004; 28:256-257.
2. Bomabello A, Galmozzi MR, Canaparo R, Isaia GC, Serepe L, Muntoni E. Dexibuprofen (S(+)-Isomer Ibuprofen) reduces gastric damage and improves analgesic anti-inflammatory effects in rodents. Anesth Analg. 2003; 97:402-408.
3. Amit K, Mahalaxmi RP, Srinivas, Deepak K. Enhancement of solubility and dissolution of poorly soluble drug: Ketoprofen as a model drug. J Chem Pharm Res. 2011; 3:268-276.
4. Neuberg C. Hydrotropy. Biochem Z. 1961; 76:107-109.
5. Maheshwari RK. Analysis of frusemide by application of hydrotropic solubilization phenomenon. Indian Pharmacist. 2005; 4:55-58.
6. Maheshwari RK. Mixed hydrotropy in spectrophotometric analysis of poorly water-soluble drug. Indian Pharmacist. 2007; 6:66-67.
7. Niazi S. Physicochemical properties affecting bioequivalence. In: Handbook of Bioequivalence Testing. Informa Healthcare, Mortimer Street, London, UK, 2007; pp. 181-182.
8. Rajesh K, Rahul Nair, Rajalakshmi R, Latha P, Arun kumar KS, Nama V. Inclusion complex of dexibuprofen and its in-vitro and in-vivo evaluation. Int Bio Pharm Res. 2011; 2:34-38.
9. Aulton ME. Pharmaceutics. The science of dosage form design (Taylor k, ed.). Churchill Livingstone, London, UK, 2002; p. 197.
10. Bastos MO, Friedrich RB, Beck CR. Effects of filler-binders and lubricants on physicochemical properties of tablets obtained by direct compression: A 22 Factorial Design. Lat Am J Pharm. 2008; 27:578-583.
11. Badawy AA, El-Nabarawwy MA, El-Houssieny BM, Kamel MM. Formulation and evaluation of albendazole solid dispersion. J Drug Res. 2011; 32:11-21.
12. Rajesh KM, Arpna I. Formulation and evaluation of aceclofenac injection made by mixed hydrotropic solubilization technique. Iran J Pharm Res. 2010; 9:233-242.
13. El-Houssieny BM, Soliman II, Mansour MM. Preparation and evaluation of etodolac spherical agglomerate crystals prepared by the quasi emulsion solvent diffusion method. Bull Fac Pharm Cairo Univ. 2009; 47:85-102.
14. Shahi SR, Agrawa GR, Shinde NV, Shaikh SA. Formulation and in-vitro evaluation of orodispresible tablets of etoricoxib with emphasis on comparative functionality evaluation of three classes of superdisintegrants. Russ J Chem. 2008; 1:292-300.
15. European Pharmacopoeia. Sixth Edition. Council of Europe, 67075 Strasbourg Cedex, France, 2007; pp. 320-321.
16. Silverstein RM. Spectrophotometric Identification of Organic Compounds. John Wiley and Sons, New York, USA, 1981; p. 112.
17. Botha SA, Lotter AP. Compatibility study between atenolol and tablet excipient using differential scanning calorimetery. Drug Dev Ind Pharm. 1990; 19:235-258.
18. Wells JI. Pharmaceutical Preformulation. The physicochemical properties of drug substances. Ellis Horwood Ltd, Chichester, UK, 1988; pp. 86-102.
19. Biliaderis CG. Structures and phase transitions of starch in food systems. Food Tech. 1992; 46:98-109.
20. Duvall RN, Koshy KT, Dashiell RE. Comparative evaluation of dextrose and spray dried lactose in direct compression system. Int J Pharm Sci. 1965; 54:1196-1200.
21. Ford JL, Stewart AF, Dobois JL. The properties of solid dispersion of indomethacin or phenylbutazone in polyethylene glycol. Int J Pharm. 1986; 28:11-22.

(Received April 7, 2014; Revised August 13, 2014; Accepted August 22, 2014)

Original Article

DOI: 10.5582/ddt.2014.01030

Formulation, optimization, and evaluation of a transdermal patch of heparin sodium

Rakesh P. Patel*, Dipika R. Gaiakwad, Nikunjana A. Patel

S. K. Patel College of Pharmaceutical Education and Research, Ganpat University, Ganpat vidyanagar, Gujarat, India.

Summary **The purpose of this research was to develop a matrix-type transdermal therapeutic system containing drug heparin sodium with different ratios of hydrophilic polymeric systems by the solvent evaporation technique by using 30% (w/w) of PEG 400 LR to the dry polymer weight, incorporated as plasticizer. Different concentrations of oleic acid and isopropyl myristate were used to enhance the transdermal permeation of heparin sodium. The physicochemical compatibility of the drug and the polymers studied by differential scanning calorimetry and infrared spectroscopy suggested absence of any incompatibility. Formulated transdermal films were physically evaluated with regard to thickness, weight variation, drug content, flatness, tensile strength, folding endurance, percentage of moisture content and water vapour transmission rate. All prepared formulations indicated good physical stability. *In-vitro* permeation studies of formulations were performed by using diffusion cell apparatus. Formulation prepared with hydrophilic polymer containing permeation enhancer showed best *in-vitro* skin permeation through Wistar albino rat skin as compared to all other formulations. Formulation F9 showed highest flux among all the formulations and 1.369-fold enhancements in drug permeation. These results indicate that the formulation containing 10% of oleic acid with 10% isopropyl myristate give better penetration of heparin sodium through rat skin.**

Keywords: Heparin sodium, transdermal patch, permeation enhancer, *in-vitro* permeation study

1. Introduction

Transdermal drug administration generally refers to topical application of agents to healthy intact skin either for localized treatment of tissues underlying the skin or for systemic therapy. For transdermal products the goal of dosage design is to maximize the flux through the skin into the systemic circulation and simultaneously minimize the retention and metabolism of the drug in the skin (*1*). Transdermal drug delivery has many advantages over the oral route of administration such as improving patient compliance in long term therapy, bypassing first-pass metabolism, sustaining drug delivery, maintaining a constant and prolonged drug level in plasma, minimizing inter- and intra patient variability, and making it possible to interrupt or terminate treatment when necessary (*2,3*).

Heparin sodium (HS) inhibits reactions that lead to the clotting of blood and the formation of fibrin clots both *in-vitro* and *in-vivo*. HS acts at multiple sites in the normal coagulation system. Small amounts of heparin in combination with antithrombin III (heparin cofactor) can inhibit thrombosis by inactivating activated factor X and inhibiting the conversion of prothrombin to thrombin. Once active thrombosis has developed, larger amounts of HS can inhibit further coagulation by inactivating thrombin and preventing conversion of fibrinogen to fibrin. HS also prevents the formation of a stable fibrin clot by inhibiting the activation of the fibrin stabilizing factor (*4*).

Intravenous or topical administration of HS has many side effects including pain, swelling, inflammation, irritation at the site of administration and even frequent doses of drug can cause hemotosis which can be avoided by preparing a transdermal patch. The bioavailability of HS transdermal patch is l-2% that

**Address correspondence to:*
Dr. Rakesh P. Patel, Pharmaceutics & Pharmaceutical Technology Department, S. K. Patel College of Pharmaceutical Education and Research, Ganpat University, Ganpat vidyanagar-384012, Gujarat, India.
E-mail: raka_77us@yahoo.com

of intravenous HS, with an elimination half life of 8 h compared to 1.5 h for *i.v.* HS hence a transdermal patch gives a sustained release profile which avoids severe patient pain and frequent application of drug in the case of topical gel.

There are reports describing the use of hydroxypropyl cellulose (HPC), hydroxyethyl cellulose (HEC), hydroxypropyl methylcellulose (HPMC) in transdermal patches and ophthalmic preparations (*5-7*) and eudragit RSPO transdermal delivery systems as well as other dosage forms for controlled release of drugs (*8-10*). HPC, HEC, and HPMC are freely water soluble, whereas eudragit RSPO is hydrophobic. Transdermal delivery systems were prepared using all of these methods to study the effect of the hydrophilic and hydrophobic nature of polymer on release of HS. A large number of fatty acids and their esters have been used as permeation enhancers. Oleic acid has been shown to be effective as a permeation enhancer for many drugs, for example increasing the flux of salicylic acid 28-fold and 5-fluorouracil flux 56-fold, through human skin membranes *in-vitro* (*11,12*). It has also been used for ketoprofen (*13*), flurbiprofen (*14*), 5-FU, estradiol (*12*), zalcitabine, didanosine, zidovudine (*15*), *etc*.

The aims of the present study were to (*i*) prepare transdermal patches of HS using hydrophilic and hydrophobic polymers; (*ii*) optimize transdermal patch formulation using 3^2 full factorial design; (*iii*) study the *in-vitro* diffusion behavior of prepared transdermal patch formulations in the presence and absence of penetration enhancer, and (*iv*) study skin irritation of HS on Albino Wistar rats. The purpose was to provide delivery of the drug at a controlled rate across intact skin.

2. Materials and Methods

2.1. *Materials*

HS was received as a gift sample from Intas Pharmaceutical Ltd., Ahmedabad, Gujarat, India. HPC and HEC were a generous gift from Famycare Pvt. Ltd., Ahmedabad, Gujarat, India and HPMC was a gift from Acme Pharma Ltd., Ganpat Vidhyanagar, Gujarat, Inida. Eudragit RSPO was purchased from Vikram Thermo Ltd., Mehsana, Gujarat, India. Oleic acid (OA), polyethylene glycol (PEG) 400 LR and Di-n-butyl-phthalate (DBP) were procured from Sigma Chemicals Ltd., Ahmedabad, Gujarat, India. Other materials used in the study (chloroform, methanol, dichloromethane, glycerol, potassium dihydrogen phosphate, *etc*.) were of analytical grade. Milli-Q water was used throughout the study.

2.2. *Investigation of physicochemical compatibility of drug and polymer*

The physicochemical compatibility between HS and polymers used in the patch was studied using differential scanning calorimetry (DSC-Shimadzu 60 with TDA trend line software, Shimadzu Co., Kyoto, Japan) and Fourier transform infrared (FTIR- 8300, Shimadzu Co., Kyoto, Japan) spectroscopy.

In DSC analysis, the samples were weighed (5 mg), hermetically sealed in flat bottom aluminum pans, and heated over a temperature range of 50 to 300°C at a constant increasing rate of 10°C/min in a nitrogen atmosphere (50 mL/min). The thermograms obtained for HS, polymers, and physical mixtures of HS with polymers were compared. The infrared (IR) spectra were recorded using an FTIR by the KBr pellet method and spectra were recorded in the wavelength region between 4,000 and 400 cm^{-1}. The spectra obtained for HS, polymers, and physical mixtures of ACF with polymers were compared.

2.3. *Preparation of transdermal films*

Transdermal patches containing HS were prepared by the solvent evaporation technique in cylindrical glass molds with both sides open (*16*). The backing membrane was cast by pouring a 2% (m/V) polyvinyl alcohol (PVA) solution followed by drying at 60°C for 6 h. The drug reservoir was prepared by dissolving polymer in Milli-Q water. PEG 400 LR 30% (w/w of dry polymer composition) was used as a plasticizer. Ten mg of the drug was added into the homogeneous dispersion with slow stirring on a magnetic stirrer. The uniform dispersion was cast on a PVA backing membrane and dried at room temperature (Table 1). The films were stored between sheets of wax paper in a desiccator.

2.4. *Physicochemical characterization of films*

2.4.1. *Thickness*

The thickness of patches was measured at three different places using a micrometer (Mitutoyo Co., Japan) and mean values were calculated (*16*).

2.4.2. *Weight variation*

Mass variation of patches was measured by individually weighing randomly selected patches. Such determinations were carried out for each formulation (*17*).

2.4.3. *Drug content*

Patches of specified area (1 cm^2) were dissolved in 5 mL of Phosphate buffer pH 7.4 and the volume was made up to 10 mL with the same buffer. A blank was prepared using a drug-free patch treated similarly. The solutions were filtered through a 0.45 µm membrane,

Table 1. Composition of transdermal patches

Formulation code	PVA (backing membrane)	HEC	HPC	HPMC K4	HPMC K15	HPMC K15: RS 100	Oleic acid	PEG 4000 LR	Water
HS 1	2%	3.0%	-	-	-	-	0.2 mL		q.s.
HS 2	2%	4.0%	-	-	-	-	0.2 mL		q.s.
HS 3	2%	-	3.0%	-	-	-	0.2 mL		q.s.
HS 4	2%	-	4.0%	-	-	-	0.2 mL		q.s.
HS 5	2%	-	-	2.0%	-	-	0.2 mL		q.s.
HS 6	2%	-	-	3.0%	-	-	0.2 mL	30 % w/v	q.s.
HS 7	2%	-	-	4.0%	-	-	0.2 mL	of total ploymer	q.s.
HS 8	2%	-	-	-	2.0%	-	0.2 mL	composition	q.s.
HS 9	2%	-	-	-	3.0%	-	0.2 mL		q.s.
HS 10	2%	-	-	-	4.0%	-	0.2 mL		q.s.
HS 11	2%	-	-	-	-	3:7	0.2 mL		q.s.
HS 12	2%	-	-	-	-	5:5	0.2 mL		q.s.
HS 13	2%	-	-	-	-	7:3	0.2 mL		q.s.

Note: * 30 % w/w of dibutyl phthalate to the polymer weight, incorporated as plasticizer.

diluted suitably and absorbance was read at 201 nm in a double beam UV-Visible spectrophotometer.

2.4.4. *Flatness*

Three longitudinal strips were cut out from each film: 1 from the center, 1 from the left side, and 1 from the right side. The length of each strip was measured and the variation in length because of non-uniformity in flatness was measured by determining percent constriction, with 0% constriction equivalent to 100% flatness (*18*).

2.4.5. *Folding endurance*

Folding endurance was determined by repeatedly folding one film at the same place until it broke. The number of times the film could be folded at the same place without breaking/cracking gave the value for folding endurance (*19*).

2.4.6. *Tensile strength*

In order to determine the elongation as tensile strength, the polymeric patch was pulled by means of a pulley system; weights were gradually added to the pan to increase the pulling force till the patch was broken. The elongation *i.e.* the distance traveled by the pointer before break of the patch was noted with the help of a magnifying glass on the graph paper, and tensile strength was calculated as $kg \cdot cm^{-2}$.

2.4.7. *Percentage of moisture content*

The films were weighed individually and kept in desiccators containing activated silica at room temperature for 24 h. Individual films were weighed repeatedly until they showed a constant weight. The percentage of moisture content was calculated as the difference between initial and final weight with respect to final weight (*20*).

2.4.8. *Water vapor transmission rate (WVTR)*

WVTR is defined as the quantity of moisture transmitted through a unit area of film in unit time (*21*). Glass cells were filled with 2 g of anhydrous calcium chloride and a film of specified area was affixed onto the cell rim. The assembly was accurately weighed and placed in a humidity chamber (80 ± 5% RH) at 27 ± 2°C for 24 h.

2.5. *In-vitro skin permeation studies*

In-vitro skin permeation studies were performed by using a Diffusion Cell Apparatus (EDC-07) with a receptor compartment capacity of 12 mL. Excised rat abdominal skin (Wistar albino) was mounted between the donor and receptor compartment of the diffusion cell. The formulated patches were placed over the skin and covered with paraffin film/or having backing layer. The receptor compartment of the diffusion cell was filled with phosphate buffer pH 7.4. The solution in the receptor compartment was constantly and continuously stirred using magnetic beads at 50 rpm; the temperature was maintained at 37 ± 0.5°C. Samples were withdrawn at different time intervals and analyzed for drug content spectrophotometrically. The receptor phase was replenished with an equal volume of phosphate buffer pH 7.4 at each sample withdrawal. The cumulative percentages of drug permeated per square centimeter of patches were plotted against time.

2.6. *Full factorial design*

A 3^2 randomized full factorial design was used in the present study. In this design two factors were evaluated, each at 3 levels, and experimental trials were performed at all 9 possible combinations. The amount of isopropyl myristate (X_1) and the amount of oleic acid (X_2) were selected as independent variables. Drug release at 10 h was selected as dependent variable. The design layout is depicted in Table 4.

2.7. *Permeation data analysis*

The flux ($\mu g \cdot cm^{-2} h^{-1}$) of HS was calculated from the slope of the plot of the cumulative amount of HS permeated per cm^2 of skin at steady state against time using linear regression analysis (*22,23*).

The steady state permeability coefficient (K_p) of the drug through rat epidermis was calculated by using the following equation (*24*): $Kp = J/C$ (**1**), where J is the flux and C is the concentration of ACF in the patch. The enhancing effect of penetration enhancer was calculated in terms of enhancement ratio (ER), and was calculated by using the following equation (*25*): *ER* = (*Kp with penetration enhancer*)/(*Kp without penetration enhancer*) (**2**).

2.8. *Kinetic modeling of drug release*

To analyze the mechanism of drug release from the patches, the release data were fitted to the following equations. Zero-order equation, $Q = K_0 t$ (**3**), where Q is the amount of drug released at time t, and k_0 is the release rate. First-order equation, $\ln(100 - Q) = \ln 100 - k_1 t$ (**4**), where Q is the percent of drug release at time t, and k_1 is the release rate constant. Higuchi's equation, $Q = k_2 t^{1/2}$ (**5**), where Q is the percent of drug release at time t, and k_2 is the diffusion rate constant.

2.9. *Skin irritation study*

The skin irritation test was performed on six rats, which were divided into 3 groups ($n = 2$), to evaluate the irritant properties of the drug HS. For this purpose, rats were shaved and an aqueous solution of formalin 0.8% was used as standard irritant. Drug reservoir patches of 2 cm^2 were used as test patches. The patches were removed after a period of 24 h with the help of an alcohol swab. The skin response was examined for development of erythema and edema for each rat at the end of 24 h, with respect to appearance of redness, flare, wheals, and rashes. The area was observed for 3 days. Finally, the application sites were graded according to a visual scoring scale from 0 to 4 (*26*).

2.10. *Stability study of optimized formulation*

A stability study was carried out for optimized patch formulation at 40°C temperature in a humidity chamber having 75% RH for 3 months. After 3 months samples were withdrawn and evaluated for physicochemical properties and *in-vitro* diffusion studies.

3. Results and Discussion

3.1. *Investigation of physicochemical compatibility of drug and polymer*

Differential scanning calorimetry enables the quantitative detection of all processes in which energy is required or produced (*i.e.*, endothermic or exothermic phase transformations). The thermograms of **(A)** HS **(B)** HS with HPMC K15, and **(C)** HS with eudragit RSPO/ammonio methaacrylate copolymer type B are presented in Figure 1. The HS showed a melting peak at 26.83°C. Peak of HS at 271.03°C was present at the same position *i.e.* near to 269°C in the physical mixture of drug with both HPMC and eudragit RSPO patch formulation excipients. This confirmed the physicochemical stability of drug with the formulation excipient used in the study.

Drug-excipient interactions play a vital role with respect to release of drug from the formulation among others. FTIR techniques have been used here to study the physical and chemical interaction between drug and excipients used. Infrared (IR) spectra of HS **(A)**, physical mixture of HS + HPMC K15 **(B)**, and physical mixture of HS + HPMC K15 + eudragit RSPO/ ammonio methacrylate copolymer type B **(C)** are shown in Figure 2. Infrared absorption spectroscopy of HS showed a band at 1,230 and 1,040 cm^{-1} due to symmetrical and asymmetrical stretching of S-O in SO_3 heparin groups, respectively. From the figure it was observed that there were no changes in these main peaks in IR spectra of mixture of drug and polymers, which show there were no physical interactions because of some bond formation between drug and polymers, and that excipients are compatible with HS within the formulation.

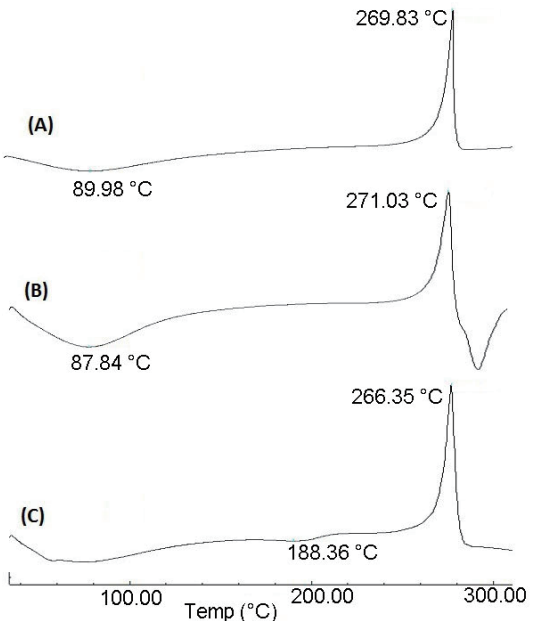

Figure 1. DSC thermogram of heparin sodium and its physical mixture with different excipients. (A) Heparin sodium. **(B)** Heparin sodium with HPMC K15. **(C)** Heparin sodium drug with eudragit RSPO/Ammonio methaacrylate copolymer type B.

3.2. *Physicochemical characterization of films*

The results of the physicochemical characterization of the patches are shown in Table 2. The thickness ranged between 0.063 and 0.146 mm, which indicate that they were uniform in thickness. The weights ranged between 5.70 mg and 9.93 mg, which indicates that different batches patch weights, were relatively similar.

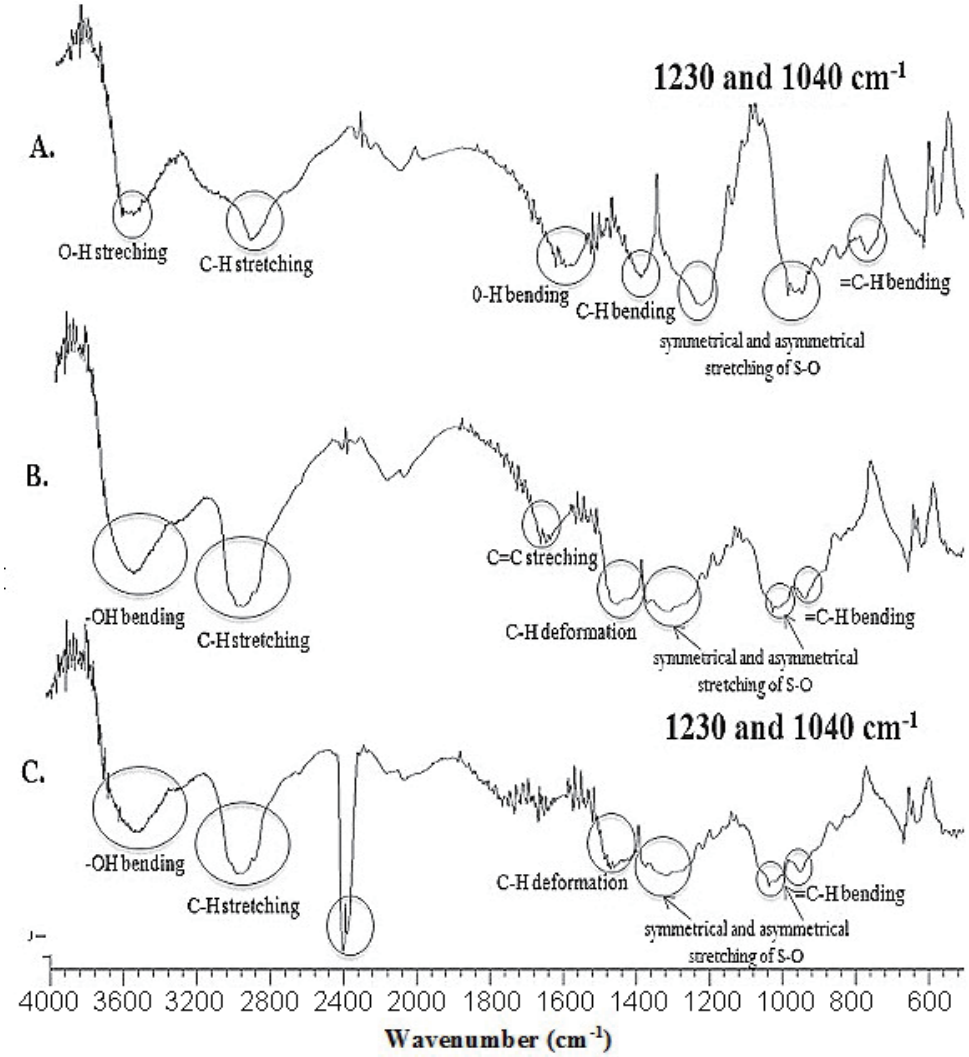

Figure 2. FTIR spectras of heparin sodium and its physical mixture with different excipients. (A): Heparin sodium. **(B)**: Physical mixture of heparin sodium + eudragit RSPO. **(C)**: Physical mixture of heparin sodium + HPMC K15 + eudragit RSPO/ ammonio methacrylate copolymer type B.

Table 2. Evaluation of transdermal patch formulations of HS

Formulation code	Thickness uniformity (mm)	Weight variation test (mgs)	Drug content (mcg/2 cm^2)	Folding endurance	Tensile strength (kg/cm^2)	Moisture Content (%)	Moisture uptake (%)	WVT (mg/cm^2 hr)
HS 1	0.063 ± 0.011	5.93 ± 0.94	9.9 ± 0.25	156 ± 9	2.0 ± 0.5	10.66 ± 0.2	1.05 ± 0.25	6.0 ± 0.45
HS 2	0.076 ± 0.005	5.70 ± 0.45	9.6 ± 0.39	165 ± 3	2.5 ± 0.5	11.23 ± 0.5	1.82 ± 0.35	5.3 ± 0.311
HS 3	0.065 ± 0.015	6.09 ± 0.56	9.7 ± 0.52	148 ± 5	2.5 ± 0.5	13.45 ± 0.4	0.90 ± 0.32	5.1 ± 0.56
HS 4	0.086 ± 0.005	6.96 ± 0.66	9.8 ± 0.70	180 ± 2	3.0 ± 0.25	12.62 ± 0.6	1.80 ± 1.15	6.0 ± 0.11
HS 5	0.113 ± 0.011	7.03 ± 0.73	9.9 ± 0.42	180 ± 3	2.0 ± 0.5	7.36 ± 0.78	1.48 ± 0.57	6.6 ± 0.26
HS 6	0.112 ± 0.01	7.00 ± 0.75	9.8 ± 0.75	205 ± 4	2.5 ± 0.25	7.50 ± 0.01	3.03 ± 0.12	6.6 ± 0.43
HS 7	0.116 ± 0.005	7.12 ± 0.45	9.5 ± 0.44	80 ± 10	3.0 ± 0.75	7.71 ± 0.78	1.02 ± 0.65	6.1 ± 0.5
HS 8	0.139 ± 0.015	7.03 ± 0.95	10.1 ± 0.43	135 ± 4	2.0 ± 0.25	8.91 ± 0.20	1.56 ± 0.95	6.9 ± 0.15
HS 9	0.143 ± 0.01	7.93 ± 0.95	9.8 ± 0.52	196 ± 2	3.5 ± 1.0	9.03 ± 0.45	2.09 ± 0.89	5.2 ± 0.45
HS 10	0.125 ± 0.01	7.98 ± 0.70	9.9 ± 0.29	92 ± 5	3.5 ± 0.5	8.76 ± 0.26	2.12 ± 0.59	5.3 ± 0.31
HS 11	0.146 ± 0.015	8.10 ± 0.54	9.7 ± 0.93	204 ± 2	2.0 ± 0.5	7.50 ± 0.40	3.21 ± 0.15	4.9 ± 0.11
HS 12	0.145 ± 0.011	9.93 ± 0.41	9.8 ± 0.42	201 ± 5	2.5 ± 0.0	7.36 ± 0.80	2.89 ± 0.35	5.1 ± 0.72
HS 13	0.144 ± 0.01	8.16 ± 0.32	9.7 ± 0.36	194 ± 7	3.5 ± 0.5	7.24 ± 0.50	2.56 ± 0.33	5.2 ± 0.115

* mean ± SD (n = 3).

Good uniformity of drug content among the batches was observed with all formulations and ranged from 97.9 to 99.2%. The results indicate that the process employed to prepare patches in this study was capable of producing patches with uniform drug content and minimal patch variability. The flatness study showed that all the formulations had the same strip length before and after their cuts, indicating 100% flatness. Thus, no amount of constriction was observed; all patches had a smooth, flat surface; and that smooth surface could be maintained when the patch was applied to the skin. Folding endurance test results indicated that the patches would not break and would maintain their integrity with general skin folding when applied. Moisture content and moisture uptake studies indicated that the increase in the concentration of hydrophilic polymer was directly proportional to the increase in moisture content and moisture uptake of the patches. The moisture content of the prepared formulations was low, which could help the formulations remain stable and reduce brittleness during long term storage. The moisture uptake of the formulations was also low, which could protect the formulations from microbial contamination and reduce bulkiness (*27*).

3.3. *In-vitro skin permeation*

The *in-vitro* release profile is an important tool that predicts in advance how a drug will behave *in-vivo* (*28*). The results of *in-vitro* skin permeation studies of HS from transdermal patches are shown in Figure 3. In the present study hydrophilic (HPC, HEC, and HPMC) and hydrophobic (eudragit RSPO) polymers were used to preparepatches. Formulation HS13 exhibited the greatest, 93.25%, drug release value, while formulation HS5 exhibit the lowest, 64.72%, drug release value. The cumulative amount of drug released from formulations containing hydrophilic polymer released drug at a faster rate than hydrophobic polymer. The cumulative amount of drug released from formulations HS9, HS12 and HS13 were much higher than other formulations. In addition to nature of polymer concentration of polymer also affected drug release. The transdermal drug delivery system HS9 (HPMC K 15 M alone) showed drug release (88.16%), and lasted only for 8 h but the transdermal drug delivery system HS13 (HPMC K15:ammonio acrylate) showed the highest prolonged drug release successfully for 10 h (93.25%). HS13 achieved a high cumulative amount of drug permeation at the end of 10 h. Based on physiochemical and *in-vitro* release experiments, HS13 was chosen for further studies.

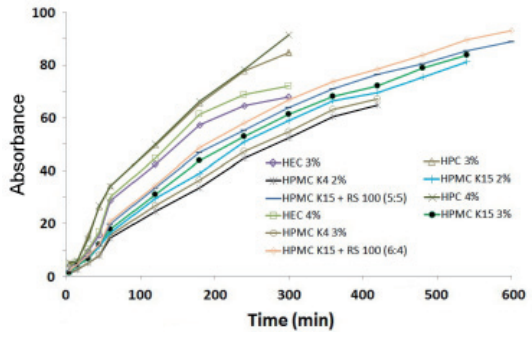

Figure 3. Release profiles of HS from patches containing different concentrations of HPC, HEC, HPMC, and eudragit RSPO, mean ± SD (*n* = 3).

3.4. *Full factorial design*

3.4.1. *Physicochemical properties of factorial design batches*

The results of the physicochemical characterization of the patches are shown in Table 3.

3.4.2. *In-vitro drug release study of factorial design batches*

The cumulative percentage of drug permeated through the rat epidermis from the patch containing different concentrations of penetration enhancer is shown in Figure 4.

An increase in concentration of oleic acid leads to an increase in Q_{10hr} because the coefficient b_1 bears a positive sign. Increasing the concentration of oleic acid from 5 to 10% the Q_{10hr} value increased from 81.13% to 88.14%. An increase in concentration of isopropyl myristate leads to an increase in Q_{10hr} because the coefficient b_2 bears a positive sign. When increasing the concentration of isopropyl myristate from 5 to 10% the

Table 3. Properties of transdermal patches containing HS

Formulation code	Thickness (μm)	Weight variation (mg)	Drug content	Folding endurance	Tensile strength (kg·cm^{-2})
HS 1	160 ± 5.60	9.61 ± 0.57	97.9 ± 2.42	198 ± 6.93	2.55 ± 0.50
HS 2	168 ± 5.88	10.12 ± 0.38	98.6 ± 2.45	202 ± 7.07	2.58 ± 0.25
HS 3	171 ± 5.95	10.23 ± 0.55	97.5 ± 2.41	215 ± 7.52	3.00 ± 0.75
HS 4	158 ± 5.53	8.20 ± 0.39	96.9 ± 2.39	218 ± 7.63	2.00 ± 0.50
HS 5	166 ± 5.81	10.73 ± 0.37	98.8 ± 2.45	201 ± 7.70	2.50 ± 0.25
HS 6	154 ± 5.39	9.97 ± 0.38	96.8 ± 3.52	200 ± 7.00	2.50 ± 0.75
HS 7	165 ± 5.77	8.21 ± 0.29	97.8 ± 2.42	208 ± 7.28	3.00 ± 0.50
HS 8	169 ± 5.61	10.87 ± 0.38	98.6 ± 2.45	196 ± 6.86	3.50 ± 0.25
HS 9	152 ± 5.28	10.52 ± 0.40	99.2 ± 1.51	220 ± 7.42	3.50 ± 1.00

* mean ± SD (*n* = 3).

Q_{10hr} value increased from 84.36% to 90.31%.

Here the coefficient of interaction terms showed a negative value. The interaction term indicated that Q_{10hr} was not significantly affected by interaction of two penetration enhancers. This indicates that by changing two factors at a time there was no effect on $Q_{10hr.}$

The maximum amount (Q_{10hr}) of ACF that permeated during the 10 h of the study was 93.06% from formulation H8. The flux was calculated by dividing the cumulative amount of drug which permeated per cm^2 of the skin with time. Thus the corresponding flux of HS was 292.03 $\mu g \cdot cm^{-2} hr^{-1}$ from formulation H8. A marked effect of penetration enhancer on HS permeation was observed when they were incorporated in the patch in varying concentrations. The cumulative percentage of HS that permeated over 10 h was found to increase ranging from 67.91 to 93.06% for patches. The corresponding flux values ranged from 208.50 to 292.03 $\mu g \cdot cm^{-2} hr^{-1}$. Formulation H8 shows highest flux among all the formulations. This result indicated that the formulation containing 10% oleic acid with 10% isopropyl myristate gave better penetration of HS through rat skin (Table 4).

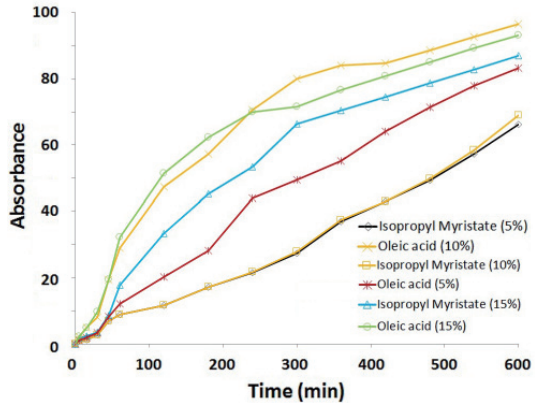

Figure 4. Release profiles of HS having different penetration enhancers, mean ± SD (*n* = 3).

3.5. *Regression analysis for Q_{10hr}*

The significance levels of the coefficients *b*1, *b*2, *b*11, *b*22 and *b*12 were found to be *P* = 6.570, 7.30, –0.540, –3.732 and –2.057 respectively, so they were omitted from the full model to generate a reduced model. The coefficient *b*1 was found to be significant; hence, it was retained in the reduced model. The reduced model was tested in proportion to determine whether the coefficients *b*1, *b*2, *b*11, *b*22, and *b*12 contribute significant information to the prediction of Q_{10hr}. The critical value of F for α = 0.05 is equal to 9.11 (df = 4.3). Since the calculated value (*F* = 2.50) is less than the critical value (*F* = 9.11), it may be concluded that the terms *b*1, *b*2, *b*11, *b*22 and *b*12 do not contribute significantly to the prediction of *Q*10 and can be omitted from the full model to generate the reduced model.

3.6. *Kinetic modeling of drug release*

The cumulative amount of drug which permeated per square centimeter of patches (H1 to H9) through rat skin plotted against time was fitted to zero, first and Higuchi kinetic models. The release profile of H followed mixed zero-order and first-order kinetics in different formulations. The release profile of patches H1, H2, H3, H4, H5, H6, H7, H8, and H9 as per Higuchi's equation was 0.937, 0.966, 0.974, 0.960, 0.980, 0.985, 0.969, 0.994 and 0.990 respectively. However, the release profile of the optimized formulation H8 (r^2 = 0.994 for Higuchi) indicated that the permeation of the drug from the patches was governed by a diffusion mechanism.

3.7. *Skin irritation study*

The skin irritation test of the transdermal formulation of optimized batch HS13 and marketed formulation on the rat gave a score less than the 1 scale for erythma as well as 0 level scale for edema as compared to the standard

Table 4. 3^2 full factorial design layouts for HS transdermal patches

Batch No.	X_1	X_2	Q_{10hr} release (%)	Flux (J) ($\mu g \cdot cm^{-2} \cdot hr^{-1}$)	Permeability co efficient (K_p) ($cm \cdot hr^{-1}$)	Enhancement ratio (ER)
HS 1	-1	-1	68.95	208.50	4.17	1.04
HS 2	1	1	87.01	263.12	5.26	1.32
HS 3	0	1	88.87	268.74	5.37	1.34
HS 4	1	-1	69.84	211.20	4.22	1.06
HS 5	1	0	83.2	251.60	5.03	1.26
HS 6	0	0	82.76	250.27	5.01	1.25
HS 7	0	-1	69.51	208.50	4.17	1.04
HS 8	-1	0	96.57	292.03	5.84	1.46
HS 9	-1	1	93.13	281.63	5.63	1.41

Translation of coded levels in actual units

Variables level	Low (-1)	Medium (0)	High (+1)
Amount of isopropyl myristate (% W/W of drug) X_1	0	5	10
Amount of oleic acid (% W/W of drug) X_2	0	10	15

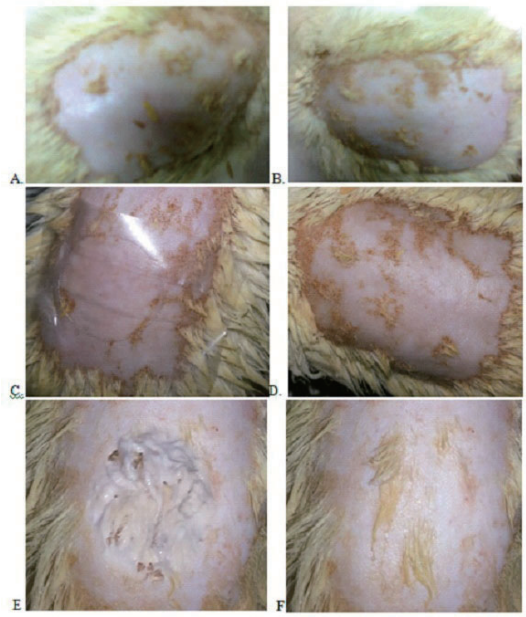

Figure 5. Skin irritation studies. (A): Control group at 0 h, **(B)**: Control group at 24 h, **(C)**: Optimized batch HS13 at 0 h, **(D)**: Optimized batch HS13 at 24 h, **(E)**: Marketed Formulation at 0 h, **(F)**: Marketed Formulation at 24 h.

Table 5. Stability studies

Stability condition	Sampling time	Folding endurance	Visual appearance	Drug content
Room tempeartue (30°C and 65% RH)	Initial (0 day)	> 200	Clear film	99.5
	After 30 days	> 200	Clear film	99.4
Accelerated condition (40°C and 75% RH)	Initial (0 day)	> 200	Clear film	99.8
	After 30 days	35	Hazy	99.1

formalin solution for 24 and 48 h after application (Figure 5). According to Draize *et al*. (*29*), compounds producing scores of 2 or less are considered negative (no skin irritation). Hence, the developed transdermal formulations are free of skin irritation.

3.8. *Stability study*

In order to determine the change in physicochemical parameters and *in-vitro* release profile on storage, a stability study was carried out. The physicochemical parameters of the optimized formulation were not significantly changed on storage. The *in-vitro* release profile before and after storage is shown in Table 5. The result indicates that the formulation was stable under the required storage conditions.

4. Conclusion

The method of preparation of transdermal patches of HS presented in this research work is simple. All formulations also showed good physicochemical properties like thickness, weight variation, drug content, flatness, folding endurance, moisture content and moisture uptake. The *in-vitro* release data showed that drug release from the patch formulation were affected by types of polymer and concentration of polymer. Effect of penetration enhancer like oleic acid and isopropyl myristate have been checked on *in-vitro* permeation of drug. These studies indicated that as the concentration of penetration enhancer increased drug permeation was increased. The finding of this result revealed that the problems of HS on i.v. administration like pain, swelling, inflammation, and short half life can be overcome by applying HS topically in the form of a transdermal patch.

References

1. Misra AN. Controlled and Novel Drug Delivery. In: Transdermal Drug Delivery (Jain NK. ed.) CBS Publisher and Distributor, New Delhi, India, 1997; pp. 100-101.
2. Chien YW. Transdermal therapeutic system. In: Controlled Drug Delivery Fundamentals and Applications (Robinson JR, Lee VHL, eds.). 2nd ed., Marcel Dekker, Inc., New York, USA, 1987; pp. 524-552.
3. Keith AD. Polymer matrix consideration for transdermal devices. Drug Dev Ind. 1983; 9:605-621.
4. *www.medsafe.govt.nz/profs/datasheet/h/HeparinSodiuminf.pdf*
5. Cohen EM, Grim WM, Harwood RJ, Mehta GN. Solid state ophthalmic medication. United States Patent No. 1979; 4: 179,497.
6. Harwood RJ, Schwartz JB. Drug release from compression molded films: preliminary studies with pilocarpine. Drug Dev Ind Pharm. 1982; 8:663-682.
7. Dumortier G, Zuber M, Chast F. Systemic absorption of morphine after ocular administration: Evaluation of morphine salt insert *in vitro* and *in vivo*. Int J Pharm. 1990; 59:1-7.
8. Kusum DV, Saisivam S, Maria GR, Deepti PU. Design and evaluation of matrix diffusion controlled transdermal patches of verapamil hydrochloride. Drug Dev Ind Pharm. 2003; 29:495-503.
9. Limpongsa E, Umprayn K. Preparation and evaluation of diltiazem hydrochloride diffusion-controlled transdermal delivery system. AAPS PharmSciTech. 2008; 9:464-470.
10. Sakellariou P, Rowe RC, White EFT. An evaluation of the interaction and plasticizing efficiency of the polyethylene glycols in ethyl cellulose and hydroxypropyl methylcellulose films using the torsional braid pendulum. Int J Pharm. 1986; 31:55-64.
11. Cooper ER. Increased skin permeability for lipophilic molecules. Pharm Sri. 1984; 73:1153-1156.
12. Goodman M, Barry BW. Lipid-protein-partitioning (LPP) theory of skin enhancer activity: Finite dose technique. Int J Pharm. 1989; 57:29-40.
13. Hu JH, Zhu Y. Effect of enhancers on the permeation of ketoprofen *in-vitro*. Yao Hsueh Hsueh Pao. 1996; 31:48-53.
14. Chi SC, Park ES, Kim H. Effect of penetration enhancers on flurbiprofen permeation though rat skin. Int J Pharm. 1995; 126:267-274.
15. Kim DD, Chien YW. Transdermal delivery of

dideoxynucleoside-type anti-HIV drugs. 2. The effect of vehicle and enhancer on skin permeation. J Pharm Sci. 1996; 85:214-219.
16. Amnuaikit C, Ikeuchi I, Ogawara K, Higaki K, Kimura T. Skin permeation of propranolol from polymeric film containing terpene enhancers for transdermal use. Int J Pharm. 2005; 289:167-178.
17. Verma PRP, Iyer SS. Transdermal delivery of propranolol using mixed grades of Eudragit: Design and *in-vitro* and *in vivo* evaluation. Drug Dev Ind Pharm. 2000; 26:471-476.
18. Arora P, Mukherjee P. Design, development, physicochemical, and *in-vitro* and *in-vivo* evaluation of transdermal patches containing diclofenac diethylammonium salt. J Pharm Sci. 2002; 91:2076-2089.
19. Devi VK, Saisivam S, Maria GR, Deepti PU. Design and evaluation of matrix diffusion controlled transdermal patches of verapamil hydrochloride. Drug Dev Ind Pharm. 2003; 29:495-503.
20. Gupta R, Mukherjee B. Development and *in-vitro* evaluation of diltiazem hydrochloride transdermal patches based on povidone-ethyl cellulose matrices. Drug Dev Ind Pharm. 2003; 29:1-7.
21. Krishna R, Pandit JK. Transdermal delivery of propranolol. Drug Dev Ind Pharm. 1994; 20:2459-2465.
22. Julraht K, Keith AP, James AW. Development of a transdermal delivery device for melotoin *in-vitro* study. Drug Dev Ind Pharm. 1995; 21:1377-1387.
23. Ho HO, Chen LC, Lin HM, Sheu MT. Penetration enhancement by menthol combined with a solubilization effect in a solvent system. J Control Release. 1998; 51:301-311.
24. Yamune M, Williams A, Barry B. Terpenes penetration enhancers in propylene glycol/water co-solvent systems: Effectiveness and mechanism of action. J Pharm Pharmacol. 1995; 47:978-989.
25. Williams A, Barry B. Terpenes and the lipid-protein partitioning theory of skin penetration enhancement. Pharm Res. 1991; 8:17-24.
26. Bagchi D, Bagchi M, Sidney J, Stohs A, Das DK, Ray SD, Kuszynski CA, Joshi SS, Pruess HG. Free radicals and grape seed proanthocyanidin extract: Importance in human health and disease prevention. Toxicology. 2000; 148:187-197.
27. Mutalik S, Udupa N. Glibenclamide transdermal patches: Physicochemical, pharmacodynamic, and pharmacokinetic evaluations. J Pharm Sci. 2004; 93:1577-1594.
28. Katayose S, Kataoka K. Water-soluble polyion complex associates of DNA and poly (ethylene glycol)-poly (L-lysine) block copolymer. Bioconjug Chem. 1997; 8:702-707.
29. Draize JH, Woodard G, Calvery HO. Methods for the study of irritation and toxicity of substances applied to the skin and mucous membranes. J Pharmacol Exp Ther. 1944; 82:377-390.

(Received August 19, 2014; Revised August 22, 2014; Accepted August 24, 2014)

DD&T
Drug Discoveries & Therapeutics

Guide for Authors

1. Scope of Articles

Drug Discoveries & Therapeutics welcomes contributions in all fields of pharmaceutical and therapeutic research such as medicinal chemistry, pharmacology, pharmaceutical analysis, pharmaceutics, pharmaceutical administration, and experimental and clinical studies of effects, mechanisms, or uses of various treatments. Studies in drug-related fields such as biology, biochemistry, physiology, microbiology, and immunology are also within the scope of this journal.

2. Submission Types

Original Articles should be well-documented, novel, and significant to the field as a whole. An Original Article should be arranged into the following sections: Title page, Abstract, Introduction, Materials and Methods, Results, Discussion, Acknowledgments, and References. Original articles should not exceed 5,000 words in length (excluding references) and should be limited to a maximum of 50 references. Articles may contain a maximum of 10 figures and/or tables.

Brief Reports definitively documenting either experimental results or informative clinical observations will be considered for publication in this category. Brief Reports are not intended for publication of incomplete or preliminary findings. Brief Reports should not exceed 3,000 words in length (excluding references) and should be limited to a maximum of 4 figures and/or tables and 30 references. A Brief Report contains the same sections as an Original Article, but the Results and Discussion sections should be combined.

Reviews should present a full and up-to-date account of recent developments within an area of research. Normally, reviews should not exceed 8,000 words in length (excluding references) and should be limited to a maximum of 100 references. Mini reviews are also accepted.

Policy Forum articles discuss research and policy issues in areas related to life science such as public health, the medical care system, and social science and may address governmental issues at district, national, and international levels of discourse. Policy Forum articles should not exceed 2,000 words in length (excluding references).

Case Reports should be detailed reports of the symptoms, signs, diagnosis, treatment, and follow-up of an individual patient. Case reports may contain a demographic profile of the patient but usually describe an unusual or novel occurrence. Unreported or unusual side effects or adverse interactions involving medications will also be considered. Case Reports should not exceed 3,000 words in length (excluding references).

News articles should report the latest events in health sciences and medical research from around the world. News should not exceed 500 words in length.

Letters should present considered opinions in response to articles published in Drug Discoveries & Therapeutics in the last 6 months or issues of general interest. Letters should not exceed 800 words in length and may contain a maximum of 10 references.

3. Editorial Policies

Ethics: Drug Discoveries & Therapeutics requires that authors of reports of investigations in humans or animals indicate that those studies were formally approved by a relevant ethics committee or review board.

Conflict of Interest: All authors are required to disclose any actual or potential conflict of interest including financial interests or relationships with other people or organizations that might raise questions of bias in the work reported. If no conflict of interest exists for each author, please state "There is no conflict of interest to disclose".

Submission Declaration: When a manuscript is considered for submission to Drug Discoveries & Therapeutics, the authors should confirm that 1) no part of this manuscript is currently under consideration for publication elsewhere; 2) this manuscript does not contain the same information in whole or in part as manuscripts that have been published, accepted, or are under review elsewhere, except in the form of an abstract, a letter to the editor, or part of a published lecture or academic thesis; 3) authorization for publication has been obtained from the authors' employer or institution; and 4) all contributing authors have agreed to submit this manuscript.

Cover Letter: The manuscript must be accompanied by a cover letter signed by the corresponding author on behalf of all authors. The letter should indicate the basic findings of the work and their significance. The letter should also include a statement affirming that all authors concur with the submission and that the material submitted for publication has not been published previously or is not under consideration for publication elsewhere. The cover letter should be submitted in PDF format. For example of Cover Letter, please visit http://www.ddtjournal.com/downcentre.php (Download Centre).

Copyright: A signed JOURNAL PUBLISHING AGREEMENT (JPA) must be provided by post, fax, or as a scanned file before acceptance of the article. Only forms with a hand-written signature are accepted. This copyright will ensure the widest possible dissemination of information. A form facilitating transfer of copyright can be downloaded by clicking the appropriate link and can be returned to the e-mail address or fax number noted on the form (Please visit Download Centre). Please note that your manuscript will not proceed to the next step in publication until the JPA form is received. In addition, if excerpts from other copyrighted works are included, the author(s) must obtain written permission from the copyright owners and credit the source(s) in the article.

Suggested Reviewers: A list of up to 3 reviewers who are qualified to assess the scientific merit of the study is welcomed. Reviewer information including names, affiliations, addresses, and e-mail should be provided at the same time the manuscript is submitted online. Please do not suggest reviewers with known conflicts of interest, including participants or anyone with a stake in the proposed research; anyone from the same institution; former students, advisors, or research collaborators (within the last three years); or close personal contacts. Please note that the Editor-in-Chief may accept one or more of the proposed reviewers or may request a review by other qualified persons.

Language Editing: Manuscripts prepared by authors whose native language is not English should have their work proofread by a native English speaker before submission. If not, this might delay the publication of your manuscript in Drug Discoveries & Therapeutics.

The Editing Support Organization can provide English proofreading, Japanese-English translation, and Chinese-English translation services to authors who want to publish in Drug Discoveries & Therapeutics and need assistance before submitting a manuscript. Authors can visit this organization directly at http://www.iacmhr.com/iac-eso/support.php?lang=en. IAC-ESO was established to facilitate manuscript preparation by researchers whose native language is not English and to help edit works intended for international academic journals.

4. Manuscript Preparation

Manuscripts should be written in clear, grammatically correct English and submitted as a Microsoft Word file in a single-column format. Manuscripts must be paginated and typed in 12-point Times New Roman font with 24-point line spacing. Please do not embed figures in the text. Abbreviations should be used as little as possible and should be explained at first mention unless the term is a well-known abbreviation (*e.g.* DNA). Single words should not be abbreviated.

Title page: The title page must include 1) the title of the paper (Please note the title should be short, informative, and contain the major key words); 2) full name(s) and affiliation(s) of the author(s), 3) abbreviated names of the author(s), 4) full name, mailing address, telephone/fax numbers, and e-mail address of the corresponding author; and 5) conflicts of interest (if you have an actual or potential conflict of interest to disclose, it must be included as a footnote on the title page of the manuscript; if no conflict of interest exists for each author, please state "There is no conflict of interest to disclose"). Please visit Download Centre and refer to the title page of the manuscript sample.

Abstract: The abstract should briefly state the purpose of the study, methods, main findings, and conclusions. For article types including Original Article, Brief Report, Review, Policy Forum, and Case Report, a one-paragraph abstract consisting of no more than 250 words must be included in the manuscript. For News and Letters, a brief summary of main content in 150 words or fewer should be included in the manuscript. Abbreviations must be kept to a minimum and non-standard abbreviations explained in brackets at first mention. References should be avoided in the abstract. Key words or phrases that do not occur in the title should be included in the Abstract page.

Introduction: The introduction should be a concise statement of the basis for the study and its scientific context.

Materials and Methods: The description should be brief but with sufficient detail to enable others to reproduce the experiments. Procedures that have been published previously should not be described in detail but appropriate references should simply be cited. Only new and significant modifications of previously published procedures require complete description. Names of products and manufacturers with their locations (city and state/country) should be given and sources of animals and cell lines should always be indicated. All clinical investigations must have been conducted in accordance with Declaration of Helsinki principles. All human and animal studies must have been approved by the appropriate institutional review board(s) and a specific declaration of approval must be made within this section.

Results: The description of the experimental results should be succinct but in sufficient detail to allow the experiments to be analyzed and interpreted by an independent reader. If necessary, subheadings may be used for an orderly presentation. All figures and tables must be referred to in the text.

Discussion: The data should be interpreted concisely without repeating material already presented in the Results section. Speculation is permissible, but it must be well-founded, and discussion of the wider implications of the findings is encouraged. Conclusions derived from the study should be included in this section.

Acknowledgments: All funding sources should be credited in the Acknowledgments section. In addition, people who contributed to the work but who do not meet the criteria for authors should be listed along with their contributions.

References: References should be numbered in the order in which they appear in the text. Citing of unpublished results, personal communications, conference abstracts, and theses in the reference list is not recommended but these sources may be mentioned in the text. In the reference list, cite the names of all authors when there are fifteen or fewer authors; if there are sixteen or more authors, list the first three followed by *et al*. Names of journals should be abbreviated in the style used in PubMed. Authors are responsible for the accuracy of the references. Examples are given below:

Example 1 (Sample journal reference):
Nakata M, Tang W. Japan-China Joint Medical Workshop on Drug Discoveries and Therapeutics 2008: The need of Asian pharmaceutical researchers' cooperation. Drug Discov Ther. 2008; 2:262-263.

Example 2 (Sample journal reference with more than 15 authors):
Darby S, Hill D, Auvinen A, *et al*. Radon in homes and risk of lung cancer: Collaborative analysis of individual data from 13 European case-control studies. BMJ. 2005; 330:223.

Example 3 (Sample book reference):
Shalev AY. Post-traumatic stress disorder: Diagnosis, history and life course. In: Post-traumatic Stress Disorder, Diagnosis, Management and Treatment (Nutt DJ, Davidson JR, Zohar J, eds.). Martin Dunitz, London, UK, 2000; pp. 1-15.

Example 4 (Sample web page reference):
World Health Organization. The World Health Report 2008 – primary health care: Now more than ever. *http://www.who.int/whr/2008/whr08_en.pdf* (accessed September 23, 2010).

Tables: All tables should be prepared in Microsoft Word or Excel and should be arranged at the end of the manuscript after the References section. Please note that tables should not in image format. All tables should have a concise title and should be numbered consecutively with Arabic numerals. If necessary, additional information should be given below the table.

Figure Legend: The figure legend should be typed on a separate page of the main manuscript and should include a short title and explanation. The legend should be concise but comprehensive and should be understood without referring to the text. Symbols used in figures must be explained.

Figure Preparation: All figures should be clear and cited in numerical order in the text. Figures must fit a one- or two-column format on the journal page: 8.3 cm (3.3 in.) wide for a single column, 17.3 cm (6.8 in.) wide for a double column; maximum height: 24.0 cm (9.5 in.). Please make sure that artwork files are in an acceptable format (TIFF or JPEG) at minimum resolution (600 dpi for illustrations, graphs, and annotated artwork, and 300 dpi for micrographs and photographs). Please provide all figures as separate files. Please note that low-resolution images are one of the leading causes of article resubmission and schedule delays. All color figures will be reproduced in full color in the online edition of the journal at no cost to authors.

Units and Symbols: Units and symbols conforming to the International System of Units (SI) should be used for physicochemical quantities. Solidus notation (*e.g.* mg/kg, mg/mL, mol/mm^2/min) should be used. Please refer to the SI Guide www.bipm.org/en/si/ for standard units.

Supplemental data: Supplemental data might be useful for supporting and enhancing your scientific research and Drug Discoveries & Therapeutics accepts the submission of these materials which will be only published online alongside the electronic version of your article. Supplemental files (figures, tables, and other text materials) should be prepared according to the above guidelines, numbered in Arabic numerals (*e.g.*, Figure S1, Figure S2, and Table S1, Table S2) and referred to in the text. All figures and tables should have titles and legends. All figure legends, tables and supplemental text materials should be placed at the end of the paper. Please note all of these supplemental data should be provided at the time of initial submission and note that the editors reserve the right to limit the size and length of Supplemental Data.

5. Submission Checklist

The Submission Checklist will be useful during the final checking of a manuscript prior to sending it to Drug Discoveries & Therapeutics for review. Please visit Download Centre and download the Submission Checklist file.

6. Online submission

Manuscripts should be submitted to Drug Discoveries & Therapeutics online at http://www.ddtjournal.com. The manuscript file should be smaller than 5 MB in size. If for any reason you are unable to submit a file online, please contact the Editorial Office by e-mail at office@ddtjournal.com

7. Accepted manuscripts

Proofs: Galley proofs in PDF format will be sent to the corresponding author *via* e-mail. Corrections must be returned to the editor (proof-editing@ddtjournal.com) within 3 working days.

Offprints: Authors will be provided with electronic offprints of their article. Paper offprints can be ordered at prices quoted on the order form that accompanies the proofs.

Page Charge: A page charge of $140 will be assessed for each printed page of an accepted manuscript. The charge for printing color figures is $340 for each page. Under exceptional circumstances, the author(s) may apply to the editorial office for a waiver of the publication charges at the time of submission.

(Revised February 2013)

Editorial and Head Office:

Pearl City Koishikawa 603
2-4-5 Kasuga, Bunkyo-ku
Tokyo 112-0003
Japan
Tel: +81-3-5840-9697
Fax: +81-3-5840-9698
E-mail: office@ddtjournal.com

DD&T
Drug Discoveries & Therapeutics

JOURNAL PUBLISHING AGREEMENT (JPA)

Manuscript No.:

Title:

Corresponding author:

The International Advancement Center for Medicine & Health Research Co., Ltd. (IACMHR Co., Ltd.) is pleased to accept the above article for publication in Drug Discoveries & Therapeutics. The International Research and Cooperation Association for Bio & Socio-Sciences Advancement (IRCA-BSSA) reserves all rights to the published article. Your written acceptance of this JOURNAL PUBLISHING AGREEMENT is required before the article can be published. Please read this form carefully and sign it if you agree to its terms. The signed JOURNAL PUBLISHING AGREEMENT should be sent to the Drug Discoveries & Therapeutics office (Pearl City Koishikawa 603, 2-4-5 Kasuga, Bunkyo-ku, Tokyo 112-0003, Japan; E-mail: office@ddtjournal.com; Tel: +81-3-5840-9697; Fax: +81-3-5840-9698).

1. Authorship Criteria

As the corresponding author, I certify on behalf of all of the authors that:

1) The article is an original work and does not involve fraud, fabrication, or plagiarism.
2) The article has not been published previously and is not currently under consideration for publication elsewhere. If accepted by Drug Discoveries & Therapeutics, the article will not be submitted for publication to any other journal.
3) The article contains no libelous or other unlawful statements and does not contain any materials that infringes upon individual privacy or proprietary rights or any statutory copyright.
4) I have obtained written permission from copyright owners for any excerpts from copyrighted works that are included and have credited the sources in my article.
5) All authors have made significant contributions to the study including the conception and design of this work, the analysis of the data, and the writing of the manuscript.
6) All authors have reviewed this manuscript and take responsibility for its content and approve its publication.
7) I have informed all of the authors of the terms of this publishing agreement and I am signing on their behalf as their agent.

2. Copyright Transfer Agreement

I hereby assign and transfer to IACMHR Co., Ltd. all exclusive rights of copyright ownership to the above work in the journal Drug Discoveries & Therapeutics, including but not limited to the right 1) to publish, republish, derivate, distribute, transmit, sell, and otherwise use the work and other related material worldwide, in whole or in part, in all languages, in electronic, printed, or any other forms of media now known or hereafter developed and the right 2) to authorize or license third parties to do any of the above.

I understand that these exclusive rights will become the property of IACMHR Co., Ltd., from the date the article is accepted for publication in the journal Drug Discoveries & Therapeutics. I also understand that IACMHR Co., Ltd. as a copyright owner has sole authority to license and permit reproductions of the article.

I understand that except for copyright, other proprietary rights related to the Work (*e.g.* patent or other rights to any process or procedure) shall be retained by the authors. To reproduce any text, figures, tables, or illustrations from this Work in future works of their own, the authors must obtain written permission from IACMHR Co., Ltd.; such permission cannot be unreasonably withheld by IACMHR Co., Ltd.

3. Conflict of Interest Disclosure

I confirm that all funding sources supporting the work and all institutions or people who contributed to the work but who do not meet the criteria for authors are acknowledged. I also confirm that all commercial affiliations, stock ownership, equity interests, or patent-licensing arrangements that could be considered to pose a financial conflict of interest in connection with the article have been disclosed.

Corresponding Author's Name (Signature):

Date: